ROCK PHYSICS-BASED CARBONATE RESERVOIR PORE TYPE EVALUATION BY COMBINING GEOLOGICAL, PETROPHYSICAL AND SEISMIC DATA

A Dissertation

by

QIFENG DOU

Submitted to the Office of Graduate Studies of
Texas A&M University
in partial fulfillment of the requirements for the degree of

DOCTOR OF PHILOSOPHY

May 2011

Major Subject: Geophysics

Rock Physics-Based Carbonate Reservoir Pore Type Evaluation by Combining Geological, Petrophysical and Seismic Data

Copyright 2011 Qifeng Dou

ROCK PHYSICS-BASED CARBONATE RESERVOIR PORE TYPE EVALUATION BY COMBINING GEOLOGICAL, PETROPHYSICAL AND SEISMIC DATA

A Dissertation

by

QIFENG DOU

Submitted to the Office of Graduate Studies of
Texas A&M University
in partial fulfillment of the requirements for the degree of

DOCTOR OF PHILOSOPHY

Approved by:

Chair of Committee,	Yuefeng Sun
Committee Members,	William Bryant
	Benchun Duan
	Mark Everett
Head of Department,	Andreas Kronenberg

May 2011

Major Subject: Geophysics

ABSTRACT

Rock Physics-Based Carbonate Reservoir Pore Type Evaluation by Combining Geological, Petrophysical and Seismic Data. (May 2011)

Qifeng Dou, B.S., China University of Petroleum (East China), P. R. China

M.S., China University of Petroleum (Beijing), P. R. China

Chair of Advisory Committee: Dr. Yuefeng Sun

Pore type variations account for complex velocity-porosity relationship and intensive permeability heterogeneity and consequently low oil and gas recovery in carbonate reservoir. However, it is a challenge for geologist and geophysicist to quantitatively estimate the influences of pore type complexity on velocity variation at a given porosity and porosity-permeability relationship. A new rock physics-based integrated approach in this study was proposed to quantitatively characterize the diversity of pore types and its influences on wave propagation in carbonate reservoir. Based on above knowledge, permeability prediction accuracy from petrophysical data can be improved compared to conventional approach. Two carbonate reservoirs with different reservoir features, one is a shallow carbonate reservoir with average high porosity (>10%) and another one is a supper-deep carbonate reservoir with average low porosity (<5%), are used to test the proposed approach.

Paleokarst is a major event to complicate carbonate reservoir pore structure. Because of limited data and lack of appropriate study methods, it is a difficulty to

characterize subsurface paleokarst 3D distribution and estimate its influences on reservoir heterogeneity. A method by integrated seismic characterization is applied to delineate a complex subsurface paleokarst system in the Upper San Andres Formation, Permian basin, West Texas. Meanwhile, the complex paleokarst system is explained by using a carbonate platform hydrological model, similar to modern marine hydrological environments within carbonate islands.

How to evaluate carbonate reservoir permeability heterogeneity from 3D seismic data has been a dream for reservoir geoscientists, which is a key factor to optimize reservoir development strategy and enhance reservoir recovery. A two-step seismic inversions approach by integrating angle-stack seismic data and rock physics model is proposed to characterize pore-types complexity and further to identify the relative high permeability gas-bearing zones in low porosity reservoir (< 5%) using ChangXing super-deep carbonate reservoir as an example. Compared to the conventional permeability calculation method by best-fit function between porosity and permeability, the results in this study demonstrate that gas zones and non-gas zones in low porosity reservoir can be differentiated by using above integrated permeability characterization method.

DEDICATION

This dissertation is dedicated to my wife, Shaohua Wang, and my mother, Hongxiang Dong, for their love, encouragement and support.

ACKNOWLEDGEMENTS

I am indebted to many for the completion of my Ph.D. as without the generous and kind help from my committee members, officemates, friends, families and many others, it would have been much harder to complete this tough work. First of all, thank you to Dr. Yuefeng Sun for being my doctoral committee chair, whose knowledge and experience in reservoir geophysics and rock physics always gave me inspiration. His constructive advice when I was stuck improved my research greatly and his sincerity toward sciences and scientific writing will benefit me in all my professional life. His approach to understanding all kinds of questions related to reservoir geophysics taught me a lot more than just knowledge. I will always remember our weekly meeting time when we discussed our questions and results about carbonate reservoir study! Even though some frustrations and failures occurred from time to time during the research as expected, we were excited about our research progress most of the time, which brought lots of encouragement and enjoyment. Meanwhile, I greatly appreciated his openness to my research all the time and his tolerance to my stubbornness some of the time.

Secondly, thanks to my other committee members, Dr. William Bryant, Dr. Mark Everett, and Dr. Benchun Dun. During the most difficult time in my first year studying at Texas A&M, the generous financial support from Dr. Bryant really helped me out, which meant a lot to me and my family. Without his help at that time, I am not sure I could have finished my studies here. It's Dr. Everett who introduced me into the geophysical inversion research field that amazed me a lot. His smiles and kindness

brought sunshine and encouragement to me throughout my studies. Many constructive discussions with Dr. Duan benefited my doctoral research greatly as well.

I am very grateful for Dr. Charlotte Sullivan. Even though I didn't work with her for my doctoral research, sincere encouragement from her helped me to make decision to study in America and this experience will be valuable throughout my entire life. I greatly appreciate her assistance with data collections and reviewing my publication. I acknowledge lots of valuable advice for my research from Drs. Kurt Marfurt and Fred Hilterman, as well, when I studied in University of Houston.

I have enormous debt of gratitude for the ConocoPhillips Oil Company, Hess Oil Company, and Devon Energy Oil Company, for their financial support. I am also very grateful to two software companies, Hampson-Russell Software Services and Landmark Company, for donating two suits of powerful software for my doctoral research.

I am so lucky to work with so many talented and kind graduate student fellows during my four-year study at Texas A&M University, such as (in alphabetic order): Hamid Adesokan, Rui Cai, Thomas Hull, Nan Ma, Elnara Mammadova, Idris Murad, Satyan Singh, Tinging Zhang, and Zhao Zhang. Special thanks to Zhao and Tingting for helping me finish the data transform and generate multiple-well normalization figures. All of them provided lots of help in many aspects even though it was during their extremely busy times.

TABLE OF CONTENTS

CHAPTER Page

LIST OF FIGURES

FIGURE Page

FIGURE Page

FIGURE Page

FIGURE Page

FIGURE Page

CHAPTER I

INTRODUCTION

SIGNIFICANCE OF RESEARCH

Carbonate reservoir accounts for 60 % oil and 40% gas reserves worldwide. For example, 62% of the world's proved oil reserves are in the Middle East and approximately 70% of these oil reserves are in carbonate reservoirs. 40% of the world's proved gas reserves are in the Middle East and 90% of these gas reserves lie in carbonate reservoirs. In Permian Basin of Texas, more than 60% of the original oil in place (OOIP) still remains in subsurface carbonate reservoirs. Recently, new giant oil and gas discoveries in ultra-deep carbonate reservoirs have been reported in Brazos and Southern China. So, carbonate reservoirs are considered as the future of oil and gas production and would remain a major focus in petroleum industry as well.

An unfortunate reality is that oil recovery is usually low in carbonate reservoirs. Fox example, the average carbonate reservoir recovery in Middle East is around 25%, however, it is around 35% in sandstone reservoir over the world. Based on the statistics from Kerans and Lucia (1994), recovery from the carbonate reservoirs in Permian Basin, USA, were still lower than 30%, which has been produced for 70 years after intensive enhanced oil recovery operations. Huge amount of oil and gas reserves worldwide still

---

This dissertation follows the style of Journal of Applied Geophysics.

remains in the subsurface carbonate reservoir using present existing technologies. With in-depth understanding of subsurface carbonate reservoir features and application of advanced technologies, it could be highly feasible to meet the increased energy demands from growing economy worldwide.

Compared to clastic reservoirs, carbonate reservoirs demonstrate complicated pore structure causing unpredictable porosity-velocity and porosity-permeability relationships. In the San Andres Reservoir, Permian Basin, Western Texas, USA, velocity difference at a given porosity of 13% is around 500 m/s and porosity-permeability crossplot represents considerable scattering. For the second studied deep low-porosity reservoir, ChangXing Reservoir, Later Permian, Sichuan Basin, China, represents a much bigger velocity difference around 1000 m/s at a porosity of 4% and higher permeability heterogeneity, varying from 0.01 MD to 1 D than Upper San Andres Reservoir, Permian Basin.

Complicated porosity-velocity relationship is a big challenge for geophysicists and geologists to characterize carbonate reservoirs by using geophysical data. For most clastic reservoirs, knowledge of porosity, shale volume and fluid information could be enough to predict seismic velocity (Vp and Vs) because of its relatively simple pore geometries. Some rock-physics models and empirical formula have been developed to estimate wave velocity from porosity, shale-volume, fluid types or the combination of above three factors (Geertsma, 1961; Han, 1986; Tosaya and Nur, 1982; Castagna and Batzle, et al., 1985).

Without considering influences of pore structure variation on rock elastic properties in carbonate reservoir, all of the direct hydrocarbon indicator (DHI) ranking, AVO classification systems and rock-physics models for sandstone reservoir are hardly applicable to carbonate rocks. Currently, most of existing rock-physics models could be used qualitatively to account for the complicated relationships between porosity and velocity based on pore type evaluation. However quantitative understanding of these relationships is a key part that is highly needed in seismic inversion to invert reservoir parameters from seismic data for carbonate reservoir characterization.

Low hydrocarbon recovery in carbonate reservoir is mainly caused by high permeability heterogeneity at all scales, which account for the water flooding failure in low permeability zones or early water breakthrough via high permeability zones (super-K layers). Studies show that pore structure variation has an equally important or even more important influence on permeability heterogeneity than porosity (Anselmetti and Eberli, 1993, 1999, Sun et al., 2004, 2006). Study from Lyndon et al., in 2006 in Abu Dhabi carbonate field also revealed not only intensive permeability heterogeneity but also inverse permeability-porosity relationship, in which highest permeability zone doesn't develop in high porosity zones. In this case, permeability is mainly controlled by pore types difference, but not the amount of total porosity.

Therefore, in order to estimate permeability heterogeneity and predict high permeability zones, it is crucial to delineate three-dimensional pore type and porosity variation in carbonate reservoirs by combing geological, petrophysical and geophysical data. However, very few publications are available in the literature on how to use

seismic data to evaluate carbonate reservoir pore structure complexity and further predict high permeability zones.

In this study, I would propose a practical approach to characterize carbonate reservoir porosity and pore structure heterogeneity by combining geological, lab measurement, petrophysical, geophysical data volume guided by rock physics models. Results from my studies are expected to be useful for reservoir quality prediction and for optimization of reservoir development strategies so as to enhance hydrocarbon recovery.

OBJECTIVES

The principle goal of this research is to characterize carbonate reservoir porosity and pore type heterogeneity by using a new rock-physics model based on poroelasticity and further predict reservoir permeability heterogeneity by integrating geology, rock physics and geophysics and using core, log, post- and pre-stack seismic data. Results from my studies are expected to be useful for optimizing oil and gas exploration and production strategy. The major objectives are:

1. To analyze paleokarst distribution and its influences on inter-well fluid communication using a field example from the Upper San Andres Reservoirs, Permian basin, Texas, USA.

2. To investigate reservoir geological features including depositional facies, rock types, mineral composition, diagenesis, pore types for the San Andres reservoirs and the ultra-deep ChangXing reservoirs.

3. To characterize pore type diversity and identify the major factors that result in complicated porosity-velocity and porosity-permeability relationships in carbonate rocks by combining lab measurement, petrophysical data, and log analysis for two studied reservoirs.

4. To study AVO response of carbonate rocks with different pore types in order to test the value of pre-stack seismic data in evaluating carbonate reservoir pore type variation using forward seismic modeling.

5. To conduct porosity and pore-structure parameter (γ) inversion and further predict high permeability zones using angle-stack seismic data.

LITERATURE REVIEW

Besides mineral composition and fluid type, porosity has usually been taken as a key factor affecting rock velocity. In most cases, this could be true for clastic reservoirs. Based on this knowledge, different equations or models have been proposed to characterize the relationships between velocity and porosity in past several decades. In 1941, Wood used the compressibility-average equation to predict velocity for suspensions and unconsolidated sediments. For homogeneous sandstones saturated with liquid phase and dominated by intercrystalline or interparticle porosity lower than 40%, Wyllie's time average equation could explain the velocity-porosity relationship and represent the most commonly used equation to predict velocity from porosity in the energy industries.

However, both of above equations don't take into account the influences of a change of pore types on the effective rock elastic properties in carbonate reservoirs. The pore type variation could result from the changes of pore shape, pore size and their distribution in the host rock. Recently, many researches revealed that pore type variation in carbonate reservoirs, including moldic, vuggy, interparticle, intraparticle, fractures and others, could have more influences on seismic velocity variation and permeability heterogeneity than porosity for a given mineral composition and fluid type (Anselmetti and Eberli, 1993, 1999, Sun et al.,2000, 2006). By measuring over 300 carbonate samples, Anselmetti and Eberli (1993) showed that pore structure could cause 2.5 km/s or even larger seismic compressional velocity difference at given porosity and further discovered that "permeability" was controlled by pore geometry rather than by the total amount of porosity. Sun (2006) also found that permeability variation can be more than four orders of magnitude at a given reservoir porosity range (20-25%) in a Middle East carbonate reservoir.

Lacking consideration of pore types diversity and physical mechanisms of wave propagation, Wyllie's equation and Wood's equations can hardly be used to interpret the velocity-porosity complexity in carbonate rocks. For example, Anselmetti and Eberli (1999) reported that Wyllie time average equation underestimates the bulk rock velocity in the presence of near-spherical pore types and overestimates the velocity in compliant rocks with crack or fracture porosity.

Based on the deviation of Wyllie's calculated velocity from measured velocity, some approaches or models are proposed to characterize carbonate rock pore types

qualitatively, such as secondary porosity indicator (Schlumberger, 1974), pseudo-fluid transit time (Meese and Walther, 1976), spherical porosity model (Brite et al., 1985), Lucia Model (Lucia, 1983), velocity-deviation log (Anselmetti and Eberli, 1999).

In velocity-deviation log method proposed by Anselmetti and Eberli (1999), a synthetic velocity log needs to be created from neutron or density porosity-log data using Wyllie time average equation. The differences between the real sonic log and synthetic sonic log can be plotted as velocity-deviation log, which could be a signature of different pore types. Basically, frame-forming pore types, for example moldic and vuggy, cause a higher real velocity than expected from porosity values. If reservoir is dominated by interparticle or micro-porosity, real velocity and synthetics velocity have almost zero deviation, which means that the rock lacks a rigid frame. Negative deviations mark zones where real sonic velocities are lower than expected, which may indicate a presence of fractures, paleokarst-related cracks or free gas.

By introducing pore shape factor, which is equivalent to cementation factor in Archie's equation for resistivity measurement, Saleh and Castagna in 2004 revised Wyllie's equation to study the velocity complexity in rocks with a mixture of intercrystalline and near-spherical pores. Instead of a single line trend between velocity and porosity given by Wyllie's time average equation, the modification Wyllie time average describe a velocity-porosity envelope. The lower limit of the velocity envelope represents the carbonate rock with interparticle and intercrystalline porosity. The upper limit describes the rock in which all pores are spherical or near spherical. Between the lower and upper limits is a mixture of spherical and interparticle or intercrystalline

porosity. This equation shows that Wyllie's velocity-porosity relation is a specific case as all pore types are interparticle or intercrystalline. With the aspect-ratio increasing, pore shape factor increases too. The modified Wyllie time average equation as the followings:

$$\frac{1}{Vp_{rock}} = \frac{1-\phi}{(Vp_{matrix})^{s}} + \frac{\Phi}{Vp_{fluid}} \quad \ldots\ldots\ldots\ldots\ldots\ldots\ldots\ldots 1.1$$

where Vp_{rock}, Vp_{matrix}, Vp_{fluid} are measured, matrix and fluid velocity. Φ_B is the porosity calculated from density-neutron log combination. S is pore shape factor, which can be expressed in:

$$S = 1 + \frac{\Phi}{6.5/Vp_{matrix} - 3\Phi + 2\Phi\phi - \Phi} \quad \ldots\ldots\ldots\ldots\ldots\ldots 1.2$$

where

$$\Phi_s = \frac{\Phi_B - \phi_p'}{1-\phi_p'} - \ldots\ldots\ldots\ldots\ldots\ldots\ldots\ldots\ldots\ldots\ldots\ldots 1.3$$

Φ_p' is the primary medium porosity calculated using Wyllie time average equation.

By extending the Xu-White model (Robert and Xu, 2002) used for velocity prediction from porosity and shale volume in clastic reservoir, Xu and Payne (2009) extended it to study porosity-velocity complexity in carbonate reservoirs.

In the modified model given by Xu and Payne (2009), total rock pore volume is divided into (1) clay-related pores, (2) interparticle pores, (3) microcracks, and (4) stiff pores:

$$\Phi = \phi_{clay} + \phi_{inter} + \phi_{crack} + \phi_{stiff} \quad \ldots\ldots\ldots\ldots\ldots\ldots 1.4$$

where Φ_T, Φ_{clay}, Φ_{IP}, Φ_{crack}, Φ_{stiff} are total, clay, interparticle, crack and stiff porosity. Φ_{stiff} represents moldic or vuggy pores in carbonate rocks. For clean carbonate rocks, the clay pores can be neglected. Differential effective medium process and Kuster-Toksoz theory are used to add micropores with bound water to account for the mechanical interaction between the pores. A reference line in porosity-velocity crossplot is used to represent rocks dominated by interparticle. Compared to this reference line, samples with P-wave or S-wave above this trend was interpreted as a mixture of interparticle and stiff pores. On the other hand, samples with P-wave or S-wave below this trend could be the mixture of microcrack and interparticle pores.

All of the above modified equations and models from Wyllie equation have been attempted to account for the important influence of pore structure on velocity in carbonate reservoir and explain the velocity-porosity complexity qualitatively. However, they can be questioned due to their nature of being highly data-driven or having a very limited physical insight, if at all. So, much effort is needed for quantifying the effect of pore structure on velocity complexity in rock physics for carbonate reservoirs.

As a special case of the Biot theory, Gassmann equation (1951) has been used to model velocity variation in consolidated and high-porosity sedimentary rock. But, a fundamental assumption in Gassmann equation is that the pore pressure needs to be equilibrated within a half cycle of a seismic wave. Because of the complex and multiscale pore systems in carbonate reservoirs, many researchers questioned the applicability of traditional Gassmann fluid substitution to seismic data.

Biot theory represents many theoretical advantages compared to other models in studying mechanical properties of porous media. It, however, does not consider cracks or fractures in a porous medium. This limits its application to rocks under lower differential pressures, especially for low-porosity rocks (Murphy, 1984, 1985).

By extending and generalizing Biot model, Sun and Goldberg (1997a, 1997b, 2000, 2004) introduced a rock physics model based on dynamical theory of fractured porous media. Meanwhile, a topological characterization of structural media that provides the features of internal structure of a fractured porous medium was used in this model, which quantitatively interpreted the causes and effects of structural complexity in carbonate rock pore space on velocity variations. In this model, Sun (2000, 2004) defined elastic parameters called frame flexibility factors and these frame flexibility factors depend less on porosity than wave velocity does. Based on these studies, these parameters are not only related to pore structure but also to solid/pore connectivity and grain size, which has been used for quantitative carbonate pore type analysis and classification (Bracco Gartner et al., 2006; Eberli et al., 2006; Weger et al., 2009). Some formula simplified by Sun (2000) from this model as the followings:

Let Vp and Vs be the compressional and shear wave velocity, respectively. Let ρ be bulk density. K and μ be bulk and shear modulus, respectively. Then, we have

$$V_p = \sqrt{\frac{K + \frac{4}{3}\mu}{\rho}} \quad \text{.....1.5}$$

$$V_s = \sqrt{\frac{\mu}{\rho}} \quad \text{.....1.6}$$

where

$$\rho = (1-\Phi)\rho_s + \Phi\rho_f \quad \text{.....1.7}$$

$$K = (1-\Phi)K_s + \Phi K_f \quad \text{.....1.8}$$

$$\Phi_k = F_k \Phi \quad \text{.....1.9}$$

$$F_k = \frac{1-(1-\Phi)f}{(1-(1-\Phi)f)\frac{K_f}{K_s} + (1-\frac{K_f}{K_s})\Phi} \quad \text{.....1.10}$$

$$\mu = \mu_s(1-\Phi)^{f_\mu} \quad \text{.....1.11}$$

$$f = 1-\Phi^{\gamma} \quad \text{.....1.12}$$

$$f_\mu = 1-\Phi^{\gamma_\mu} \quad \text{.....1.13}$$

where ρ_s, K_s, μ_s, ρ_f, K_f, $\varnothing$ are solid matrix density, solid matrix bulk modulus, solid matrix shear modulus, fluid density, fluid bulk modulus and porosity, respectively. f, f_μ, γ, γ_μ are frame flexibility factors. "γ" parameter is not only independent on porosity but also related to pore connectivity so that it has been used to evaluate permeability in carbonate reservoir as well (Bracco Gartner et al., 2006; Eberli et al., 2006; Weger et al., 2009).

This poroelasticity model has been successfully proven at the core-plug scale by measured core data for its effectiveness in quantifying pore structure (Sun, 2006).

Petrophysical data calibrated by core measurement and thin section analysis, has been widely used to evaluate pore type complexity in carbonate reservoirs (Schlumberger, 1974; Meese and Walther, 1967; Brite et al., 1985; Lucia, 1983;

Anselmetti and Eberli, 1999; Sun et al., 2000, 2003, 2006), however, no reports were published about how to apply 3-D seismic data to characterize carbonate reservoir properties based on rock-physics model analysis. Only Bracco Gartner et al. (2005) reported a successful field study by combining rock-physics model introduced by Sun (2000) and post-stack seismic data to evaluate carbonate reservoir pore types and further predict average interval matrix permeability in Middle East oil field. This rock physics model has subsequently been referred to as the Sun model by Shell Oil Company and others.

Sun (2006) also found that carbonate rocks of different pore types with similar porosity have different AVO response. For the samples with different pore types, their seismic and AVO response results in not only different critical angle but also different reflection coefficient variation. This implies that we might get more accurate evaluation of pore type variation and prediction of high permeability zones in carbonate reservoirs from pre-stack seismic data than that from post-stack seismic data. However, no papers have been reported on this important pre-stack seismic study for pore type evaluation, which is among my major research work in my dissertation.

DATABASE

The datasets include core data, petrophysical analysis results, log and seismic data in a Upper San Andres reservoir, Permian Basin, west Texas, USA. The seismic survey used in this studied field covers an area of 104 km^2. The seismic volumes consist of a zero-phase post-stack 3D time migration volume as well as several calculated multi-trace

seismic attribute volumes such as maximum positive curvature, maximum negative curvature and coherence from the zero-phase volume as input. For the producing Upper San Andres Formation, over 270 feet of whole core intervals are available from two wells drilled through this interval. Core descriptions and photos and petrophysical data, including 60 full-diameter core porosity and permeability measurements, are available for each well. We also have twelve full digital suites of well logs including spectral gamma, neutron porosity, density, sonic, caliper and resistivity logs. Production data from the producing wells and pumping test reports were also available. The core images provide us information about reservoir lithology, rock texture and visible vuggy pore space.

The second reservoir to be studied is the ChangXing reservoir, Sichuan Basin, Southern China. The reservoir depth is about 7 km below the surface which is one of the few ultra-deep carbonate reservoirs discovered in the world.

There are much abundant data available in this reservoir. Not only poststack but also prestack seismic data volume is available. Separate angle-stack seismic data volumes are also available, having three angle ranges of 0-8 °, 8-16 ° and 16-24 °. For each well, conventional and dipole well logs are available including caliper, resistivity, SP, GR, AC, neutron porosity, sonic and Vs logs. Some petrophysical analysis and core measurement results including porosity, water saturation, mineral composition volume, core description, core physical properties (porosity, permeability and density), thin-section and mercury capillary analysis in cored interval have also been made available to us. Compressional and shear ultrasonic velocity measurement and thin section analysis

of 34 core samples will be conducted to evaluate sonic velocity and pore type relationship in a direct method. The effective pressure is varying for velocity measurement, which simulates reservoir condition.

In addition, much published work about this two studied fields help us to understand regional and local conditions of the studied reservoirs. The combination of these various data volume provides a rare opportunity to conduct an integrated study of the subsurface carbonate reservoir porosity and pore structure heterogeneity.

METHODS

A rock-physics model based approach by integrating geological, lab measurement, petrophysical and seismic data will be used to characterize carbonate reservoir porosity and pore type heterogeneity in order to better predict reservoir quality. The schematic framework of this research is indicated in Figure 1.1. The detail information of methods applied in this study would be discussed in the later chapters.

DISSERTATION STRUCTURE

Depositional facies, mineral composition and diagenetic events after carbonate rock deposition are the major controlling factors on reservoir porosity and permeability. So, reservoir geological features study was conducted so as to estimate geological factors affecting the reservoir quality, pore types variation and development of high-permeability zones by combing the core-description, petrophysical and post-stack seismic acoustic impedance data volume and summarized from previous studies.

Lab measurement data, including rock porosity, permeability and acoustic velocity, are the most accurate methods to study rock physical properties. Thin section analysis will be used to estimate reservoir mineral composition, pore type and diagenetic features. By using ultrasonic velocity measurements on core samples, velocity-porosity complexity resulting from pore type changes could be better understood, which can be used to calibrate petrophysical data analysis as well.

Forward-model-based seismology study is helpful to evaluate the feasibility for inversing γ parameter from prestack seismic data The AVO response difference caused by pore type variation will be evaluated by building two layers forward and solving Zoeppritz wave equation.

3-D seismic data is the best approach to characterize porosity and pore-type heterogeneity calibrated by geological and petrophysical data. From pre-stack and post-stack seismic inversion, several conventional impedance and AVO parameter data volumes could be extracted, including the acoustic impedance, elastic impedance (Connolly, 1999), shear impedance. Using rock physics model as bridge, impedances would be connected with reservoir porosity and pore structure indicating parameter (γ). Permeability heterogeneity evaluation would be conducted by integrating porosity and pore structure indicating parameter (γ) study.

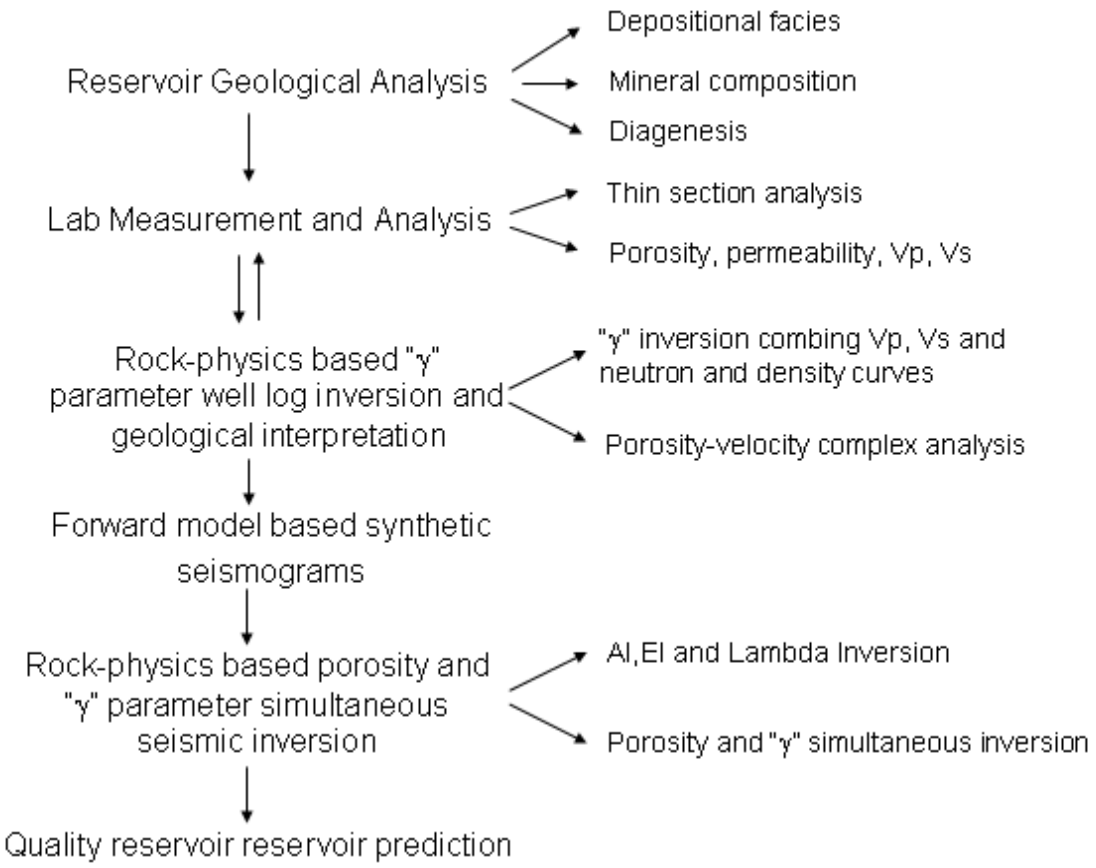

Figure 1.1 Schematic Framework of Research

CHAPTER II

PALEOKARST SYSTEM DEVELOPMENT IN THE SAN ANDRES FORMATION, PERMIAN BASIN, WESTERN TEXAS, USA, REVEALED BY SEISMIC CHARACTERIZATION

OVERVIEW

Paleokarst system is one of major factors resulting in carbonate reservoir heterogeneity and compartmentalization, however, it is huge challenge for geologist and geophysicist to detect and characterize its 3D distribution due to the lack of appropriate methods and limited data. A detailed seismic characterization approach integrating core, well log and rock physics analysis was proposed to reveal a complex subsurface paleokarst system in the San Andres Formation, Permian basin, West Texas. In the area of high volume production, the collapsed paleokarst system is characterized by irregularly developed crackle and fracture breccias, mosaic breccias and cave fillings in the Upper San Andres Formation, which are delineated from seismic acoustic impedance. The transition from platform to basin is marked by a linear collapse with occurrences of sags and small vertical faults that are recognizable in seismic imaging. Production data indicates that tight paleokarst zones consisting of karst-controlled collapsed features of different sizes and patterns cause reservoir compartmentalization and influence fluid communication between wells. The complex paleokarst system development is explained using a carbonate platform hydrological model, similar to modern marine hydrological

environments within carbonate islands. Our method of modeling development for complex subsurface paleokarst systems may be applicable to other paleoenvironments.

INTRODUCTION

Karst systems develop on emergent portions of carbonate platforms or islands whenever the platform is subaerially exposed in hot and humid conditions for significant time periods. The level of exposure is controlled by either eustatic or tectonic sea level change during geologic history (Mylroie and Carew 1995). As a result, karst regions usually develop interconnected cave systems with a significant thickness as seen in the modern karst terrain analogs. The paleokarst features preserved in the stratigraphic record are usually collapsed paleocave systems, which may be further complicated by later mechanical compression and diagenetic processes.

Paleokarst systems prove to be important hydrocarbon reservoirs in world class oil fields. Karst-controlled collapsed paleocave systems, whether subsequently filled or unfilled, are significant factors in the development of carbonate reservoir heterogeneity and compartmentalization. Additionally, fill sediment and collapse during burial may destroy most of the original cavernous porosity (Kerans 1988).

The detection and characterization of subsurface paleokarst environments present immense challenges for geologists and geophysicists (Hardage, et al. 1998; Dembicki, 1996; Sullivan, et al. 2006; Zeng, et al. 2006). Many examples of modern karst and paleokarst environments are discovered through the common and straightforward method of observing of outcrop exposures(Hayes, 1964; Kerans, 1988; Kerans, et al.

1994; Kerans and Fitchen, 1995; Kittridge, et al. 1990; Lucia, 1995; Loucks, 1999). However, subsurface paleokarst systems important for indicating ancient sea level fluctuation and predicting reservoir quality are less commonly reported due to lack of data and proper imaging tools.

Our case study addresses the aforementioned research challenges. Specifically, we focus on the east central flank of the Permian Central Basin Platform of West Texas. The San Andres Formation in this area experienced paleokarst development due to several periods of substantial subaerial exposure during the Guadalupian period. As a result, reservoir production from the Upper San Andres interval is highly variable, due in part to the fluid barriers created by anhydrite-cemented dolostones. We developed a method of identifying subsurface paleokarst systems by integrating core, well logs, seismic inversion and seismic 3D geometric attribute analysis. In this way, we obtained a detailed knowledge of the 3D distribution of the paleokarst system, which is essential for the optimized development strategies and enhanced hydrocarbon recovery. Our study of the associated reservoir indicates that the occurrence of the tight flow barriers is related to a fully developed paleokarst system with vertical and lateral spatial complexity. Using results from our seismic characterization, we further propose a carbonate platform hydrologic model to explain the development of this paleokarst system and its control on reservoir quality and compartmentalization.

GEOLOGICAL SETTING

The Permian Basin of southeastern New Mexico and western Texas has an area of ~115,000 mile^2 and consists of the Delaware basin to the east, the center basin platform in the center, and the Midland basin to the west (Fig 2.1 and French 2000). The Central Basin Platform is a complex uplifted block with world class oil and gas reservoirs on the platform and along its margin. Our study area lies on the eastern Central Basin Platform, Crane County, Texas (Fig.2.1).

The Permian basin underwent several stages of tectonic movements including uplift, sedimentary basin fill, and compressional tectonics related to the Marathon-Ouachita Orogeny, as well as a second period of quiescence associated with basin subsidence (Hills 1970, 1972, 1984; Keller et al. 1980; Yang and Dorobek 1995; Adams and Keller 1996). The interior structural configuration of the Permian Basin was established by the early Permian period (Hills 1970; Keller et al. 1980). The major filling stage of the basin is from Cambrian through Triassic age. During the Guadalupian time, carbonate shelves developed and prograded into the basins. Guadalupian depositional environments varied from supratidal, to shallow intertidal, to high-energy ramp crest shoals, and to deep subtidal (Pranter 1999; French 2000; French and Kerans 2004).

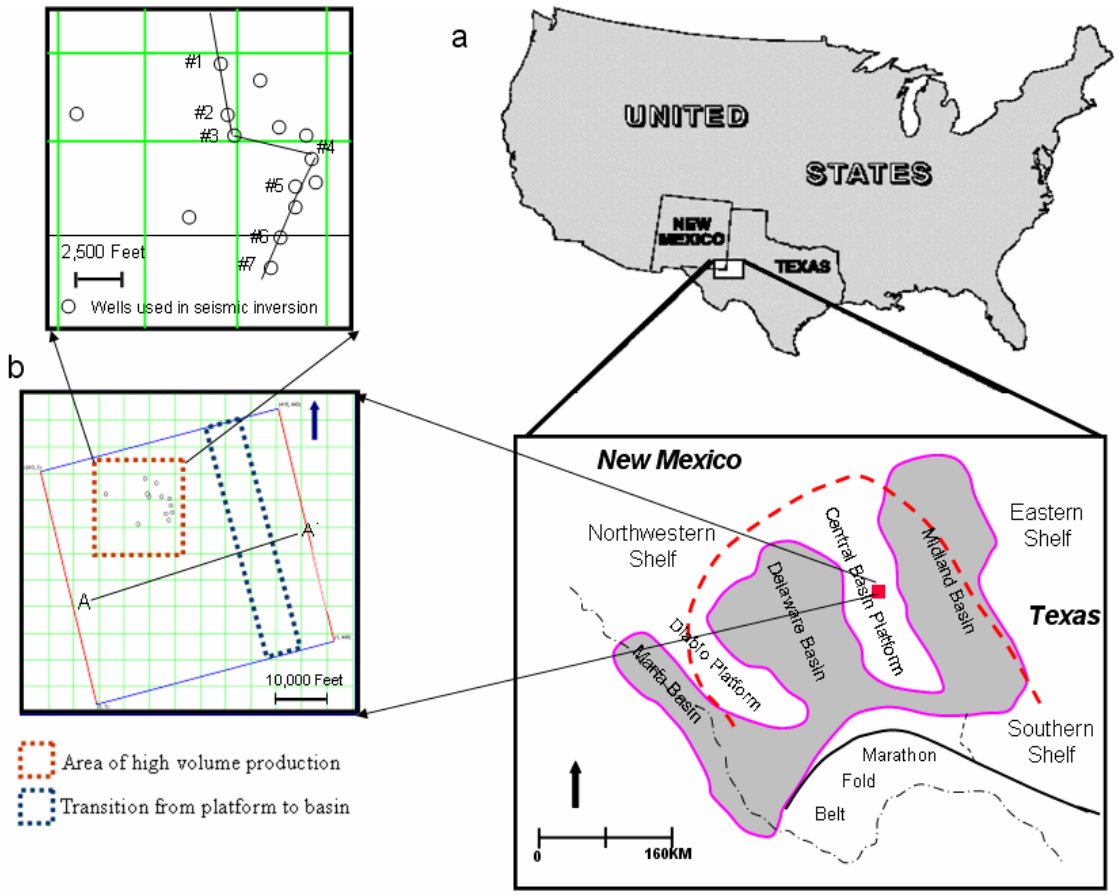

Figure 2.1 Location of Studied Field, Well Location and Seismic Survey, San Andres Reservoir, Permian Basin

During the Ochoan time, evaporate deposition dominated the Delaware and Midland Basins due to restricted marine conditions, basin filling, and an arid climate

(Hills 1970). By the end of Permian period, the Delaware and Midland Basins coalesced to form one large evaporative basin (Hills 1984).

Production in our study field occurs in the San Andres Formation which was deposited during the Guadalupian epoch (Kerans and Fitchen 1995; French 2000; French and Kerans 2004). Stratigraphicly, the San Andres Formation can be subdivided into two third-order composite sequences: the Upper San Andres and the Lower San Andres (Kerans and Fitchen 1995). The Lower San Andres consists of six fourth-order high frequency sequences (HFS), which include the Leonardian L7, L8 and the Guadalupian G1 through G4. The L7 and L8 HFS are a transgressive sequence set and the G1 through G4 HFS are an overlying highstand sequence set. The Upper San Andres consists of nine fourth-order HFS. The lower seven HFS, from G5 to G11, consist of basin-restricted, deep-water siliciclastic sediments, which often occurred during very low sea-levels and onlapped a regionally extensive unconformity at the top of the Lower San Andres (Kerans and Fitchen 1995; Gardner and Sonnenfeld 1996). The uppermost two HFS within the Upper San Andres composite sequence, G12 and G13, directly and unconformably overlie the top of Lower San Andres G4 on the Central Basin Platform (Kerans and Fitchen 1995; Gardner and Sonnenfeld 1996). In this research, we focus our study on the platform top and platform margin expression of the HFS G4 of the Lower San Andres and the HFS G12 and G13 of the Upper San Andres.

METHODS

An integrated seismic characterization method was used to delineate paloekarst system development in Upper San Andres Formation. The first steps in our integrated approach consists of identifying petrographic and rock physical features using available core data as well as interpreting paleokarst facies in the San Andres Formation in the 12 suites of well logs. With the understanding from core and the synthetics from logs, we perform the first iteration of conventional seismic interpretation to pick the key HFS in the zero phase volume. Identification and correlation of the amplitude data with the paleokarst facies recognized from cores and logs proved difficult. Next we transformed our amplitude volume into the impedance domain through an inversion process in order to upscale our observations from wells and cores. Compared to the conventional seismic interpretation, seismic inversion can transform the seismic reflection data into quantitative estimations of rock properties (Buenafama and Gibson 2004). When compared to conventional seismic reflection data, post-stack acoustic impedance, a widely used seismic inversion approach, provides more detailed and accurate insights into the lithology, fluid types and porosity features of a reservoir. In this study, we perform model-based seismic impedance inversion to determine the distribution of the paleokarst system. The original forward model was built from the well logs and the horizons picked in the first iteration of seismic interpretation. The tight paleokast zones are more recognizable in the impedance volume and correlate well with the fluid barrier recognized from production data. Production data analysis results were used to evaluate the influences of tight paleokarst zones on the interwell fluid communication.

Geometric seismic attributes, including coherence and multispectral curvatures, helped detect macro-scale collapsed paleokarst in the transitional section between the carbonate platform and basin where well log and core data were not available. Unlike inversion attributes, geometric attributes such as curvature and coherence are calculated from the aggressive comparisons of the geometrical property of a target trace with nearby neighboring traces in a sliding analysis window. The geometric seismic attribute analysis is an independent and powerful tool for the qualitative and quantitative mapping of subsurface geological features in siliciclastic, carbonate, and volcanic reservoirs, and forms an integral part of most interpretation work (Chopra and Marfurt 2008).

By integrating previous empirical experiences from analogs, outcrops and the subsurface with the seismic paleokarst features within the San Andres Formation, we propose a conceptual hydrological model to explain the driving mechanism of the evolution of the collapsed paleokarst systems in the study area. We think that this model is also applicable to other fields with similar geologic settings and thus provides a conceptual tool to help interpreters to infer the reservoir properties for exploration.

RESULTS

Core from well #1 drilled through the upper San Andres Formation in the study area contains lithologies and fabrics in the top 35 feet of cored interval that indicate multiple karst overprinting events on the fine dolomudstone and dolowackstone lithofacies as evidenced by cave fill, collapse breccia, and mosaic/fracture breccia (Fig.2.2, modified from the core description report of study field, Burlington/Schlumberger IPM, 2003).

Vertically, several cycles of brecciation and clastic fill are repeated in the interpreted paleokarst interval.

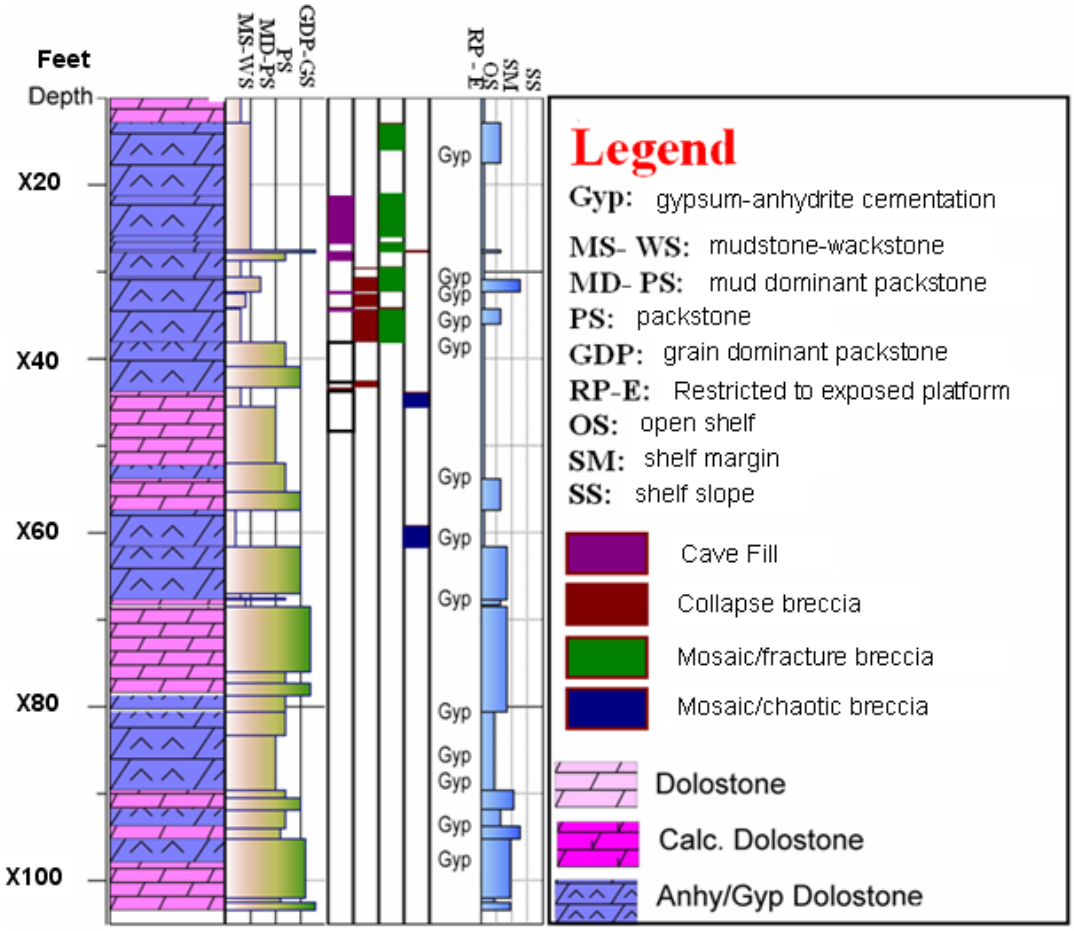

Figure 2.2 Lithological Column of Cored Interval in Well #1, Paleokarst Events Developed in the Top 35 feet in the Upper San Andres Formation (Modified from description report of study field, Burlington/Schlumberger IPM, 2003)

All of the collapsed paleocave facies proposed by Loucks and Mescher (2001), except the Fine Chaotic Breccia Facies, can be interpreted in the paleokarst interval of well # 1 based on key textures, fabrics and structures. The core photos shown in Figure

2.3, from the uppermost 1.5 feet of the Undisturbed Strata Facies, illustrate excellent bedding continuity in the gray dolomudstone. The middle 8 feet of the core can be assigned as paleocave filling facies, including the Coarse-Clast Chaotic Breccia Facies and Sediment-Fill Facies. The Coarse-Clast Chaotic Breccia Facies are composed of poorly sorted, granule- to boulder-size dolomudstone and dolopackstone clast. The chaotic breccias represent extensive displacement, rotation and deformation of the host rock, however, original structures, including laminae, bioturbation, burrows and skeletal material are still evident in the clastic breccia. In the Sediment-Fill Facies, the main lithology is brown siliciclastics that probably record infiltration from an exposure-related sabkha environment. Several thin layers of mosaic breccia, assigned to the Highly Disturbed Strata Facies of cave roof and cave wall, are also present in this interval. In the bottom 1.5 feet, the Disturbed Strata Facies is indicated by the presence of crackle breccias and soft sediment deformation features. Intensive cavernous dissolution is suggested by the large clasts that appear to "float" in the blue anhydrite.

Pore space related to paleokarst events include the cavernous pores, interclast pores, crackle and mosaic breccia fractures. However, except for few open fractures stained by oil, most of the matrix porosity, original collapse fractures and dissolution pore-network are occluded by anhydrite cementation. Open fractures are related to younger, possibly Laramide age fracturing of the anhydrite cemented breccias (Lorenz, et al. 2002). The pervasive secondary cementation by anhydrite may be in large part responsible for the development of "tight" karst zones in the Upper San Andres Formation. Compared with well #1, anhydrite cemented breccias are about twice as thick

in the upper San Andres of the second cored well, but appear to represent similar fabrics and events as observed in well #1 (from the core description report of study field, Burlington IPM, 2003) . This difference in thickness suggests irregular lateral distribution of these paleokarst passages.

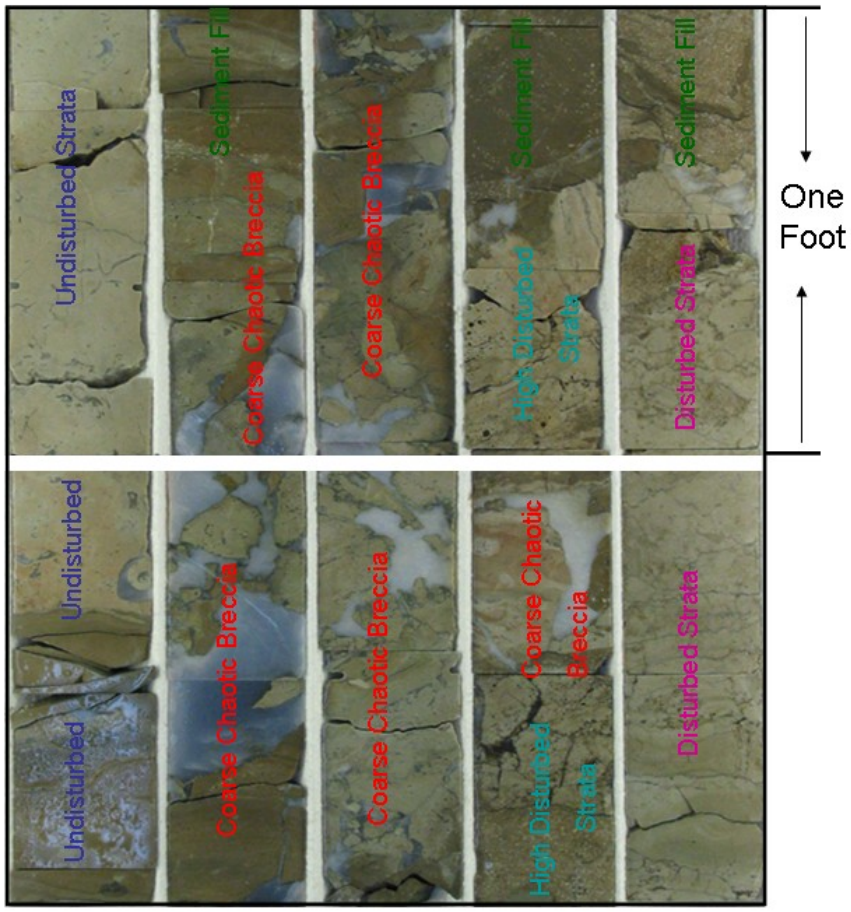

Figure 2.3 Paleokarst Facies Interpreted from Core Photos from X 5 to X15 feet

In the cored wells where paleokarst intervals are identified, well log data are used for the log signatures of the "tight" paleokarst zone. The paleokarst zones have anomalously high velocity, high bulk-density, high resistivity and low neutron porosity when compared with the lower non-paleokarst zones. The average neutron porosity in paleokarst zones is lower than 5%; however, it is between 5 % and 25% in the non-paleokarst zone. The average velocity and bulk density are higher than 6.0 km/s and 2.75 g/cm^3 respectively, for the paleokarst zones calibrated by core description (see Figure 2.4). Compositional analysis by combining the bulk density and photoelectrical curves shows that the volume percent of anhydrite in the formation is around 20% (Figure 2.4), which may explain the high velocity and high bulk density in paleokarst zones. Because there were few open, big caves in the target interval, no apparent excursion occurred on the caliper curve.

Figure 2.5 shows the cross-plot of bulk density and transit time log data in the cored interval, in which the pink points are from paleokarst zone and other points are from non-paleokarst zones. It could be found that the bulk density for non-paleokarst zones is lower than 2.75 g/cm^3 and Δt is higher than 50 us/feet. From the cross-plot, the cutoff value of the acoustic impedance (AI) for the paleokarst zones is established as >57000 (FT/S)*(G/CC), which is used to differentiate the tight paleokarst zones from seismic acoustic impedance data volume quantitatively.

The distinctive petrophysical difference between anhydrite-filled paleokarst zones and the non-karst zones revealed by log data enables us to use seismic impedance

inversion to delineate the lateral and vertical distribution of the paleokarst zones in the study area.

For the area of HVP, the model-based seismic inversion is performed, which can transform the reservoir information contained in conventional seismic data into a recognizable and quantitative reservoir description parameter.

Model based inversion is done by minimizing the error between a forward model and real seismic signal (Buenafama and Gibson, 2004; Xu, et al. 2006). Generally, the forward geophysical model is built from the reservoir stratigraphy and synthetic information which are crucial to seismic inversion. Figure 2.6 is the synthetics of Well #5, which demonstrates a good match with the real seismic response. Figure 2.7 is a conventional seismic section and Figure 2.8 is its acoustic impedance section in south-north direction. Compared with Figure 2.6, the tight karst zones with high acoustic impedance are revealed clearly in Figure 2.8 (pink areas). The tight paleokarst areas close to the top of the San Andres Formation are extensive with widely variable thickness. For example, Well #3 shows the thickest karst interval of 110 feet. In adjacent Well #2, however, the karst is as thin as 20 feet. This acoustic impedance section also illustrates that the distribution of the tight karst zone follows the paleotopographic trend. Thick paleokarst zones occur on the high paleotopographic positions where the exposed carbonates experienced relatively longer and stronger karst-processes than other places. As the paleotopography declines from the north to the south and east, the paleokarst processes are weakened.

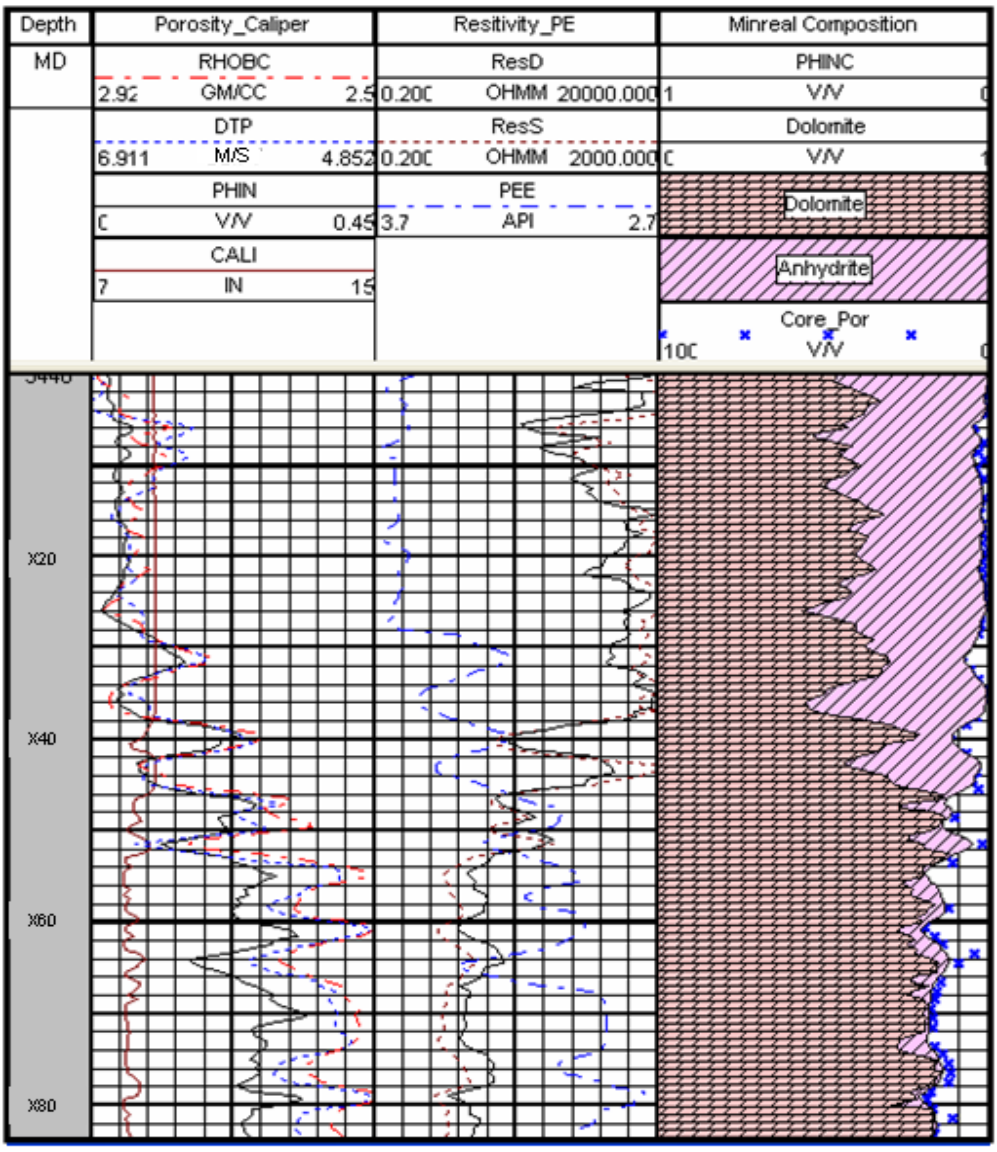

Figure 2.4 Composite Well Log Curves of Well #1 within Upper San Andres Formation

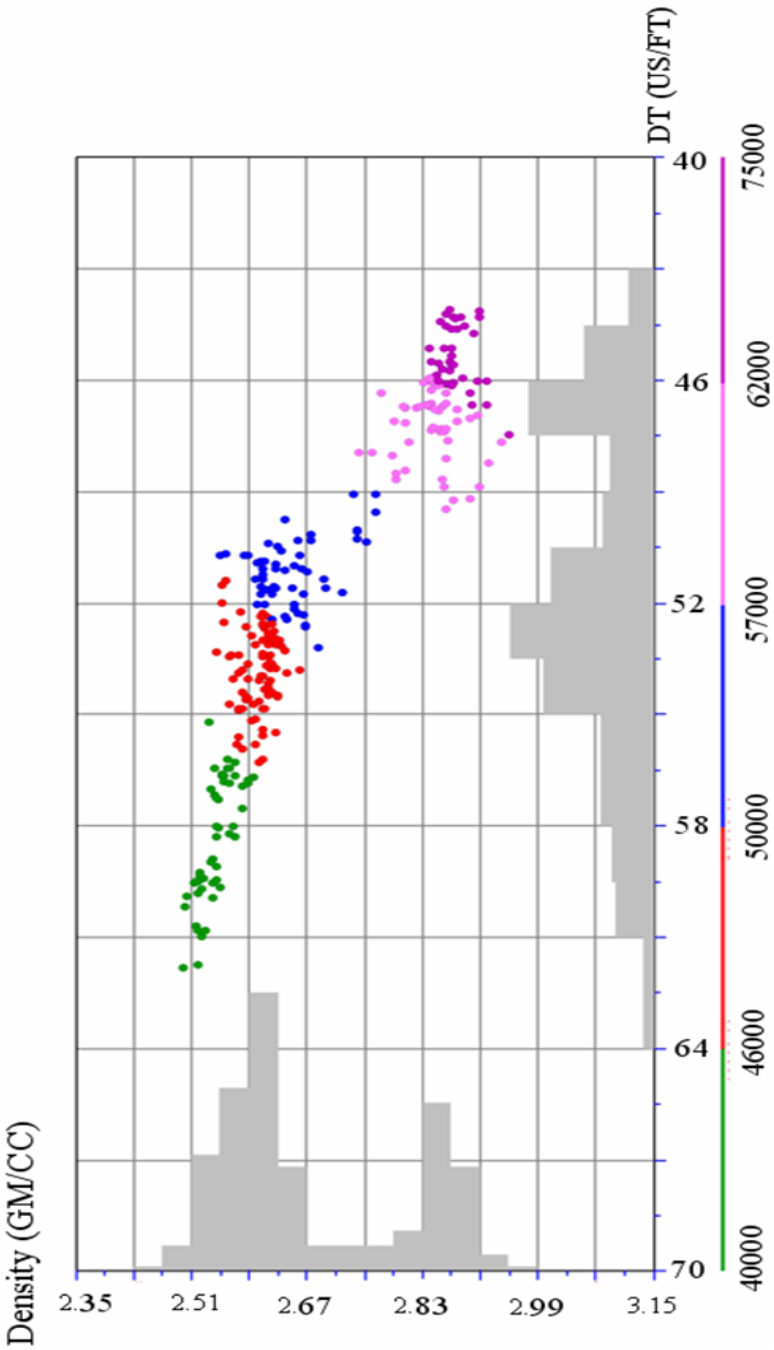

Figure 2.5 Bulk Density and Slowness Crossplot with an Acoustic Impedance Color Bar

In contrast to the HVP area where core and log data are available and seismic inversion can be used to determine the fine-scale paleokarst systems, seismic imaging and geometric attribute analysis are used to determine the large-scale collapse paleokarst systems along the transition from platform to basin where no core and log data are available. In seismic, karst-controlled collapses are characterized by distinctive sags and multiple small faults (Fig. 2.9). Figure 2.9 demonstrates that a collapse event can extend from G3 HFS through G4 HFS and into the upper San Andres Formation, having a vertical height of about 500 feet. In order to delineate the lateral extension of this macro-collapsed paleokarst system, 3-D coherence and negative curvature data volumes are calculated. Figures 2.10-2.11 show the coherence and negative curvature slices along the top of G4 HFS. Features having low coherence and negative curvature are interpreted as collapsed paleokarst zones. This reveals the linear distribution of a paleokarst system parallel to the platform margin. This huge collapsed paleokarst system extends from the south to the north across the entire seismic survey.

DISCUSSION

The development of a collapsed paleokarst system can be caused by many geological processes, including subaerial exposure, cavern collapse, hydrothermal brecciation and dissolution, tectonic movement or a combination of these processes (Berger and Davies, 1995; Mylroie and Carew, 1995; Loucks, 1999). Building a correct geological model for karst events requires Identification of the dominant processes for a given paleokarst system.

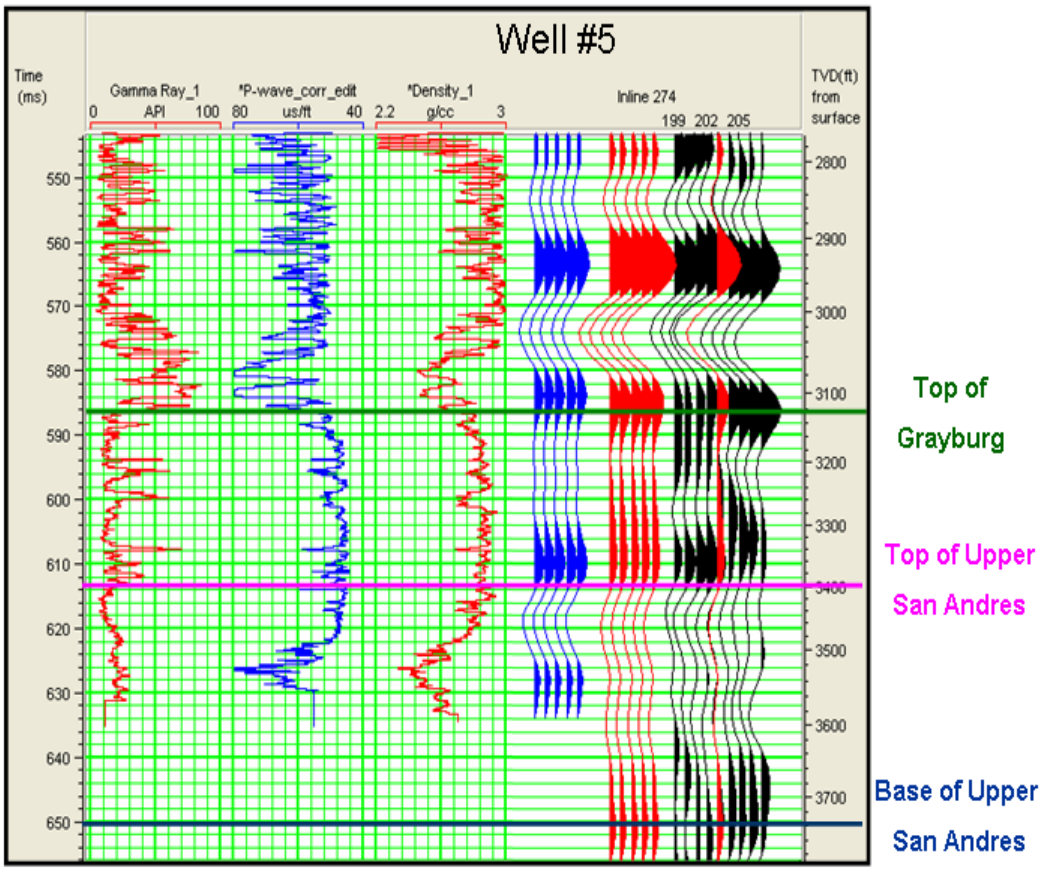

Figure 2.6 Synthetics of Well # 5 within Supper San Andres Formation

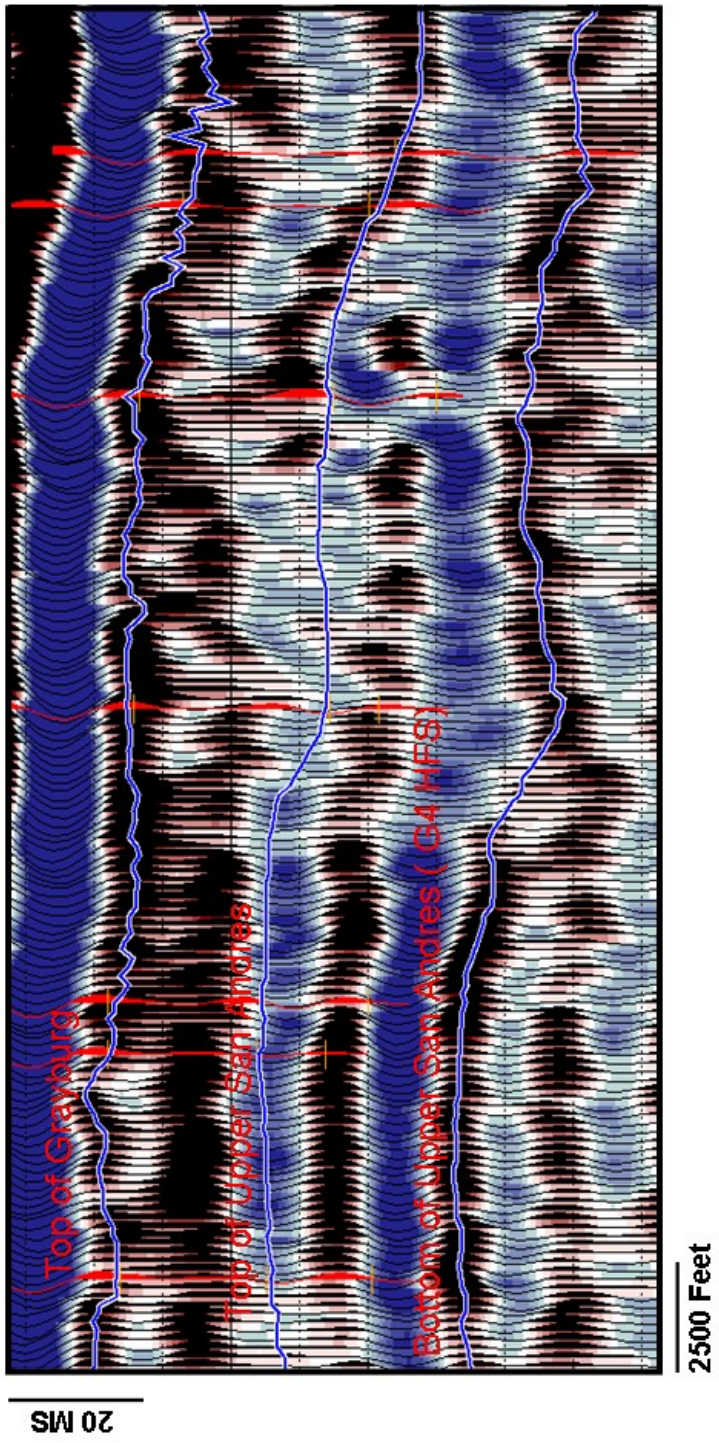

Figure 2.7 Arbitrary Seismic Section across Well #1 through Well # 7 with Synthetics of Each Well Overlapped

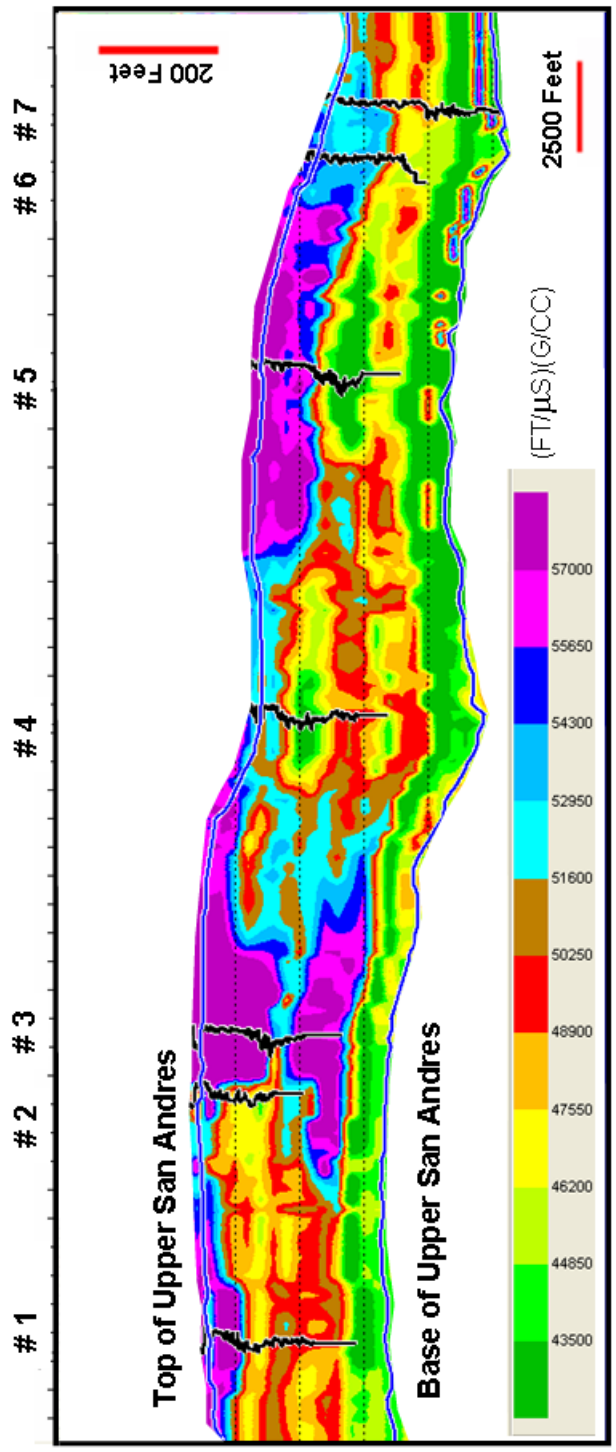

Figure 2.8 Arbitrary Acoustic Impedance Section across Well #1 through Well # 7 with P-wave Velocity Curve f Each Well Overlapped

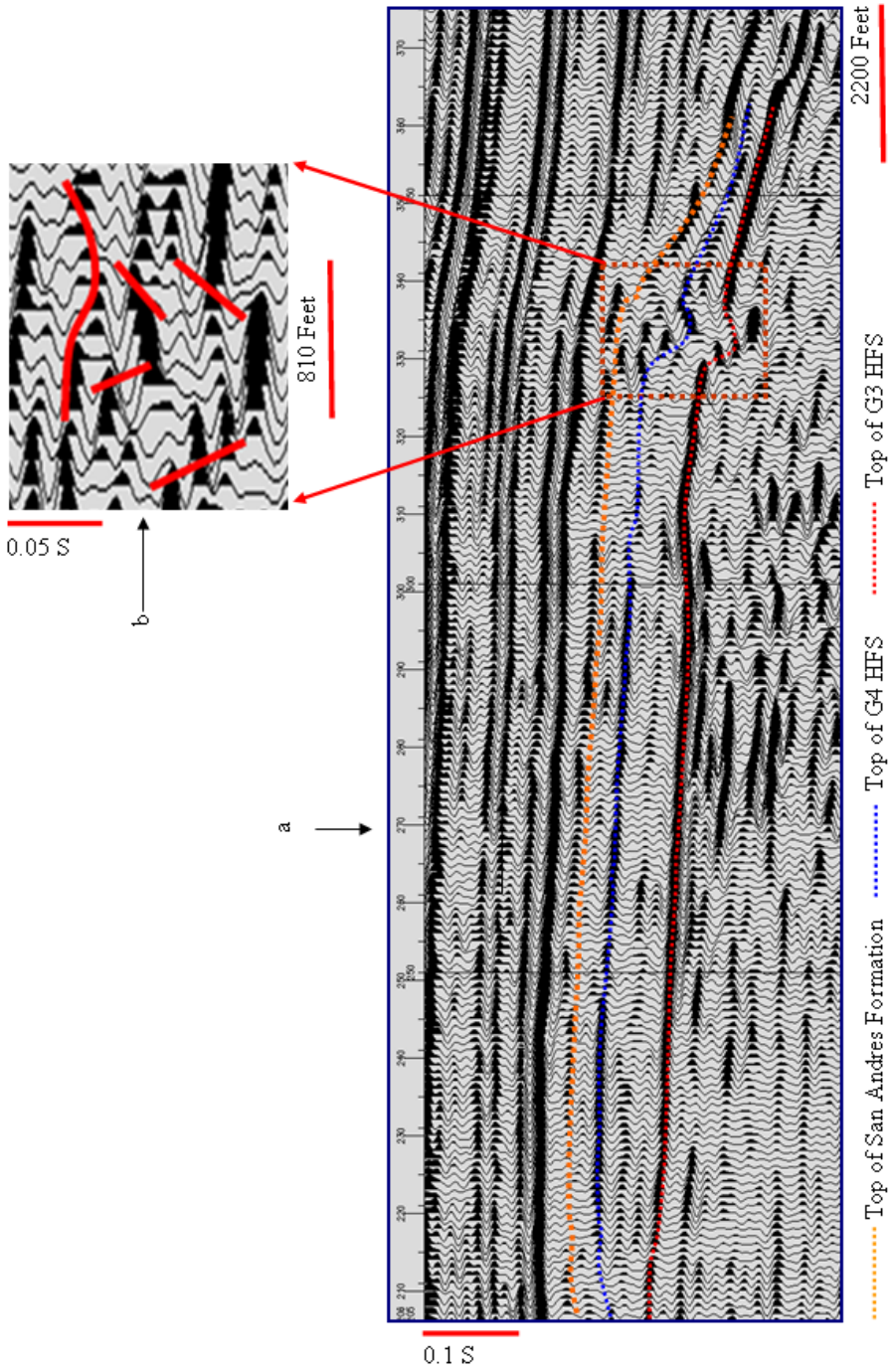

Figure 2.9 Seismic Section Representing Paleokarst Events along Transition from Platform to Basin

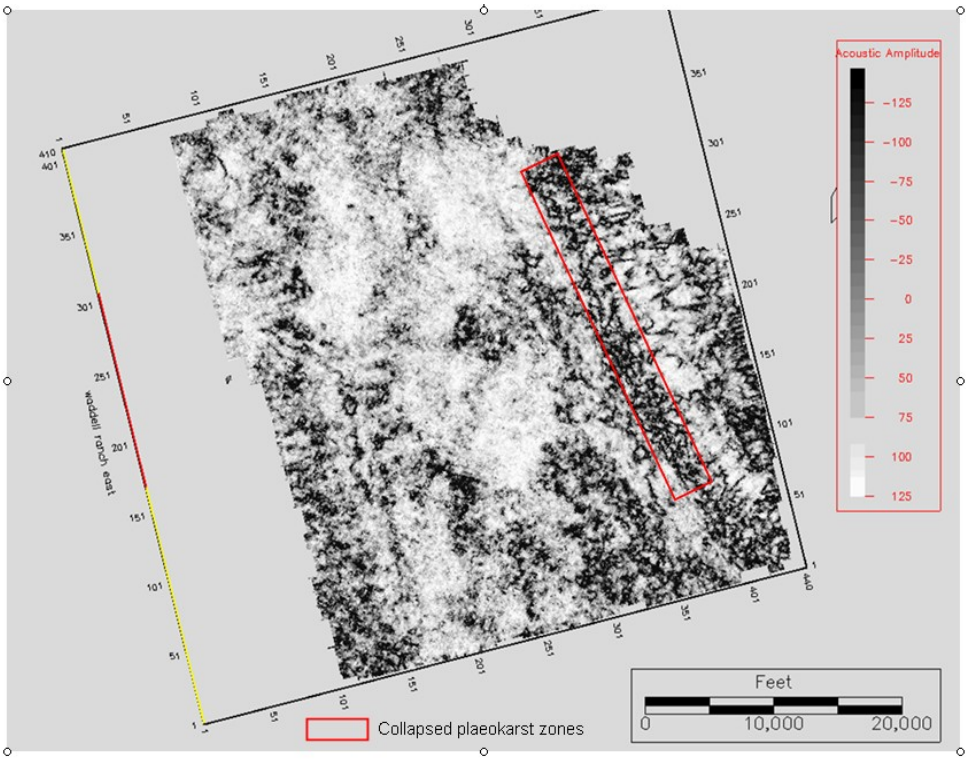

Figure 2.10 Coherence Slice along G4 HFS

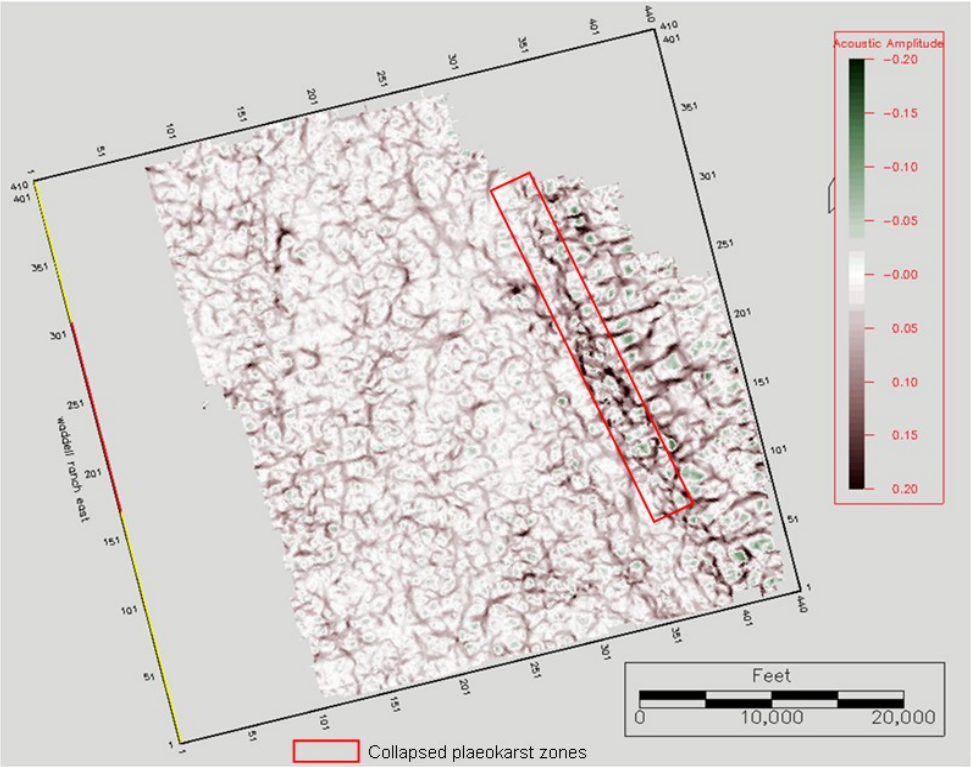

Figure 2.11 Curvature Slice along G4 HFS

From our study of the regional geology, we knew that the overall configuration of the Permian Basin was tectonically established by the early Permian period and experienced a period of structural quiescence during San Andres Formation deposition. The lack of large offset faults through the San Andres Formation in seismic also suggests tectonic stability during the Guadalupian period. Major changes in San Andres strata in the study area may be related to variation in the hydrological environments from the Central Basin platform to the Midland Basin.

The karst development model for carbonate islands in an oceanic realm, as studied by Smart and Whitaker (1993), illustrates a complicated hydrological environment consisting of the Vadose zone, Phreatic zone and Halocline or mixing zone. Based on hydrological characteristics typical of carbonate platforms, an island hydrologic model (Craig, 1988) is used to explain karst events and the subsequent development of karst associated features. Using conditions of Quaternary carbonate settings, Mylroie and Carew (1995) further tested the validity of this model and predicted that numerous similar subsurface paleokarst events have occurred within carbonate islands during their geological history.

Our analysis and seismic characterization results lead us to propose a carbonate platform hydrological model as the development mechanism for karst systems in our study area. Our model is similar to the island hydrologic model. In the area of HVP, slightly acidic meteoric water entered the Vadose zone through preexisting fractures or crackles and produced pit caves. These pit caves show varying depth depending on vertical extension of the existing joints and fractures. Consequently, the collapsed paleokarst packages created during the later burial also show varying thickness, as illustrated in the seismic inversion section.

Why do the study area paleokarst packages show a more extensive distribution laterally in the HVP area than that of most modern karst-controlled cave packages? Later burial and mechanical compression processes may account for this difference. Based on the coalesced collapsed-paleocave system model proposed by Loucks in 1999, multiple isolated karst-forming episodes can be connected and combined into paleokarst systems

hundreds to several thousand meters long in the later burial processes. This coalescing has been proven in our study.

According to the carbonate platform hydrological model, large dissolution voids called flank margin caves are produced. These flank margin cave systems are prone to be in the discharging margins of the freshwater lens where the freshwater and saltwater mix, increasing the dissolution potential (Plummer, 1975). Compared to the Vadose waters that existed in the partially exposed interior platform area, more chemically active mixing zone waters could created larger dissolution caverns and collapsed structures that underwent later mechanical compaction, as shown in Figures 2.10. After karst dissolution and collapse processes, later diagenesis, including gypsum or anhydrite cementation would further modify the original pore spaces. Figure 2.12 is a conceptual model for karst events within study area.

Paleokarst system development can be an important factor in controlling carbonate reservoir heterogeneity. It can either benefit or degrade the reservoir quality. The intense post-karst anhydrite cementation dramatically occluded the original depositional and secondary karst associated pore space as well as reduced connectivity within the reservoir. Core measurements showed average porosity and permeability of the San Andres within paleokarst zones to be lower than 2% and 1 MD, respectively. These conditions are referred to as the tight karst zone (Fig 2.13). For quality reservoir without paleokarst influence, their porosity and permeability are higher than 10% and 30 MD. The paleokarst system probably contributes to highly variable fluid production. Oil

and gas recoveries for wells in and adjoining area of HVP vary from 1MM BOE to 100 M BOE per well (Nissen, et al. 2008).

The operator-interpreted tracer and pressure data also support our interpretation that the anhydrite occluded paleokarst system is a dominant factor controlling carbonate reservoir compartmentalization in the HVP portion of the study area. Fluid barriers can be correlated to high acoustic impedance areas by comparing the production data analysis and seismic inversion results. Figure 2.14 is the acoustic impedance slice at 12ms below the Upper San Andres. Figure 2.14 demonstrates that two low acoustic impedance zones (green and yellow areas) are separated by one high impedance zone (pink area), which represents reservoir area and paleokarst area, respectively. There are two reservoir areas; one between wells #1 and #2 while another is around well #4. Paleokarst areas in the middle of HVP extend from the northwest to the southeast. Based on the production data analysis (Nissen, et al. 2005, DOE research report), two engineering-based reservoir compartment boundaries (blue curves) existed between #2 and #4. From acoustic impedance slice, we can see that these two boundaries are mainly created by the tight paleokarst areas characterized by high acoustic impedance and low porosity. The compartment created by tight paleokarst areas blocks fluid communication between these two wells. Nevertheless, well log and production data are needed to quantify the influence of the flank macro-collapsed paleokarst system on reservoir production performance.

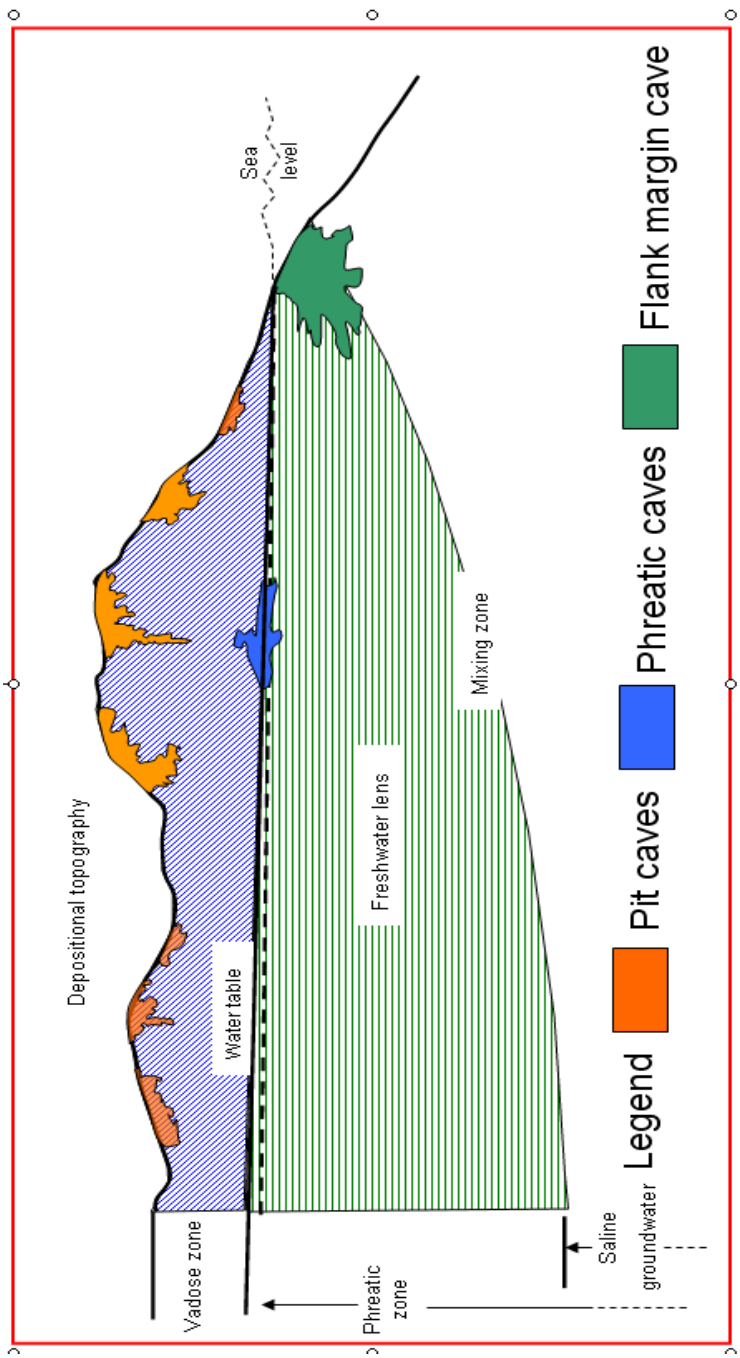

Figure 2.12 Concept Model Explaining Paleokarst Development on Carbonate Platform

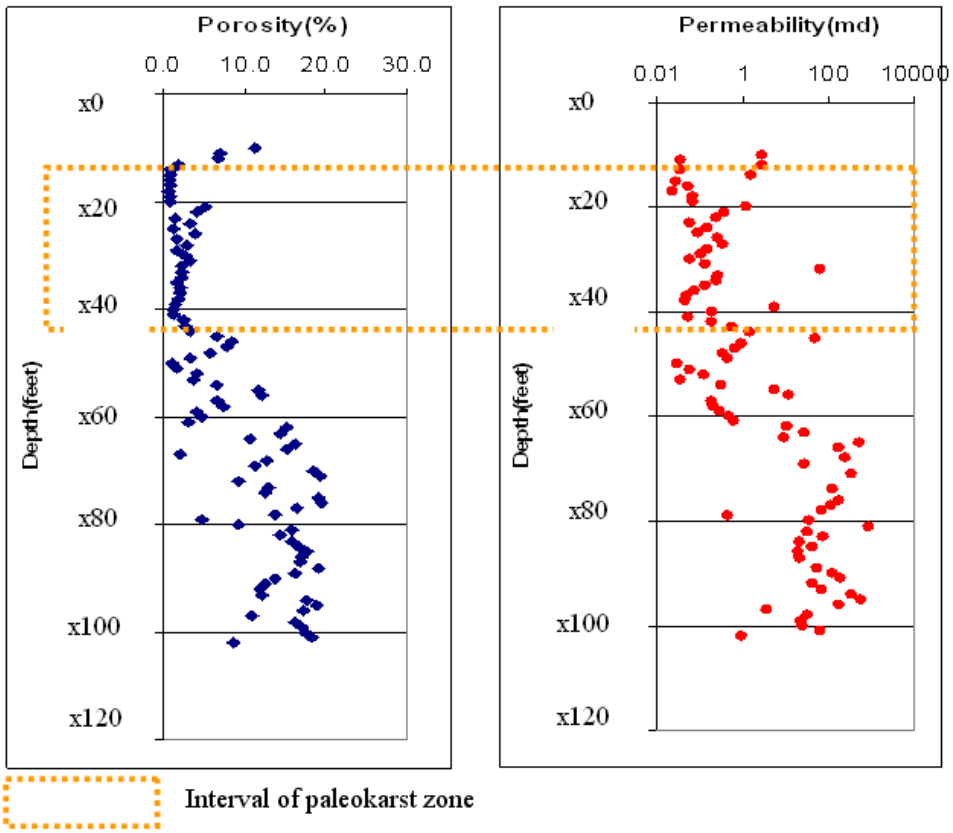

Figure 2.13 Porosity and Permeability Variation with Depth in Cored Interval, Well #1

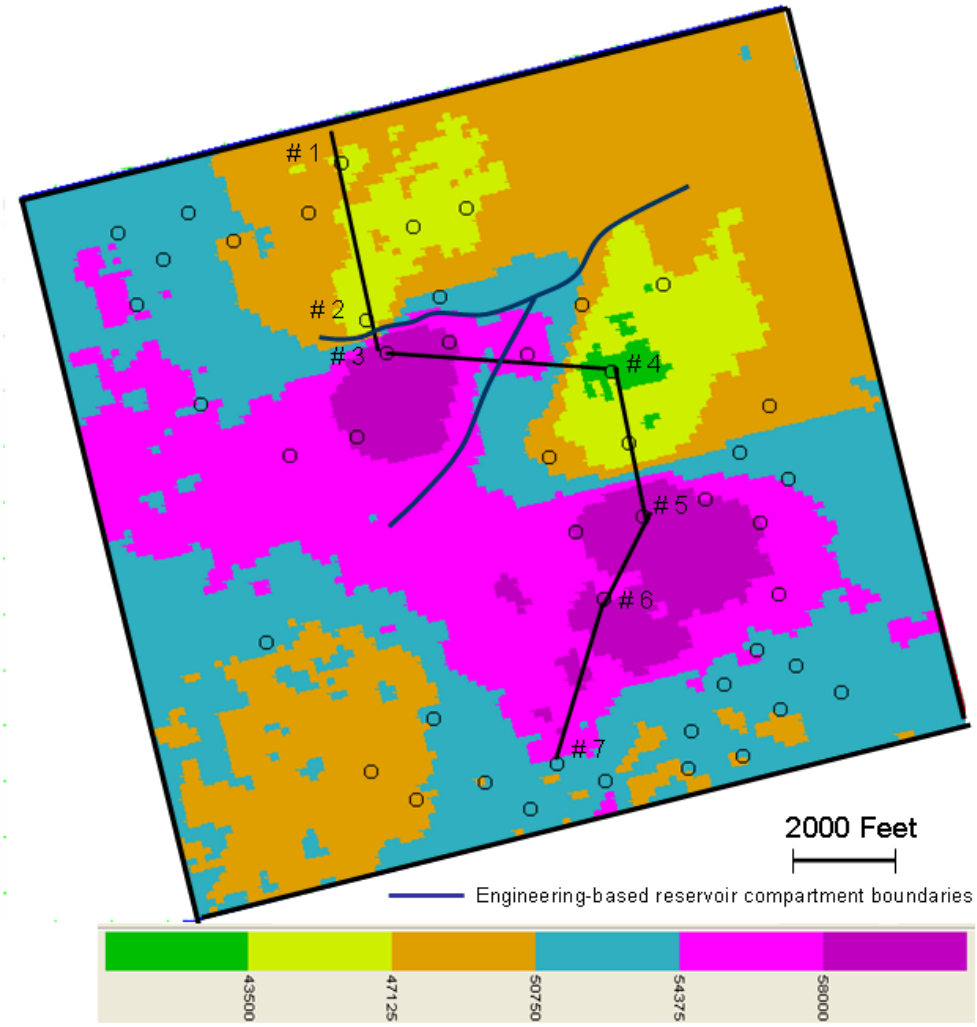

Figure 2.14 Acoustic Impedance Slice at 12ms Below the Top of Upper San Andres Formation, and Blue Lines is the Engineering-based Reservoir Compartment Boundaries

CONCLUSIONS

We propose an integrated method to identify paleokarst systems by combining core and log, seismic inversion and 3-D geometric attribute analysis. This method enables us to delineate the 3-D distribution of the collapsed paleokarst system observed in the study field as well as determine its influence on reservoir compartmentalization. The tight, fine-scale collapsed paleokarst system developed in the area of high volume production exhibits higher acoustic impedance compared to non-paleokarst zones, which have lower more uniform porosity development. The model-based seismic inversion method is thus a useful tool to characterize the vertical and lateral extent of this paleokarst system. For large-scale collapsed paleokarst systems, seismic geometric attribute analysis is a good tool to map its 3D spatial distribution. The proposed carbonate platform hydrological model explains the development of the paleokarst complex system detected in the San Andres Formation. Based on our analysis, it is expected that a collapsed paleokarst system, similar to the Upper San Andres Formation studied here, should also develop in the structurally high area of the lower San Andres Formation, G3 and G4 HFS. Our method may be useful in determining the occurrence and interpreting similar subsurface paleokarst systems in other areas.

CHAPTER III*

ROCK-PHYSICS-BASED PORE TYPE CHARACTERIZATION AND ITS APPLICATION IN CARBONATE RESERVOIR PERMEABILITY HETEROGENEITY EVALUATION, UPPER SAN ANDRES RESERVOIR, PERMIAN BASIN, WEST TEXAS

OVERVIEW

In addition to mineral composition and pore fluid, pore type variations play an important role in affecting the complexity of velocity-porosity relationship and permeability heterogeneity at a given reservoir temperature and pressure in carbonate reservoirs. Without consideration of pore type diversity, most rock physics models applicable for explaining the rock acoustic properties and reservoir parameters relationship in clastic rocks don't work well for carbonate reservoir. A frame flexibility factor (γ) defined in a new carbonate rock physics model has been found to be able to quantify effect of pore structure changes on seismic wave velocity and permeability heterogeneity in carbonate reservoir. Our study of an Upper San Andres carbonate reservoir, Permian Basin, shows that for core samples of given porosity, the lower the frame flexibility factor (γ), the higher the sonic wave velocity. In this case, samples with frame flexibility factor (γ)

*Reprinted with permission from "Rock-physics-based carbonate pore type characterization and reservoir permeability heterogeneity evaluation, Upper San Andres reservoir, Permian Basin, west Texas" by "Qifeng Dou, Yuefeng Sun, Charlotte Sullivan, 2011. Journal of Applied Geophysics, 74, 8-18, Copyright [2011] by Journal of Applied Geophysics.

<3.85 represent either visible moldic pore space in or dolopackstone or intercrystalline classified with clear geologic interpretation such as pore type and rock texture variations so as to improve porosity and permeability prediction accuracy. Two-layer forward model study represents AVO signature response differences between each kind of pore type, which implies frame flexibility factor (γ) can be evaluated by combining pre-stack and post-stack data. Testing results using petrophysical data prove that an integrated approach by combing rock-physics-model and prestack and poststack impedance inversion is applicable for porosity and frame flexibility factor (γ) calculation in carbonate reservoir New porosity-permeability relation with γ classification helps to delineate permeability heterogeneity in the Upper San Andres reservoir, and could be useful for other similar carbonate reservoir characterization as well.

INTRODUCTION

Intensive reservoir heterogeneity causes low recovery in carbonate reservoirs, even though they contribute ~50% oil and gas production worldwide. The intensive reservoir heterogeneity is caused by complicated mineral composition, pore structure and rock texture variations. Compared to porosity, the complexity of pore types in carbonate reservoir, including moldic, vuggy, interparticle, intraparticle, crack and so on, present more influences on reservoir permeability heterogeneity and seismic velocity variation at the given mineral composition and fluid types (Anselmetti and Eberli, 1993, 1999, Dou, et al., 2009, Xu, et al., 2007). For example, at a given reservoir porosity (20-25%), permeability variation can be more than four orders of magnitude (Sun, et al., 2006)

caused by pore structure changes in a Middle East carbonate reservoir. Recent experimental results using the data from Middle East carbonate reservoirs also show that pore type variations can cause 2.5 km/s or even larger seismic compressional velocity difference at given porosity (Sun, 2000). Basically, moldic or vuggy pore types with large aspect ratio tend to be rounded and make rock hard, however, interparticle or crack types with low aspect ratio tend to be flat and make rock soft. Consequently, seismic wave propagate faster in the rocks dominated by moldic and vuggy pore spaces than it does in the rocks with interparticle or crack pore spaces.

A robust and practical rock physics model considering pore type variations is important for understanding the complicated relationships between acoustic properties and reservoir parameters and evaluating reservoir heterogeneity at low effective pressure in carbonate rock, which could link rock properties with AVO response as well. For homogeneous sandstones saturated with liquid phase and porosity lower than 40%, Wyllie's average time equation could explain the velocity-porosity relationship. Because there are no insight physical mechanisms of wave propagation in Wyllie's equation and multiple pore types existing in carbonate reservoir, it can't interpret velocity complexity in structural carbonate rocks. Based on the deviation of Wyllie's calculated velocity from measured velocity, some approaches and models were proposed to evaluate carbonate rock pore types complexity, such as secondary porosity indicator (Schlumberger, 1974), pseudo-fluid transit time (Meese and Walther, 1976), spherical porosity model (Brite et al., 1985), Lucia Model (Lucia, 1983), velocity-deviation log (Anselmetti and Eberli, 1999). By introducing pore shape factor, which is equivalent to

cementation factor in Archie's equation, Saleh and Castagna in 2004 revised Wyllie's average time equation to discriminate intercrystalline and near-spherical pore spaces. Xu and Payne in 2009 extended Xu-White model to interpret clay-related, interparticle, microcrack and stiff pore types from petrophysical data by using differential effective medium process and the Kuster-Toksöz theory. All of these studies account for the important influence of pore type changes on velocity in carbonate reservoirs, however, more efforts are needed for evaluating its effect quantitatively.

Sun and Goldberg (1997a, 1997b, 2000, 2004) introduced a rock physics model based on dynamical theory of fractured porous media. This model is developed by extending Biot theory. In this model, they defined elastic parameters called frame flexibility factors and these frame flexibility factors depend less on porosity than wave velocity does. Meanwhile, these parameters are not only related to pore structure variation but also to solid/pore connectivity and rock texture in carbonate reservoir (Sun, et. al., 2004). This poroelasticity model has been successfully proven at the core-plug scale by measured core data for its effectiveness in quantifying pore structure and used for carbonate reservoir permeability inversion from seismic data (Bracco Gartner, et al., 2005).

In this paper, we use the rock physics model introduced by Sun (2000) to analyze the velocity-porosity complexity and understand the permeability heterogeneity of an Upper San Andres carbonate reservoir, Permian basin, west Texas. This progress report is based on analysis of core measurements and well logging data. Results will be used for simultaneous porosity and permeability inversion from seismic data.

GEOLOGICAL SETTING

The Permian Basin of southeastern New Mexico and West Texas, occupies an area of 115,000 mile^2 (French, 2000). The current subsurface structure of Permian Basin is composed of the deep, asymmetric Delaware Basin to the west, the shallow Midland Basin to the east, and the Central Basin Platform between the two basins (Hills, 1970; Keller, et al., 1980), see Fig 3.1. Our study field lies on the eastern Central Basin Platform, Crane County, Texas (Fig 3.1).

The Permian Basin experienced deposition from Cambrian through Triassic age. Currently, it is widely accepted that the strata of the San Andres Formation were deposited during the Guadalupian epoch (Kerans and Fitchen, 1995; French and Kerans, 2004). Learning from the core data and analogy outcrop, the San Andres formation is an overall upward shallow finer grain size and basinal progradation section, a typical carbonate ramp depositional environment. The depositional environment is composed of out ramp (windward), ramp crest and middle ramp (leeward). Sea-level, paleotopography and accommodation variation control the depositional environment change and meanwhile cause the rock texture complexity (Figure3.2).

The homogeneous dolomudstone or uniform mud-dominant dolowackstone is the main rock type in the middle ramp lagoon subfacies, which representing a quite, lower energy and restricted environment. The shallow water fossils, for example bivalve and gastropod, were found. In the middle ramp facies, the main pore type is intercrystalline pore space. Most of dissolution pore space between the brecciated and intraclast fabrics,

related to paleokarst event (Dou, et al., 2009), were almost occluded by the anhydrite tightly except some fair thin cracks and fractures (Figure3.3-a,b).

Ramp crest develops within water, high-energy environment, such as a shoal or barrier bar and the deposition in ramp crest dominated by skeletal grain-dominant fabrics consisting of dolograinstone interbedded with dolopackstone. Skeletal constituents consist of peloid, mollusk fragment, ooid and fusulinid grains. Most of the dolograinstone is oil stained. The primary pore types are good to fair visible biomoldic and intraparticle, which represent good quality reservoir in study (Figure3.3-c,d).

Proximal outer ramp environment is fusulinid dolopackstone interbedded with thin ooid-skeletal dolograinstone. The dominant fossil is fusulinid and the other skeletal grains include bivalve, gastropod scattered within the dolopackstone. The dolopackstone in the out ramp presents two kinds of pore spaces, and one is moldic from skeletal grains dissolution and the other is interparticle. Learned from core photos, the second one is main pore type in outer ramp depositional environment (Figure3.3-e,f).

The above depositional facies, lithology variation and later digenesis events complicate porosity-velocity and porosity-permeability relationships in studied reservoir.

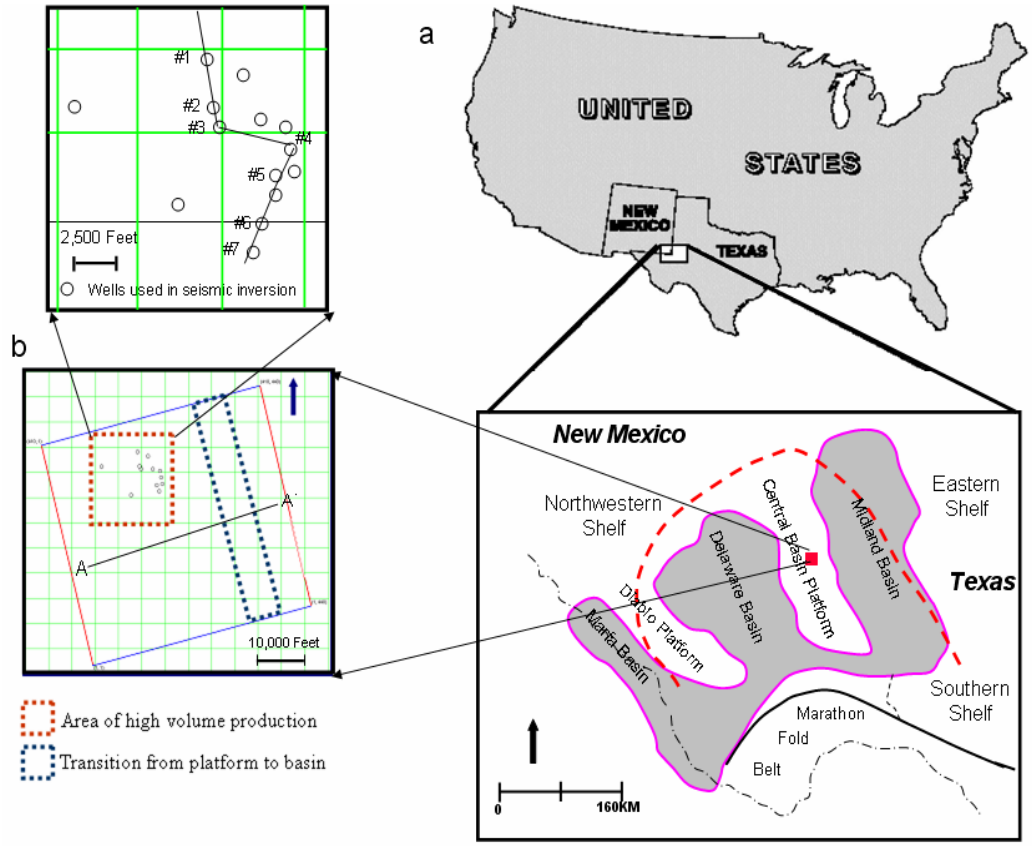

Figure 3.1 Location of Studied Field, Well Location and Seismic Survey, San Andres Reservoir, Permian Basin

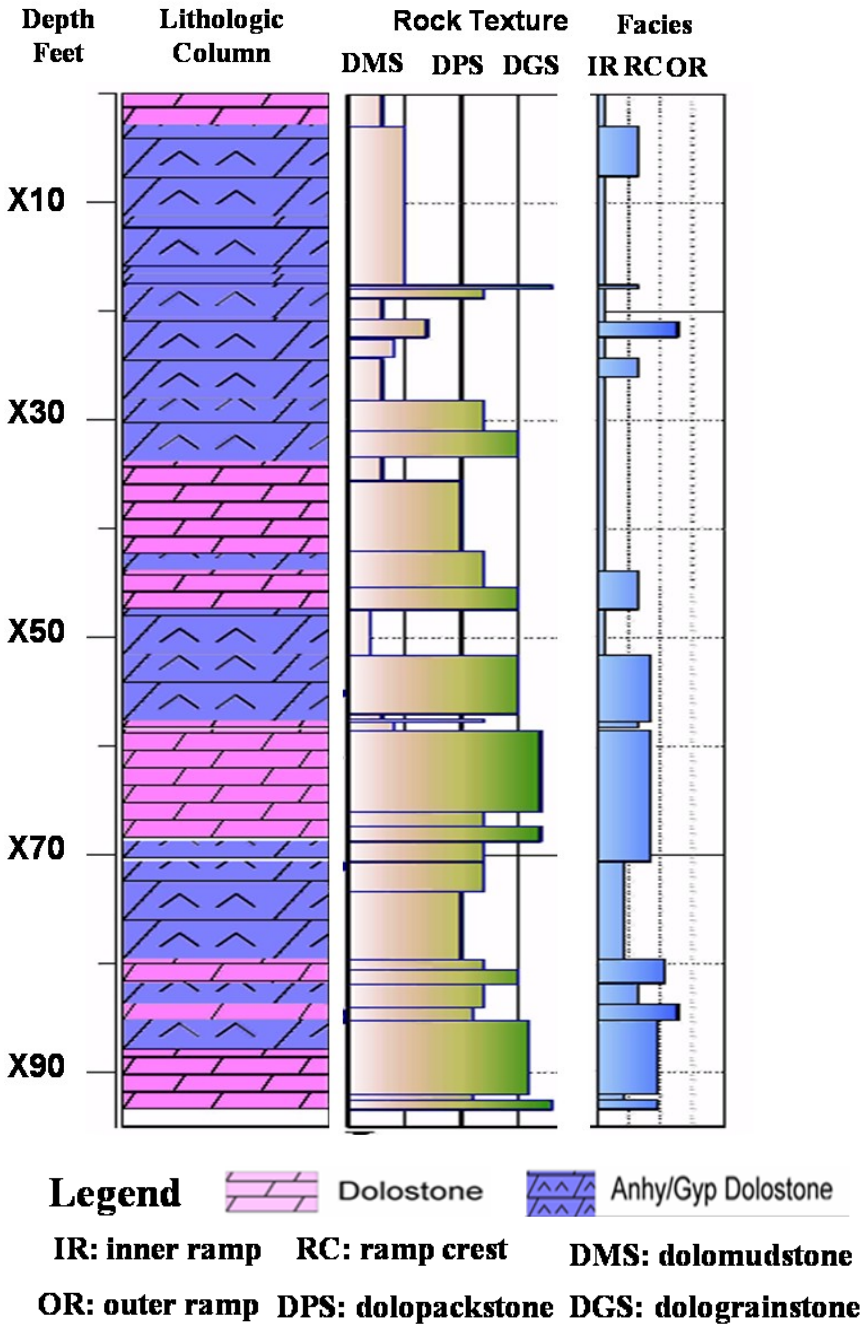

Figure 3.2 Lithological Column, Rock Texture and Depositional Facies in Cored Interval

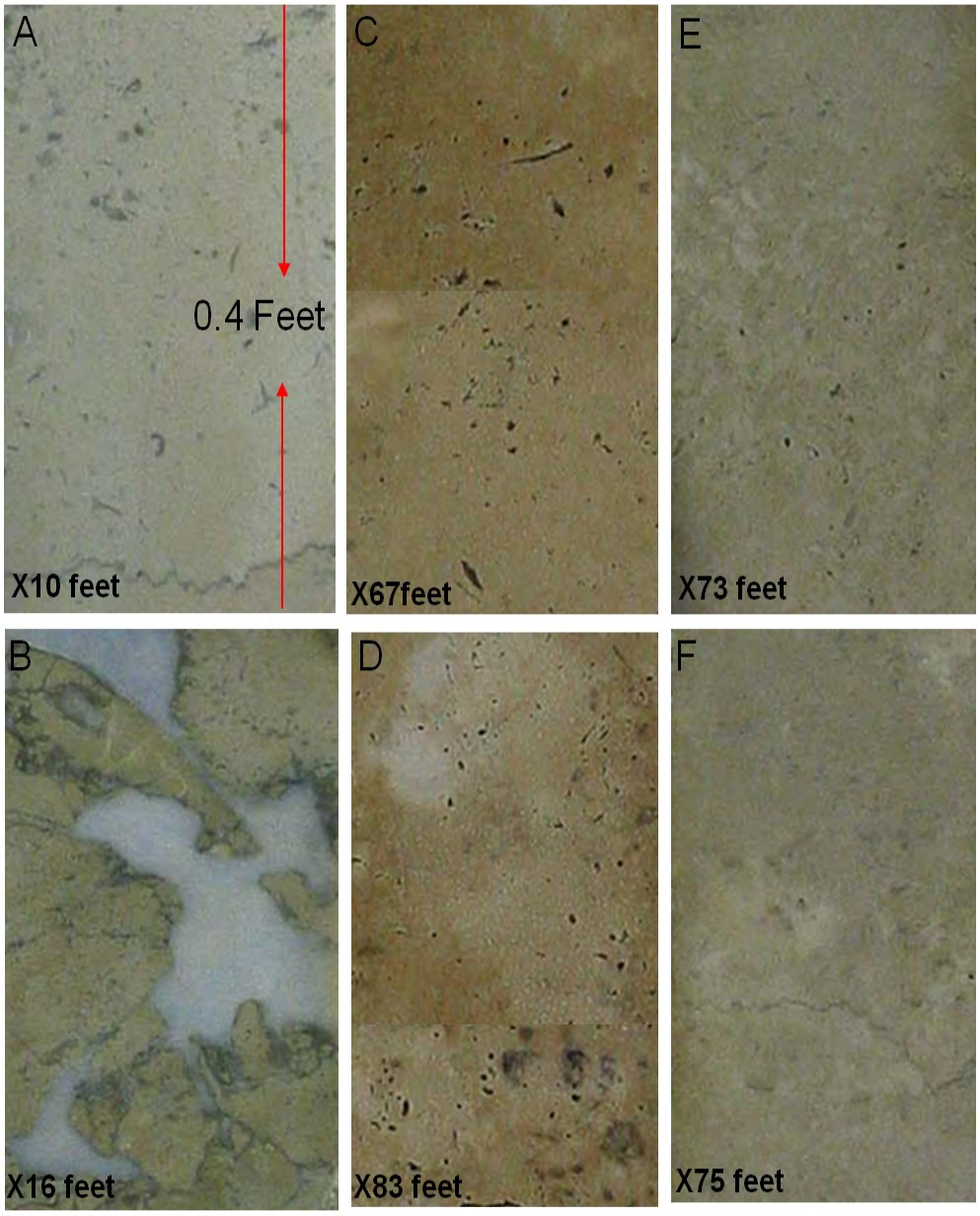

Figure 3.3 Core Photos Showing Rock Texture, Pore Types and Paleokarst Events

METHODS

Based on an extended Biot theory of poroelasticity, Sun (2000, 2004) derived a simplified rock physics model for carbonate rocks reservoir. In this model, he introduced frame flexibility factors to characterize carbonate reservoir pore structure. The formula to calculate the frame flexibility factors are summarized below:

Let V_p, V_s and ρ be compressional velocity, shear velocity and bulk density, respectively. Let K and μ be bulk and shear modulus, respectively. We have

$$\gamma = + \frac{\ln(f)}{\ln(1-\phi}$$ 3.1

where

$$f = \frac{1 - \frac{k_f}{k_s} + 1 - \frac{k_f}{k_s})\phi F_k}{(1-\phi\ (1 - \frac{k_f}{k_s} F_k)}$$ 3.2

$$F_k = \frac{K_s - \zeta}{\phi\ K_s - \zeta_f)}$$ 3.3

$$K = V_p^2 - \frac{4}{3} V_s^2)\rho$$ 3.4

where γ, f and F_k are frame flexibility factors defined by Sun (2000, 2004), K_s and K_f are matrix and fluid bulk modulus. The frame flexibility factor (γ) is inversely proportional to aspect ratio in theory. In this study, we use the γ factor to quantify carbonate pore types and permeability heterogeneity.

Mineral composition is necessary for matrix bulk modulus calculation. Thin section observation reveals that dolomite and anhydrite are two main mineral compositions in the San Andres reservoir (French, 2000). Combining the density and

photoelectric curves, we calculate the volume percentage of each mineral composition of the reservoir, and formula is as follows.

Let ρ and P_e be bulk density and photoelectric factor, respectively.

$$\rho = \phi\rho_f + V_d\rho_d + V_a\rho_a \quad \text{.....3.5}$$

$$Pe = \phi Pe_f + V_d Pe_d + V_a Pe_a \quad \text{.....3.6}$$

$$1 = \phi + V_d + V_a \quad \text{.....3.7}$$

where ρ_f, ρ_d and ρ_a are the bulk density of fluid, dolomite and anhydrite, respectively, Pe_f, Pe_d and Pe_a are the photoelectric factor of fluid, dolomite and anhydrite, respectively. After determining the percentage of each mineral, we use the Voigt-Reuss-Hill mixing models to calculate the bulk modulus of matrix, K_s. Voigt-Reuss-Hill mixing models is written as

$$M_{CRH} = \frac{M_V + M_R}{2} \quad \text{..... 3.8}$$

where

$$M_v = \sum_{i=1}^{n} f_i M_i \quad \text{.....3.9}$$

$$\frac{1}{M_R} = \sum_{i=1}^{n} \frac{f_i}{M_i} \quad \text{.....3.10}$$

The terms of f_i and Mi are the volume fraction and modulus of ith mineral component, respectively.

Xu et al. (2007) showed that the mud-filtrate invasion around the well bore was more pervasive in carbonates than clastic rock and the zones measured by sonic and bulk density well log are almost invasion zones with 100% water saturation. So, an assumption in our study is that the fluid type in above equations is brine.

How to connect seismic inversion with reservoir porosity and pore structure indicating parameter (γ) is the key for applying the prestack and poststack data to evaluate carbonate reservoir heterogeneity. From angle stack and poststack data, the elastic impedance (Connolly, 1999), acoustic impedance and lambda, one of Lame's constant could be inverted. Physically, these impedance parameter can be expressed with porosity and γ by replacing V_p and V_s with bulk and shear modulus. By combining these three kinds of impedance data, bulk density can be removed from the following equations, which make it simple for porosity and frame flexibility factor (γ) calculation using seismic impedance inversion:

$$\frac{EI}{AI^{(2c-\ -\ )}} = K + \frac{4}{3}\mu^{(a+.5b-\ )}\mu^{.5b} \quad \text{...... ....3.11}$$

$$\frac{Lambda}{AI^{2}} = \frac{3K-4\mu}{3K+\ \mu} \quad \text{........................... ....3.12}$$

and

$$K = \frac{K_s[(1-\Phi)^{\gamma}(\Phi K_f - \Phi K_s + K_f) - K_f]}{K_f(1-\phi)^{\gamma} - K_f + (K_f - K_s)\Phi} \quad \text{.....................3.13}$$

$$\mu = \mu_s(1-\Phi)^{\gamma} \quad \text{.. ...3.14}$$

where *EI* is elastic impedance; *AI* is acoustic impedance; Lambda is lame's constant; *K* and μ are bulk and shear modulus; a, b, c are constant coefficient in elastic impedance calculation (Connolly, 1999); $\varnothing$ and γ are porosity and frame flexibility factor, respectively; K_s, K_f, and μ_s are frame and fluid bulk modulus, matrix shear modulus, respectively; d is gamma ratio (Sun, 2004).

The above four equations reveal the non-linear relations between the impedances and frame flexibility factor γ as well as the porosity. By solving above equations, the porosity and γ can be determined from *EI, AI* and Lambda. One assumption in applying the above method to calculate porosity and γ is that K_s, K_f, and μ_s are needed to be known in advance.

RESULTS

Figure 3.4 is a composite well logs, calculated porosity and mineral composition, and core photos near the top of the reservoir formation. The second panel from the right shows calculated volume percentage of each kind of mineral composition and porosity. The interval with high anhydrite content is the paleokarst zone with very low porosity called tight zones. Core photos show the intensive anhydrite cementation in this zone with light-blue color. The lower reservoir zone shows weak anhydrite cementation and high porosity. The frame flexibility factor (γ) in the upper paleokarst zone shows a large variation from about 0 to 10, however, small changes from 3 to 5 in lower reservoir zone.

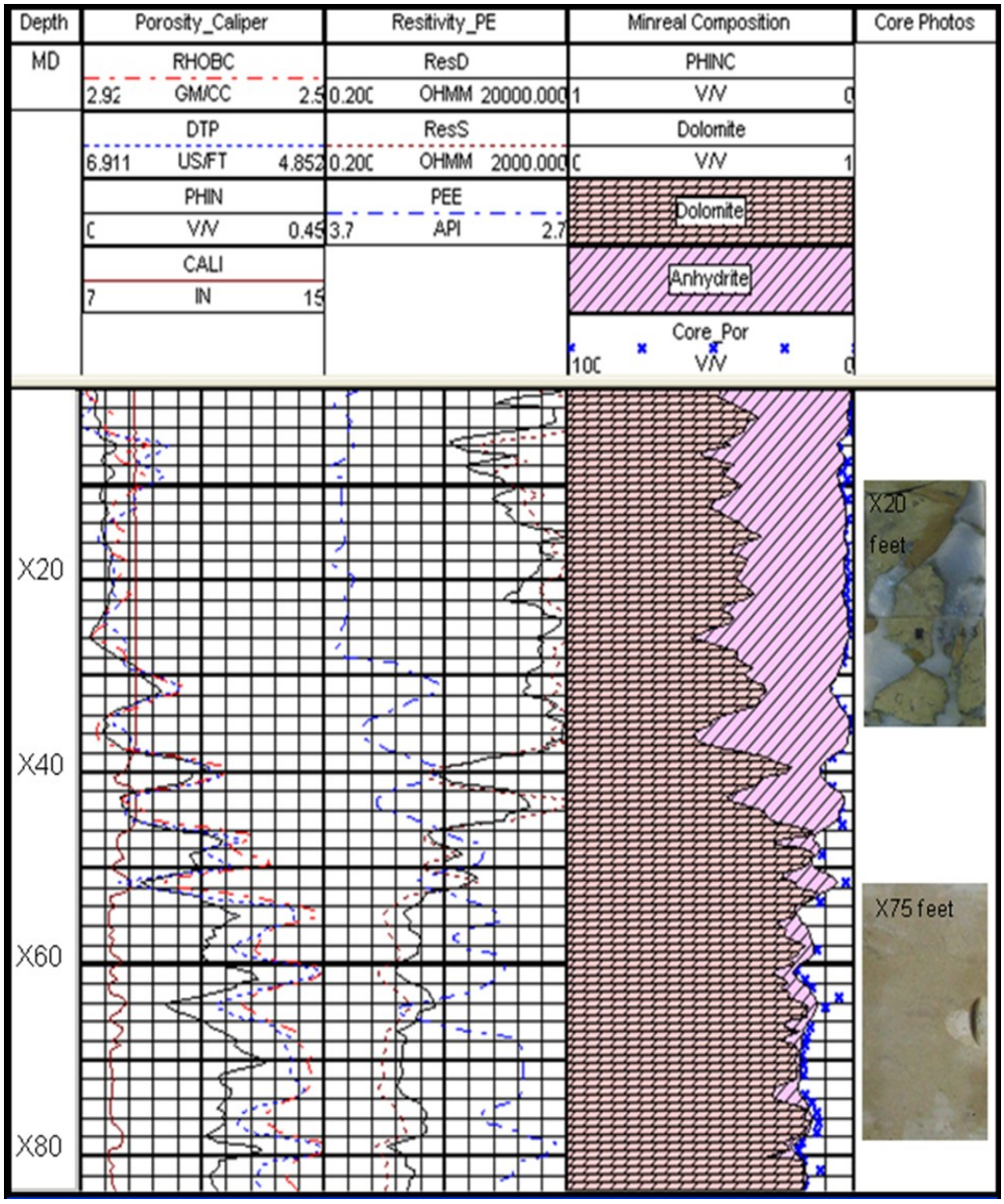

Figure 3.4 Well Log Curves and Mineral Composition of Well #1, San Andres Reservoir

As the other carbonate reservoir, complicated porosity-velocity relationship exists in Upper San Andres reservoir. Figure 3.5 is the crossplot of porosity against compressional velocity in log scale, of # well 1 and the color indicator is frame flexibility factor (γ). An inverse porosity-velocity relationship is apparent in the trend line, however, big scattering existing at a given porosity. For example, the minimum and maximum velocity difference at a porosity of 13.5 % is 900 m/s. In terms of (γ), the scattering points can be grouped into several clusters with different γ value range and this separation between different clusters is much better for samples with high porosity than that with low porosity. For example, samples with (γ) < 2 and >3.5 is around red trend line and blue trend line, respectively, and the other sample points with γ between 2-3.5 follows the green trend line, which delineates that high velocity is featured by low γ and low velocity is featured high γ at a given porosity. With porosity decreasing (< 7%), the separation among these three groups of samples becomes poor.

Another well (well #2) with core photos and measurement data was used to interpret porosity-velocity complexity in geology and how (γ) could indicate these geological influences. Figure 3.6 is the crossplot of core measured porosity against compressional velocity in log scale for cored interval of well #2 and the color bar is frame flexibility factor (γ). Similar to Figure 3.5, the inverse trend between porosity and velocity is apparent, and the data in the reservoir zone are considerably more scattered than the data in the upper paleokarst zone. Apparently, the frame flexibility factor (γ) can be used to cluster these scattering samples at given porosity, for example, the points with $\gamma < 3.85$ and > 3.85 along the yellow and blue trend lines, respectively.

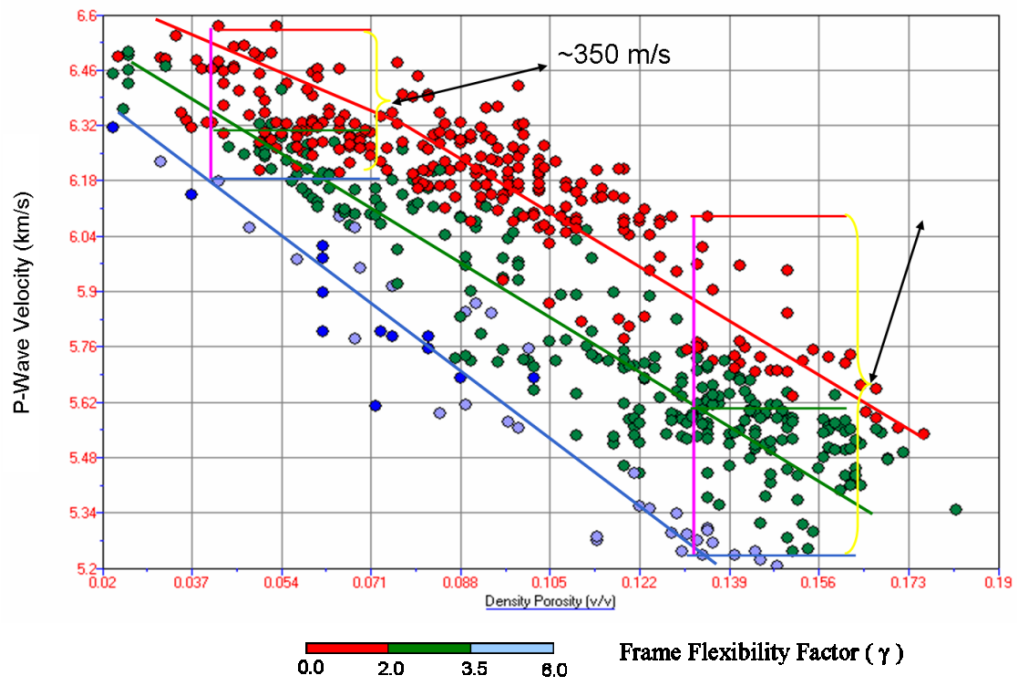

Figure 3.5 Crossplot of Density Porosity versus P-wave Velocity with γ color Indicator

Some samples were used to analyze the geological features in these two clusters. In the three groups of samples, A1 and B1, A2 and B2, A3 and B3, porosity are ~16.2%, ~15.5% and ~14.3%, respectively, but the velocity difference is ~500m/s. Core images of these samples reveal that rock texture of samples A1 and A2 are dolograinstones, however, samples B1 and B2 are primarily dolopackstones. Another apparent difference between these two groups is that there are much more visible moldic pore space in A1 and A2 samples than that in samples B1 and B2. Above observation from two groups data indicates that rock texture difference might be the major reason to causes pore type differences. Samples A3 and B3 are both dolopackstones with the same porosity of

14.3%. Sample A3 has a much higher velocity (> 500 m/s) than sample B3. Core images of these two samples show that sample A3 have more visible moldic pore space than that in sample B3. Using hand lens to observe core samples, it can be found that the major pore types of samples in B group is interparticle. The above analysis demonstrates that pore type difference is a major factor causing large velocity differences at given porosity. Similar observations have been reported in other studies (Anselmetti and Eberli, 1993; Sun, 2004; Saleh and Castagna, 2004). Higher percentages of micropores (interparticle or crack) in carbonate reservoirs make the rock weaker and cause slower velocities compared to reservoir rocks with more macropores (moldic or vuggy), as illustrated by the difference between the A and B group samples. For samples with porosity < 5%, the porosity-velocity trend is less scattered than that from high porosity samples. However, samples A4 and B4 of similar porosity of 3.2% still have a velocity difference of about 300 m/s. Core photos reveal that microcracks exist in low-velocity sample B4, which is related to paleocave collapse.

The above results also proved that frame flexibility factor (γ) can be used to the geological factors that cause complicated porosity-velocity relationship. For the sample with visible moldic pore in dolograinstones and dolopackstones (yellow and red points in Figure 3.6), its frame flexibility factor (γ) is < 3.85 in this case. For samples with dominant interparticle pore space in dolopackstones, or with microcracks in dolowackstone and dolomudstone, its frame flexibility factor (γ) is >3.85 (blue, green and pink points in Figure 3.6. But for each specific study reservoir, this cutoff could be varying and core data is required to calibrate inverted γ to determine its cutoff.

Frame flexibility factor (γ) is helpful classifying trend lines of porosity-impedance crossplot so as to improve porosity prediction accuracy from seismic inversion data volume. A traditional approach of evaluating reservoir porosity is to transform impedance data volume from seismic inversion into porosity by the best-fit of

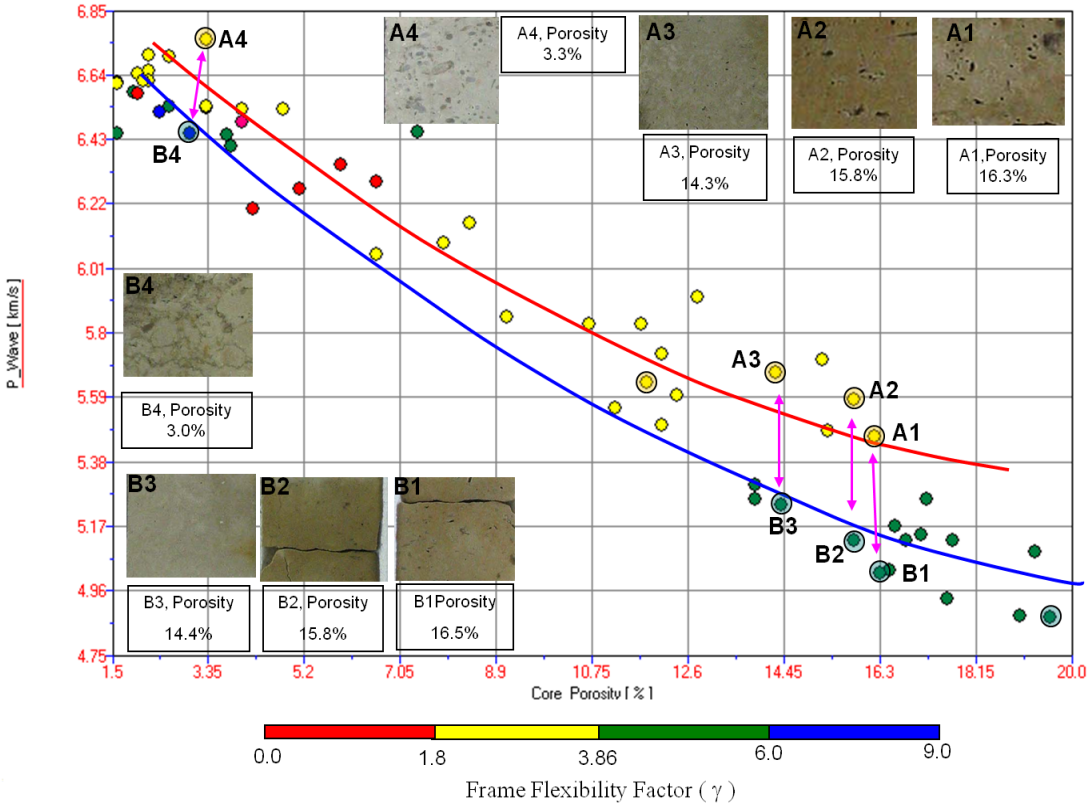

Figure 3.6 Core Porosity and P-wave Crossplot with γ Color Bar

porosity-impedance. Because there are much complicated pore types in carbonate reservoir than that in clastic reservoir, which complicate porosity-velocity relationship, this simple transforming method isn't work well in carbonate reservoir. Figure 3.7 is the

crossplot of density porosity against shear wave impedance (shear velocity* bulk density) and it represents a big scattering, which is the same as the crossplot of porosity against

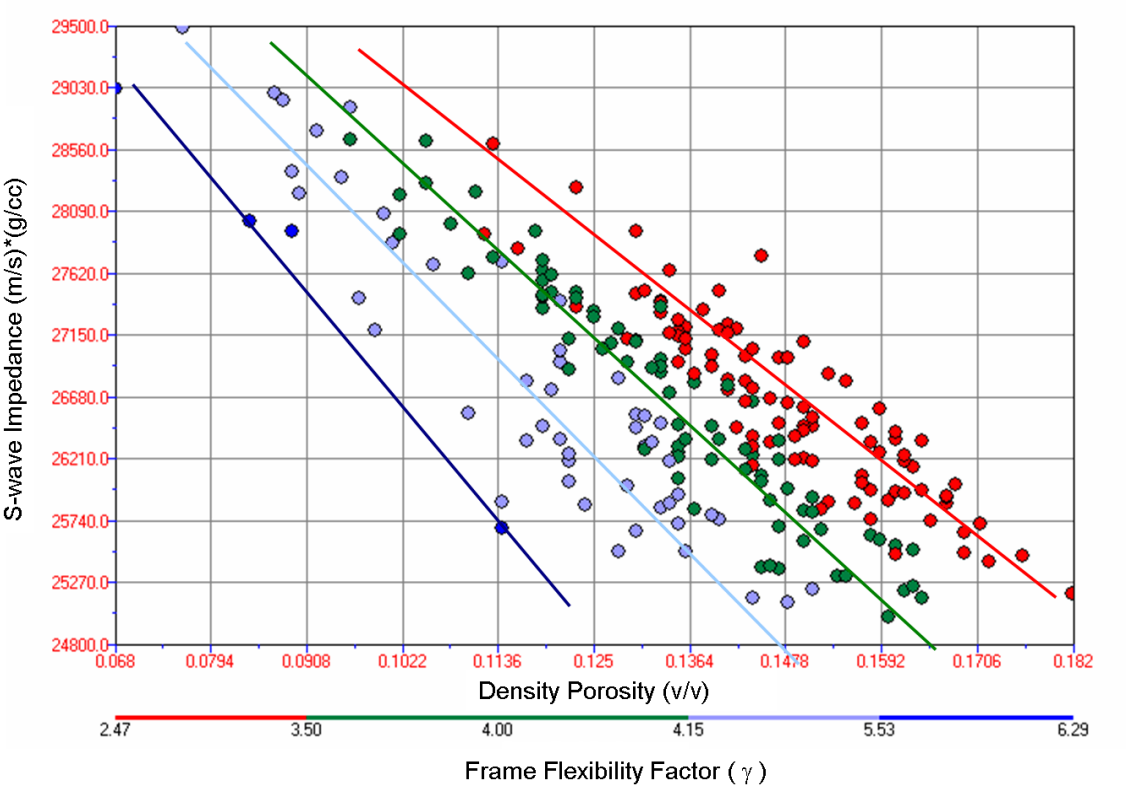

Figure 3.7 Crossplot of Density Porosity and S-wave Impedance with a γ Color Indicator

velocity. The reason is that the pore structure is a major factor that affects velocity complexity in carbonate reservoir, and consequently it also causes complicated impedance-porosity relationship. In terms of frame flexibility factor (γ) different trend

lines can be built between porosity and shear wave impedance so that porosity prediction accuracy from impedance data volume can be improved dramatically (Figure 3.7).

Combining porosity and Frame flexibility factor (γ) is a good approach to characterize carbonate reservoir permeability heterogeneity. In carbonate reservoir, permeability heterogeneity is much intensive than that in clastic reservoir because of its complicated mineral composition, pore types and rock textures. In this study reservoir, frame flexibility factor (γ) is also helpful to evaluate permeability heterogeneity in carbonate reservoirs. Figure 3.8 shows a crossplot of porosity and permeability for the cored interval and it could be found that the samples with highest permeability aren't that with highest porosity. In this Figure, samples (porosity >6%) with frame flexibility factor (γ) >3.85 have a relatively lower permeability than the samples (porosity > 6%) with frame flexibility factor (γ) <3.85 at a given porosity. For example, samples A2 and B2 have the same porosity of 15.8%, but their permeability difference is more than one-order, which are 858md and 75.8md, respectively. The frame flexibility factor (γ) also displays a certain difference between the two samples, which is 3.45 and 4.26, respectively. Because permeability is related to the pore type and rock texture in carbonate rock, which can be represented by frame flexibility factor (γ), it is understandable that the frame flexibility factor (γ) is useful evaluating permeability in carbonate reservoir. The traditional porosity-permeability best-fit is shown by the black dashed line in Figure 3.8 and its regression coefficient factor is 0.64. It could be found that there is large error for samples with porosity higher than 10% using this best-fit line.

In terms of the frame flexibility factor (γ), two distinct trend lines can be built defining two permeability zones, one with (γ) < 3.85 and the other one with (γ) >3.85.

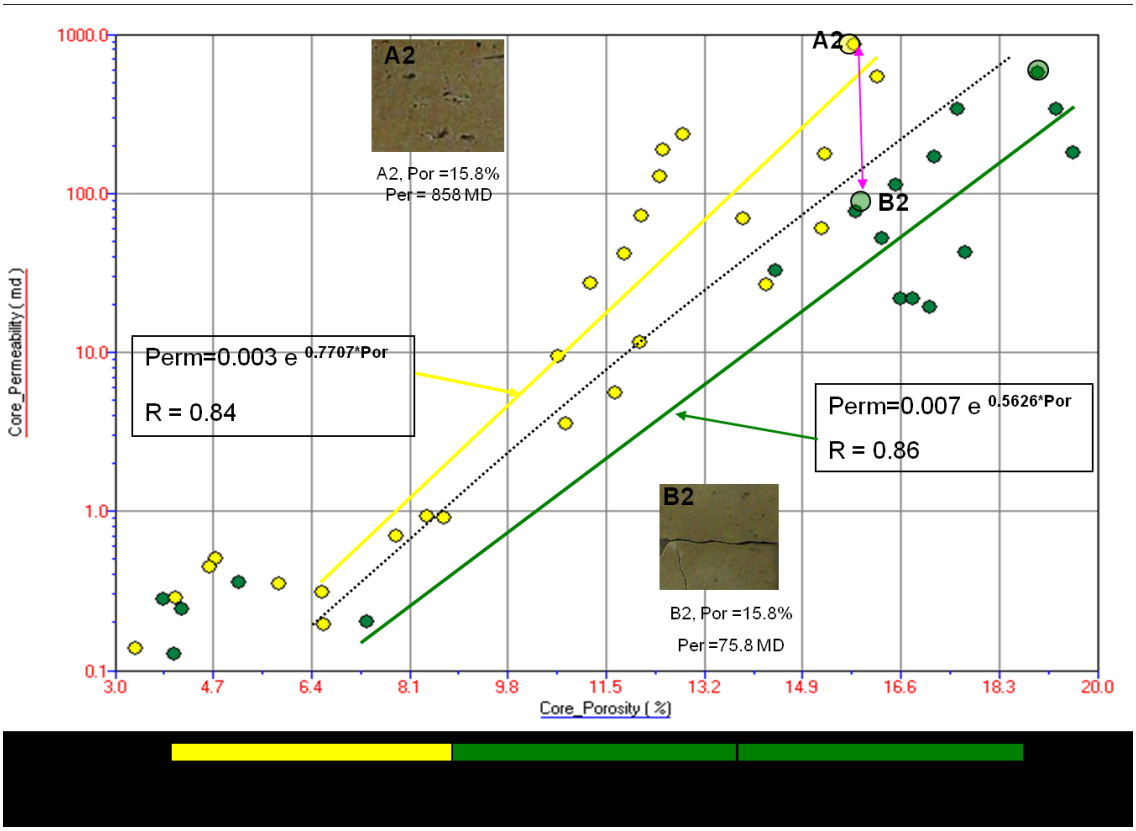

Figure 3.8 Crossplot of Core Porosity to Core Permeability with γ Color Indicator

Using these two different trend lines, regression coefficient factor of porosity-permeability is improved to 0.84 and 0.86, respectively. So, the above study shows that frame flexibility factor (γ) permeability prediction accuracy from porosity in carbonate reservoirs.

DISCUSSION

3-D seismic data survey is widely used to characterize carbonate reservoir, including depositional facies, structure and stratigraphy sequence to build carbonate reservoir 3-D. In order to evaluate the feasibility of inverting the frame flexibility factor (γ) and porosity simultaneously from prestack and poststack data so as to characterize reservoir permeability heterogeneity, AVO response of three kinds of pore type and the approach proposed in methods part for porosity and frame flexibility factor (γ) inversion from impedances would be discussed and tested in the following part.

Two layers model consisting of shale layer overlying a dolomite reservoir with a porosity of ~10% was applied for AVO response analysis of each kind of pore types. Three points were selected from # well 3 with three different pore structure types PTSI, PTSII and PTSIII, which is defined by Sun in 2006, see Figure 3.9. Point one, point two and point three represent PTSIII, PTSII and PTSI, respectively with similar porosity but different compressional and shear wave velocity. Based on above analysis, the model with PTSII, PTSII and PTSI might represent the moldic or vuggy, interparticle and crack pore types.

By solving the full Zoeppritz equation, the seismic reflection coefficients (RC) including reflection compressional wave (Rpp) and converted compressional wave (Rps) versus incident angle for each kind of pore types in model were calculated, see Figures 3.10 and 3.11. Figure 3.10 is the Rpp variation against incident angle and Figure 3.11 is the Rps variation against incident angle for three kinds of pore types. From Figure 3.10, it could be found that three Rpp curves with PSTIII, PSTII and PTSI pore types,

respectively, represent different critical angles. From PTSIII to PTSI, critical angle of each Rpp curves increases. For Rpp against incident angle, the Rpp difference between each two kinds of pore types increases with the incident angle increasing. For example, the Rpp difference between PTSIII and PTSI at incident angle of 0° is 0.03, however, it increases up to 0.15 at incident angle of 23°. For Rps against incident angle (Figure 3.11), Rps is the same at the low incident for three kinds of pore types. However, Rps difference between each two kinds of pore types increases with incident angle as well. For example, it increases to 0.12 at incident angle of 23° between PTSIII and PTSI. This analysis implies that the far offset seismic data is better to discriminate the pore type variations in carbonate reservoir than the near offset seismic data does. In above model, we assume that the fluid types in three kinds of pore spaces are the same as brine. However, the fluid variation in in-situ reservoir would weaken this AVO signature separation between each kind of pore types (Sun, et al., 2006).

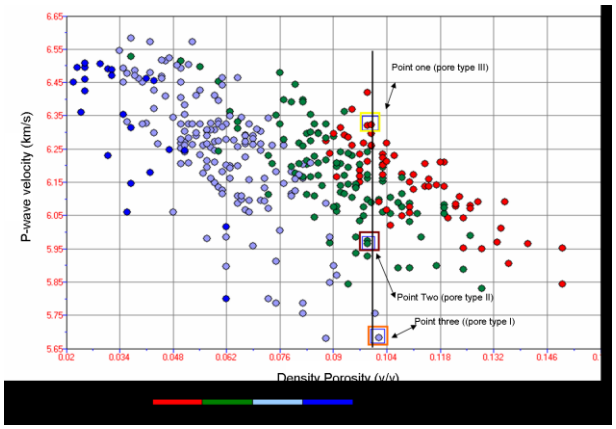

Figure 3.9 Crossplot of Density Porosity versus P-wave Velocity with γ Color Indicator and Shows Three Points Selected for Forward Model Study

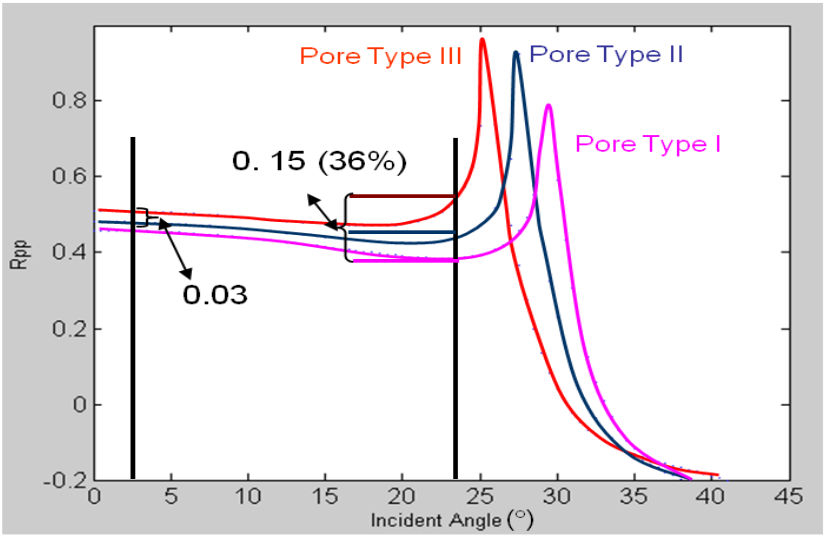

Figure 3.10 Crossplot of Incident Angle to P-wave Reflection Coefficient

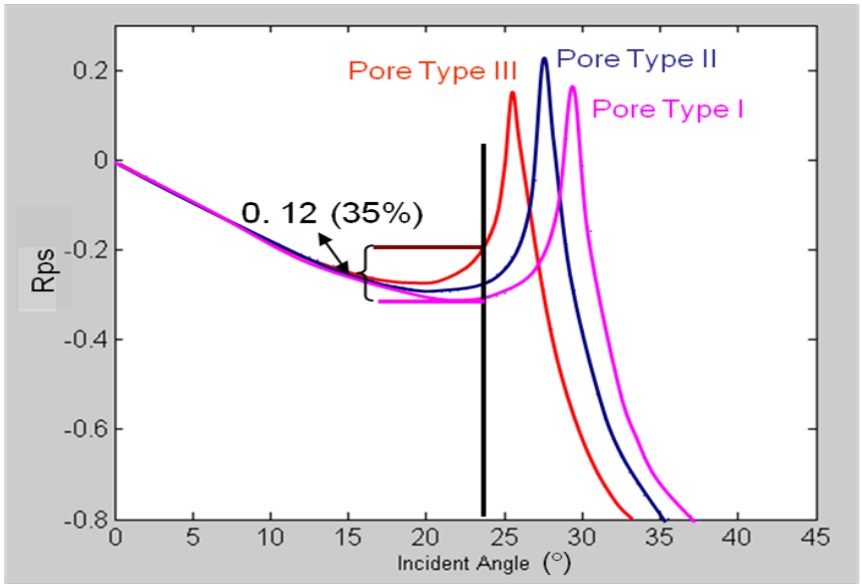

Figure 3.11 Crossplot of Incident Angle to PS-wave Reflection Coefficient

Petrophysical data from well #3 is used to test the approach about how to inverse porosity and γ from impedance data. During this procedure, acoustic impedance, elastic impedance and lambda were calculated from compressional velocity, shear velocity and bulk density firstly. Using the equation 11 and 12, bulk modulus and shear modulus were calculated. Based on the assumption that the fluid types, mineral composition and gamma ratio are known, porosity and frame flexibility factor (γ) are calculated using equation 13 and 14. Figure 3.12 and Figure 3.13 are the comparison of frame flexibility factor (γ) from impedance data volume with that rock-physics model calculation, and porosity from impedance data volume and that from bulk density curve, respectively. The absolute maximum, minimum and average error of porosity inversion from impedance data volume is 0.02, 0.002 and 0.0097 V/V, respectively. For frame flexibility factor (γ), The absolute maximum, minimum and average error is 2.78, 0.02 and 0,36, respectively. This result proves that the approach mentioned above is applicable for porosity and frame flexibility factor (γ) simultaneous inversion from anglestack and poststack impedance inversion. Another requiring in above calculation is that parameter d, gamma ratio, is supposed be approximately constant in study zones.

CONCLUSIONS

Field study of San Andres carbonate reservoir from west Texas demonstrates that the frame flexibility factor (γ) derived from an extended Biot theory is helpful for understanding the porosity-velocity complexity and improving porosity and permeability prediction accuracy in carbonate reservoirs. Variations in carbonate pore type, rock

texture and mineral composition are the major causes for poor porosity-velocity and porosity-permeability relationships. The frame flexibility factor (γ) can be used to characterize and carbonate rock pore types and high permeability zones. AVO response differences between each kind of pore types encourage us to use 3-D seismic data to evaluate carbonate reservoir pore type complexity and consequently permeability heterogeneity, which is helpful for building an accurate reservoir modeling.

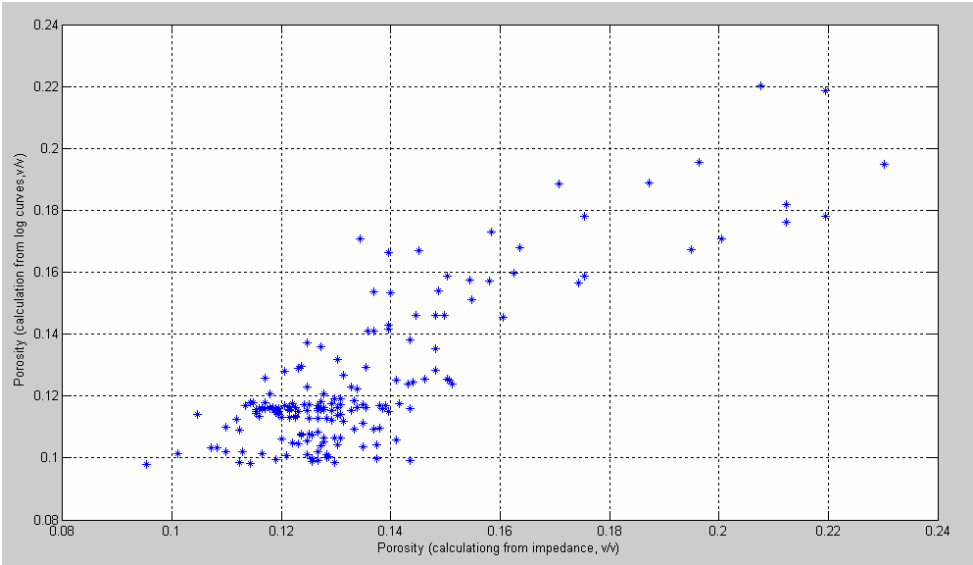

Figure 3.12 Crossplot of Inversed Porosity by Using Rock Physics Model against Porosity Calculated from Log Curves

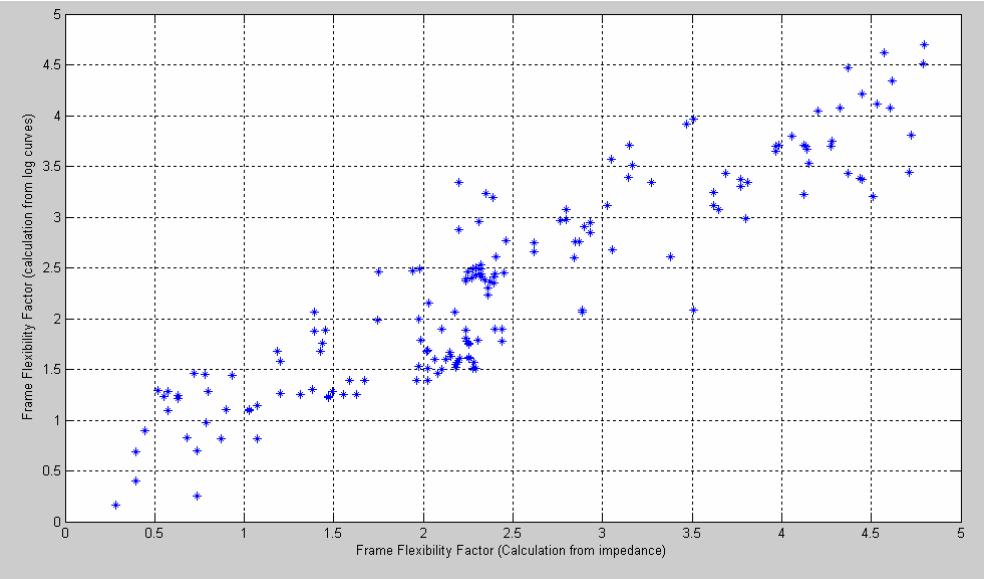

Figure 3.13 Crossplot of Inversed γ by Using Rock Physics Model against γ Calculated from Log Curves

CHAPTER IV

ROCK-PHYSICS-BASED PORE TYPE CHARACTERIZATION AND ITS INFLUENCES ON POROSITY AND VELOCITY COMPLEX RELATIONSHIP AND PERMEABILITY HETEROGENEITY IN LOW POROSITY CHANGXING CARBONATE RESERVOIR, SICHUAN BASIN, CHINA

OVERVIEW

Owing to the high-pressure and high-temperature environment and the complex history of diagenesis, ultra-deep reservoirs with depth of greater than 6 km usually exhibit much higher degree of reservoir heterogeneity than their counterparts in shallower depths. In the recent discovered gas fields, Sichuan Basin, China, reservoir units could have variable porosity ranging from less than 5% to greater than 20%, while producing units having a porosity of less than 5% are most common. Prediction of the occurrence of high-quality reservoir zones has been one of the many greatest challenges encountered in low-porosity, ultra-deep exploration.

Combining geological description and core analysis with rock-physics-based petrophysical study, we find that in low-porosity reservoir rocks (porosity <5%), variations of pore types play an important role in causing complexity of permeability-porosity relationship and spatial variations of gas occurrence. A frame flexibility factor (γ) defined in a new rock physics model is found to be useful in classifying different pore types and quantifying their effects on acoustic wave velocity and permeability heterogeneity in low-porosity carbonate reservoir rocks. For the studied reservoirs, it is

found that samples with frame flexibility factor (γ) <2.2 represent a mixed pore type of intercrystalline and interparticle pores where porosity is < 5%, or a mixture of interparticle and dissolution pores where porosity is > 5%. Samples with frame flexibility factor (γ) between 2.2 and 6 show either intercrytalline pore space in low porosity range (<5%) or dominant interparticle pore space in relatively high porosity range (>5%). Fractures usually have high frame flexibility factor (γ) of > 6. It is observed that low-porosity (<5%) gas-bearing reservoir rocks with intense dolomitization tend to have lower frame flexibility factor and higher sonic velocity than water-saturated limestone rocks in the similar porosity range.

It is also found that frame flexibility factor (γ) could be a good indicator to differentiate relatively high permeability zones (>~0.1md) from non-reservoir zones (average permeability < ~0.001md). Once this frame flexibility factor (γ) is calibrated using core and petrophysical data, it can then be estimated from log and seismic data to help determine high-permeability gas-bearing zones in low porosity carbonate reservoir rocks.

GEOLOGICAL SETTING

Studied reservoir discovered in ChangXing Formation is located in northeastern Sichuan Basin, southwest China. As a western part of the Yangtze Craton, northeast-trending Sichuan Basin covers an area of 180,000 km^2 (Ma et al., 2006). Tectonically, Longquanshan fault and Huayingshan fault divided Sichuan Basin into three major subdivisions created at late Mesozoic-Cenozonic: the northwestern depression, the

central uplift and the southwestern depressions. To the northwest, it is bounded by the Longmenshan fold belt, the Hubei-Hunan-Guizhou fold belt to the southeast, the Micangshan uplift in the north, the Dabashan fold belt to the northeast and the Emeishan-Liangshan fold belt in the southwest (Figure 4.1).

Several tectonic movements and episodes starting at Late Proterozoic governed Sichuan Basin evaluations. The uplifting and folding of pre-Sinian geosyncline and the consolidation of the metamorphic and granitic basement of the Yangtze Craton was created by the Chengjiang tectonic movement. The basement framework of Sichuan basin is established during the Chengjiang tectonic, with western and eastern lows of ductile basement and central uplift of brittle lithologies (Ma et al., 2006). The northeast-trending central uplift was formed by the late Caledonian Orogeny movement at the end of the Silurian.

Sichuan Basin is composed of a 6000-12,000m thick Sinian to Cenozoic sedimentary succession overlaying pre-Sinan Proterozoic basement. The oldest depositional rock in basin consists of the Precambrian Doushantuo and Dengying formations during a major marine transgression. Shale, siltstone, limestone and dolostone were deposited in an open- to restricted-marine environments resulting by the second major marine transgression during Cambrian period. The third marine transgression from Early Ordovician to the Early Silurian lead to a widespread deposition of black shale in an open-marine environment, which provided an important hydrocarbon source rocks to gas fields in the eastern Sichuan. Another major marine transgression occurred during the Early Permian resulted in a shale and carbonate

deposition in a shallow-marine environment, which are another important source and reservoir rocks. Under the influences of Dongwu tectonic movement, another deposition of coal-bearing shale and shallow-marine carbonate occurred at the Late Permian through Early Triassic marine transgression. The major reservoir rock including reefal dolomites and shelf and platform-marine shoal oolitic dolomites were deposited during the Upper Permian ChangXing Formation and Lower Triassic Feixianguan Formation, respectively. A major regression across the basin from the Late Triassic to the Middle Triassic led to a widespread anhydrite, halite and gypsiferous dolomite. These evaporate rock depositions provided a regional seals for the gas reservoirs in Sichuan Basin. By the end of the Late Triassic, fluvial-lacustrine clastic depositions dominated with the marine influences diminishing. Figure 4.2 is astratigraphic column of Sichuan Basin.

ChangXing reservoir was deposited in Late Permian in a shallow-marine and platform-margin environment and its dominant reservoir rock is dolomitized oolite and reefal carbonate. The dolomitization is a major controlling factor for reservoir quality, which produces lots of large-sized interparticle pore spaces. With acid liquid moving into reservoir from source rock, large amount of dissolution pore space was created which provided quality reservoir in this super-deep formation. Because of large overburden pressure in super-deep formations, micro-fractures developed widely in the ChangXing reservoir, a largely low-porosity reservoir (Figure 4.3).

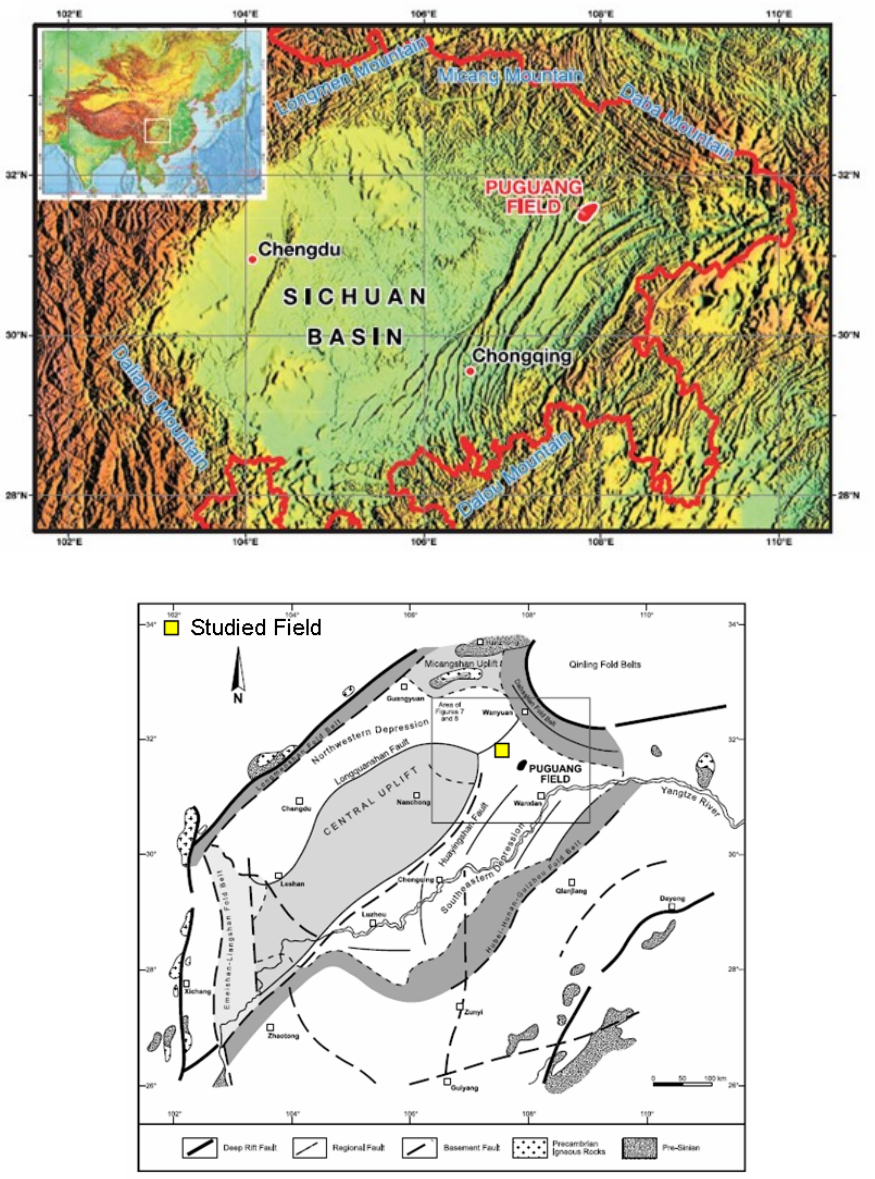

Figure 4.1 Main Tectonic Structure Component of Sichuan Basin and Studied Feld Lcation (Modified from Ma et al., 2006)

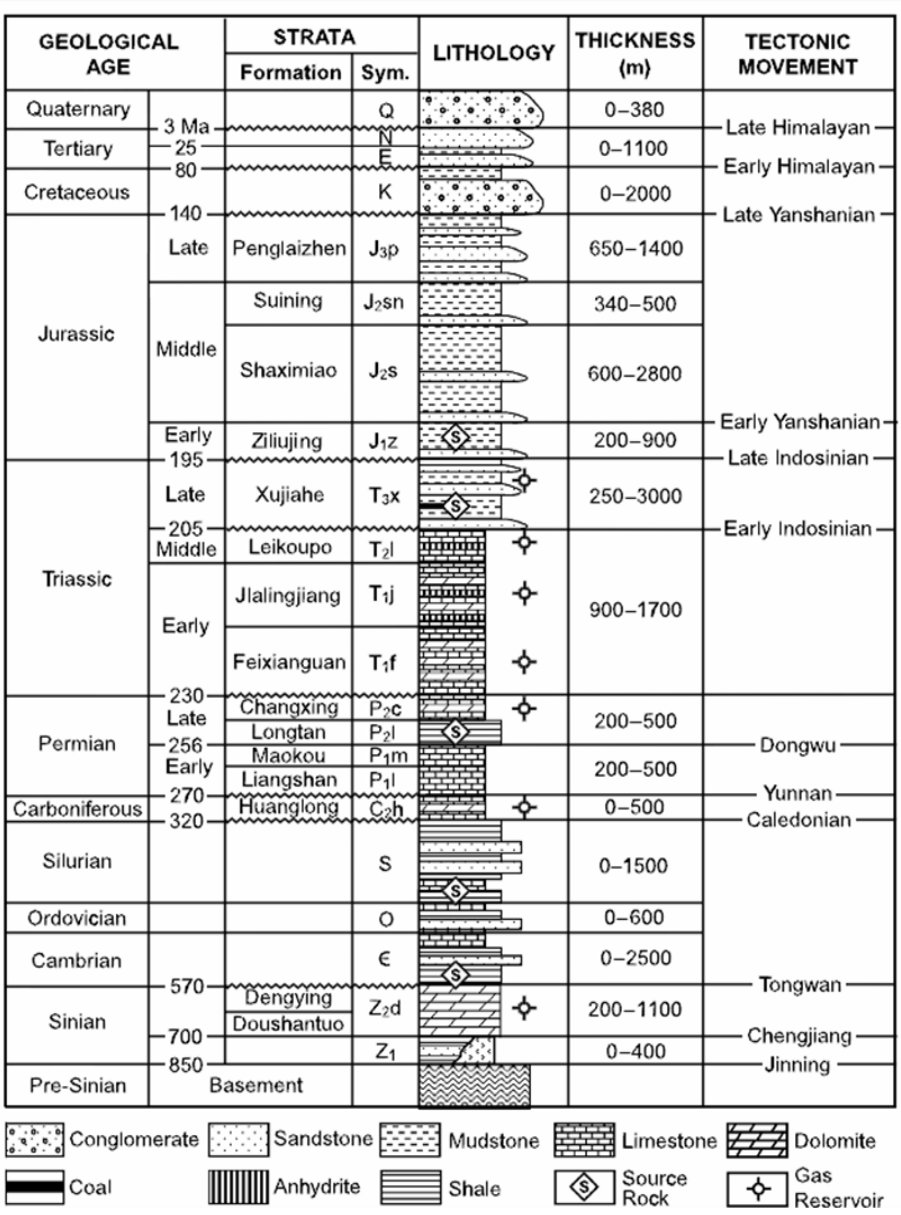

Figure 4.2 Formation Column of Sichuan Basin (Modified from **Ma et al., 2006)**

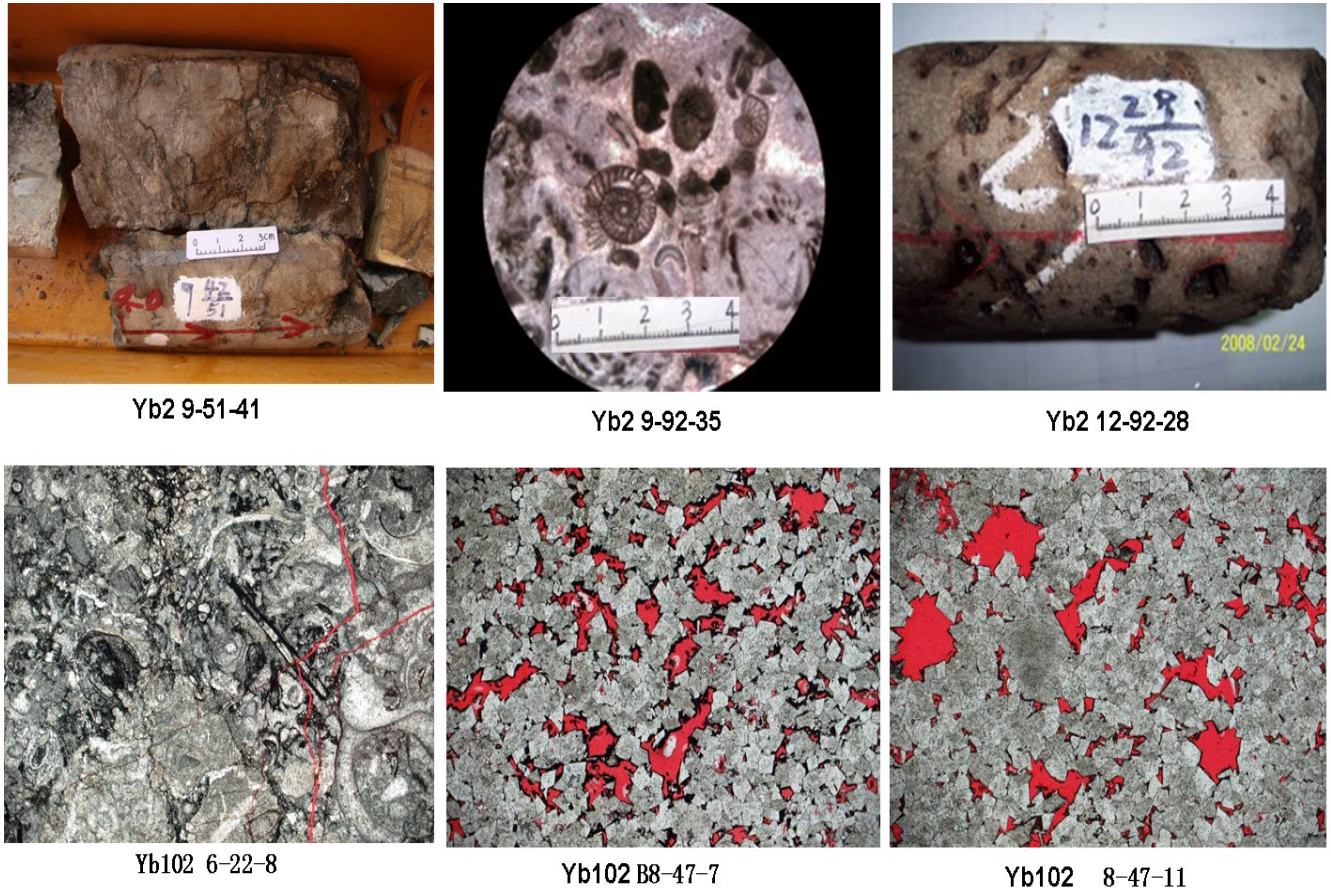

Figure 4.3 Core and Thin Section Photos Representing Rock Types, Mineral Compositions and Pore Spaces, ChangXing Reservoir, Sichuan Basin

RESULTS

ChangXing gas reservoir is a super-deep gas reservoir in early Permian, which located in Sichuan basin, Central China. ChanXing (~7000 meters) gas reservoir presents a very low porosity and the porosity of 80% samples is <5% based on statistics from all the wells within this area. The volume fraction of each kind of mineral composition, porosity and water saturation from petrophysical evaluation of Well #12 in ChangXing gas reservoir is represented in Figure 4.4. From the reservoir zones to nonreservoir zones, volume fraction of dolomite decreases, however, calcite volume percentage increases. In the nonreservoir zone of this well, its average porosity is lower than 2% and reservoir zone shows a big porosity variation from 2 to 20%. Based on porosity criteria for reservoir classification, ChangXing reservoir is classified into three kinds, which are type I, type II and type III with porosity higher than 10%, 5-10% and 2-5%, respectively. Based on above criteria, major reservoir type in ChangXing formation is type III, a low-grade reservoir.

A complex porosity-velocity relationship is found in the studied reservoir, Sichuan Basin. Figure 4.5 is the crossplot of compressional velocity versus porosity representing a large velocity scattering at given porosity, however, at lower porosity range, <~7%. Data in this crossplot consists of the whole reservoir interval in Well 12, and cored interval in Well 101, Well 102 and Well 11 and color bar represents data sources. From this crossplot, it could be found that velocity variation at a given porosity higher than 7% is less than 500m/s, especially for the samples with porosity higher than 13%, this velocity change is lower than100m/s at a given porosity. However, with

porosity decreasing, the velocity demonstrates huge variation at a given porosity. For example, the velocity variation at a velocity of ~ 2% is ~1250m/s and it is ~1600m/s at a porosity of ~6.5%.

Similar to the study in San Andreas reservoir, Permian basin, γ parameter is helpful to characterize the porosity and compressional velocity complex relationships. Figure 4.6 is the crossplot of compressional velocity to porosity and color indicator is γ parameter instead of well numbers in Figure 4.5. Using the γ parameter, the velocity variations can be characterized at a given porosity and meanwhile velocity-porosity crossplot can be classified into 3 different trends in terms of γ parameter, which are <2.2, 2.2-6 and >6.

What kinds of geological events cause velocity-porosity complexity in ChangXing gas reservoir? Basically, there are five major factors causing rock velocity variation, including porosity, mineral compositions, fluid features, pore structure and rock texture variation. Definitely, with porosity increasing, velocity decreases which has been shown in Figures 4.5 and 4.6. However, dramatic velocity variation at a given velocity might be caused by the factors other than porosity. Besides the above four controlling factors on velocity variation, fracture or crack related to tectonic movement or paleokarst events which happened after deposition or syn-deposition may have a big influence on velocity too, and this influence could be much bigger than that from the above four factors. In the following part, controlling factors on velocity complexity in ChangXing reservoir will be analyzed using thin section, core physical measurement,

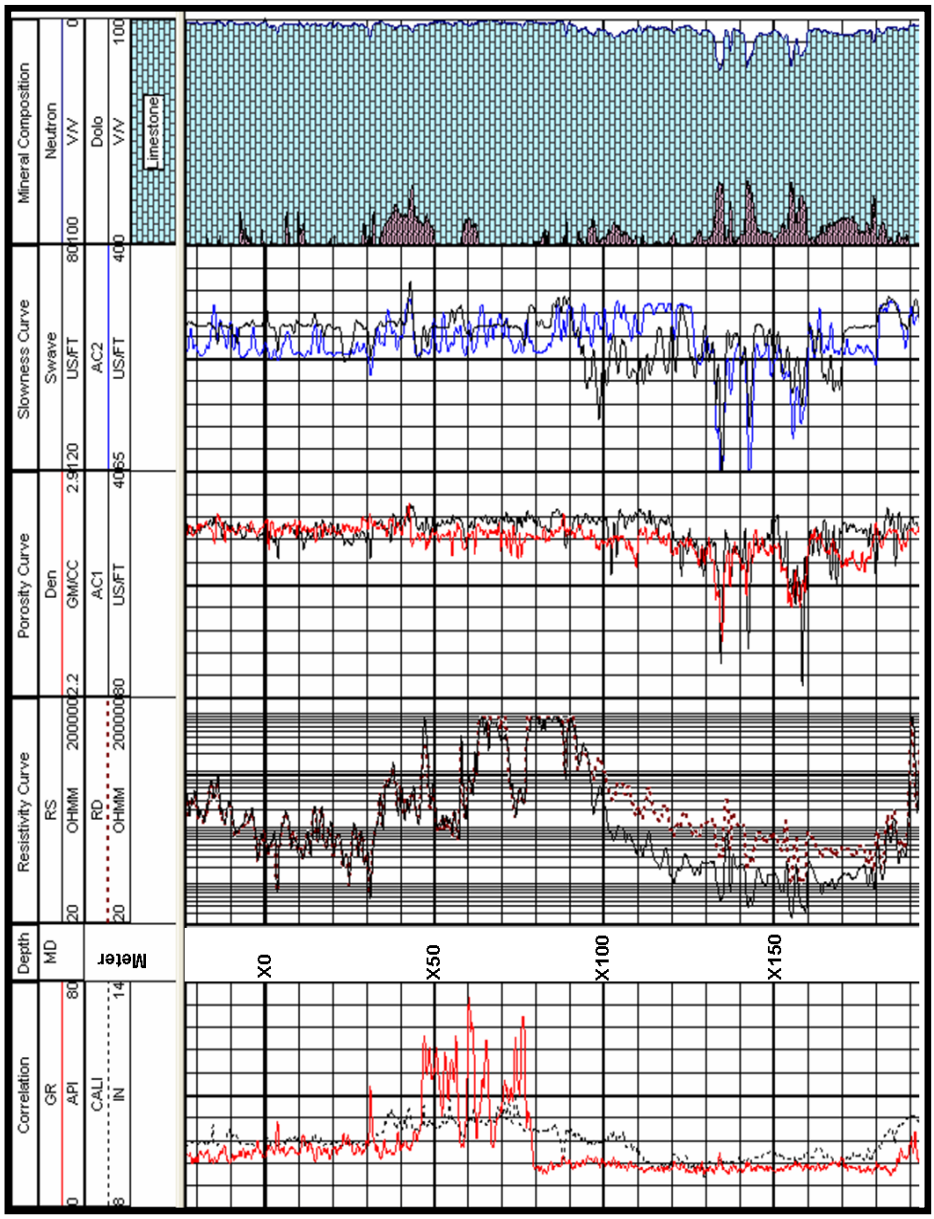

Figure 4.4 Composite Well Log Curves and Mineral Composition of Well 12, ChangXing Reservoir

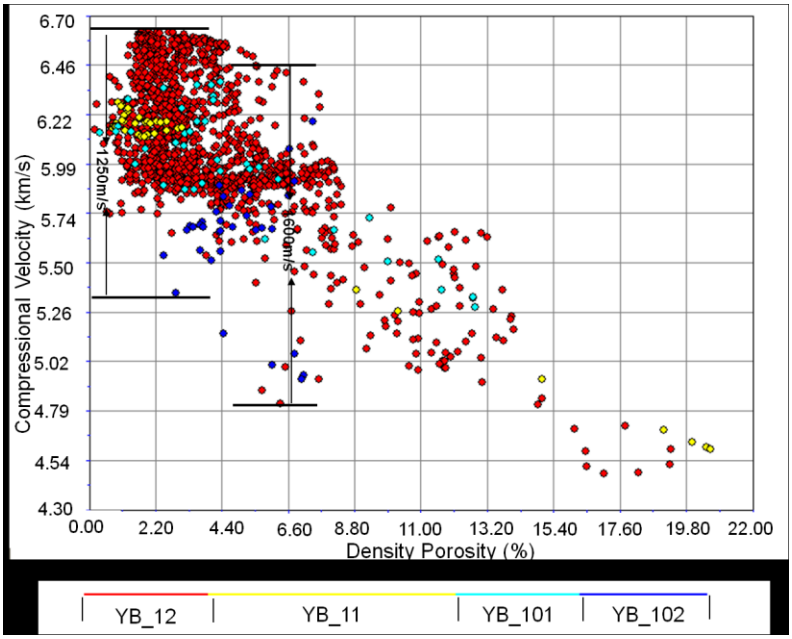

Figure 4.5 Density Porosity and Compressional Velocity Crossplot

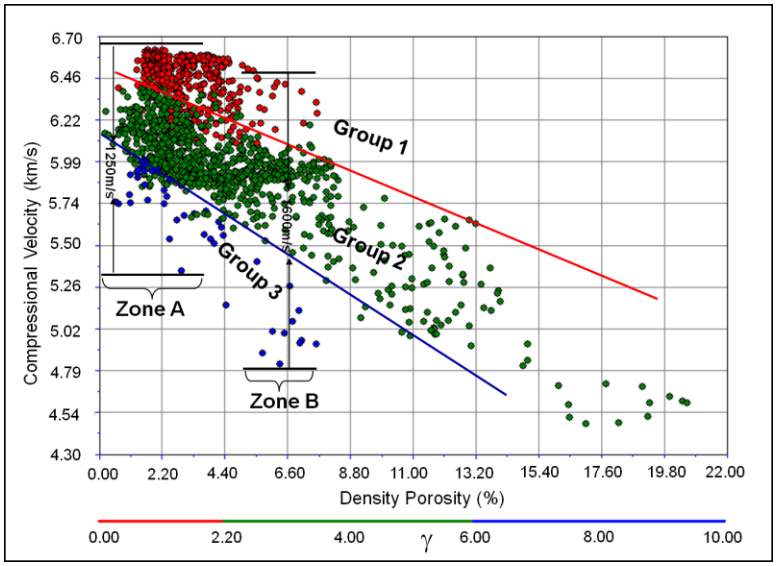

Figure 4.6 Density Porosity and Compressional Velocity Crossplot with γ Indicator

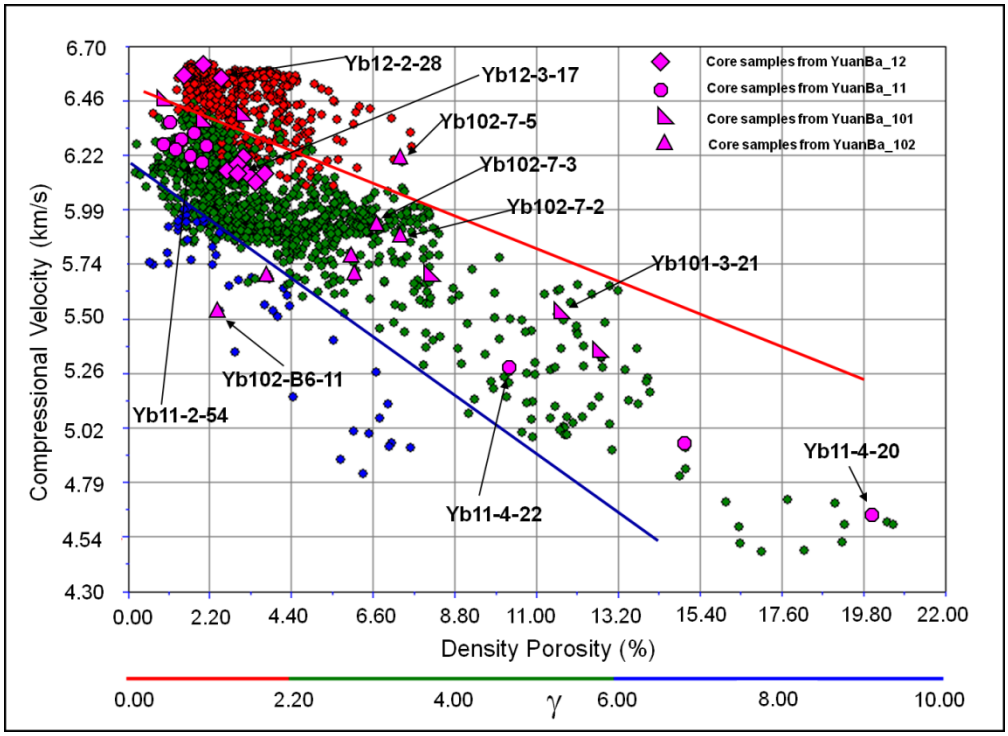

Figure 4.7 Density Porosity and Compressional Velocity Crossplot, in which the Samples Used for γ Interpretation were Indicated

capillary curves and petrophysical processing results. Figure 4.7 shows the core samples used in the following study.

The fluid influence on velocity variation is discussed firstly. In zone A (Figure 4.8), the maximum and minimum velocity difference is ~1250m/s and γ parameter is varying from 0 to 10. Consequently, the data points in this zone also could be populated into three groups with γ parameter values < 2.2, between 2.2 and 6, as well as >6. The fluid influence on velocity variation was studied first in terms of water saturation which is calculated using Archie's equation by combining porosity and resistivity curves. In

zone A, 90% of the samples in group 2 have water saturation > 50%, however, for the group 1 in zone A, the water saturation of 95% samples are <50%, see Figure 4.5. If all the other reservoir properties are identical, the rock velocity should be decreasing as water saturation decreases. However, the observation from group 1 and group 2 are inverted. That is, the water saturation of samples in group 1 is lower than that in group 2, however, their compressional velocity in group 1 is higher than that in group 1 at the similar porosity. This result indicated that there are some other factors that controlling velocity variations and fluid variation may not be the major factor affecting velocity changes here.

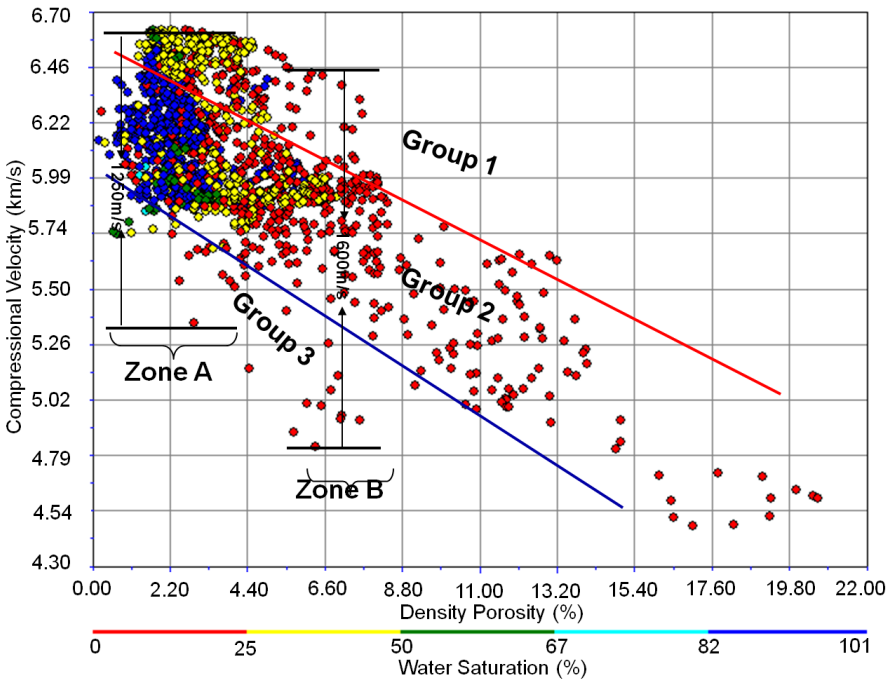

Figure 4.8 Density Porosity and Compressional Velocity Crossplot with Water Saturation Color Bar

By analyzing the thin sections, differences in mineral composition could be found between these two groups first as shown in Figure 4.9. For group 2, the major mineral composition is biomicrite in which the residual of fossil fragment is visible (Fig. 4.9-b,c). For the group 1, it isn't pure limestone but dolomitized limestone (Fig. 4.9-a). The dolomite is observed clearly in the thin sections of samples in group 1 with rhombic crystal shape. Because of dolomitization, some large and visible interparticle pore spaces (filled by red color) are observed in group 1, however, not shown in group 2. The difference in these geological features in these two groups could explain the velocity differences between them. Based on lab measurements, the average velocity of pure dolomite is much higher than that of limestone, which is ~6.89km/s and ~6.70km/s (Mavko, et.al, 2003), respectively. So, as these two groups represent a similar total porosity variation, it is understandable that the velocity of samples in group 1 with much more dolomite contents caused by dolomitization diagenesis is higher than that in group 2 without dolomite contents.

Besides mineral composition difference, diagenesis results in pore type differences between two group samples as well. In group 2, a dominant pore type is micropore space, for example intercrystalline which is invisible in thin section. However, there is a mixture of two kinds of pore types existing in group 1, which is composed of interparticle related to dolomitization due to diagenesis and intercrystalline (Figure 4.9-a). Physically, micropores have lower aspect ratio than round pores and they have a much lower compressional velocity at similar porosity. So, the pore space differences between these two groups also explain their compressional velocity differences at a

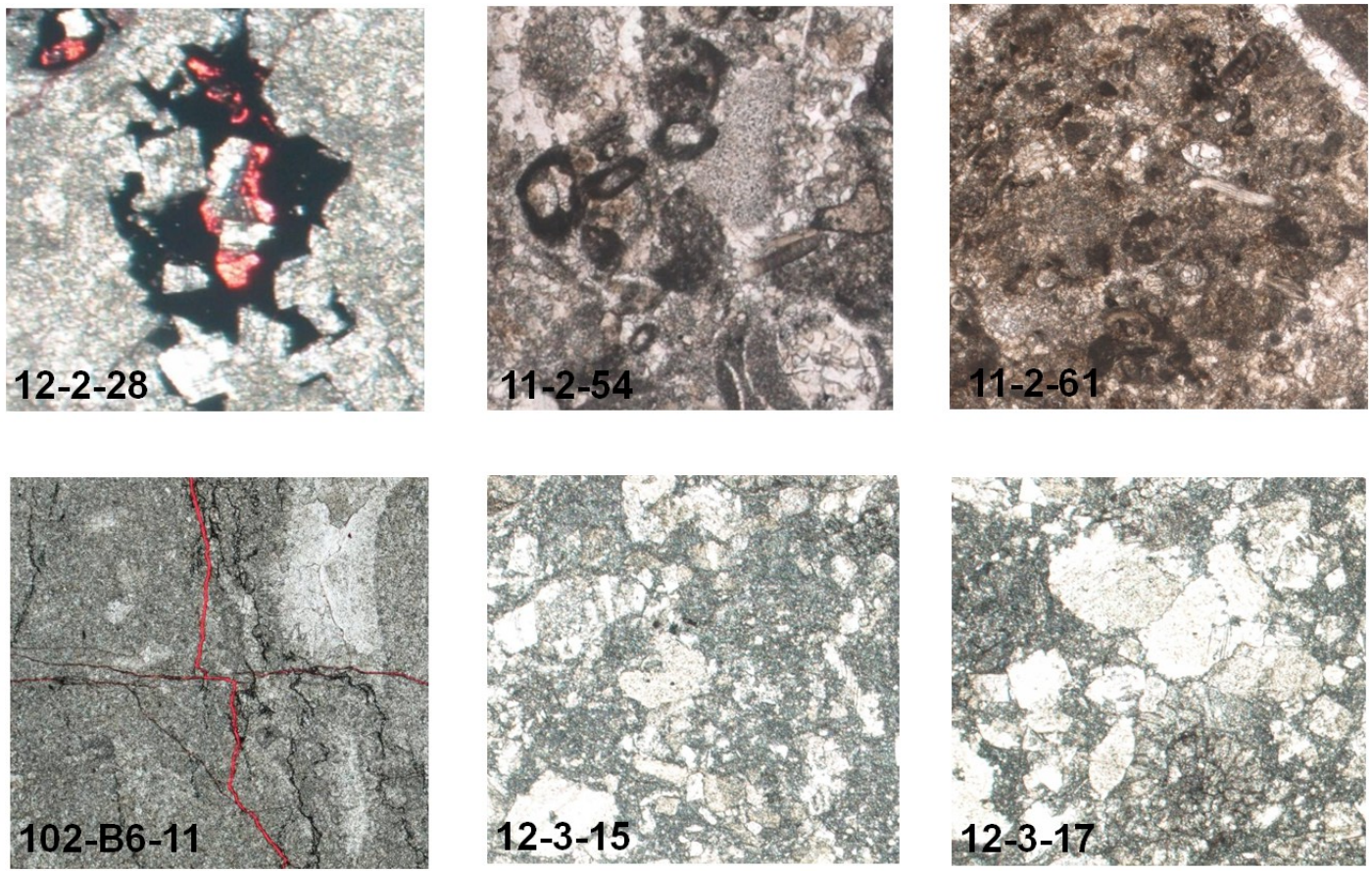

Figure 4.9 Thin Section Photos to Represent Mineral Composition, Pore Types and Diagenesis Events of Selected Samples, ChangXing Reservoir

given porosity as well.

Fracture or crack can cause a dramatic velocity decrease in low porosity reservoir. The velocity in group 3 is the lowest in zone A. As observed from the thin section analysis, the fracture which tends to make rock soft and decrease the aspect ratio dramatically in the carbonate rock accounts for the low velocity data in this group. A long and red color filled fracture is clearly visible across the tight matrix rock, which causes velocity decrease, however, an increase in reservoir permeability (Figure 4.9-d).

For the second zone B with a velocity variation of ~1500m/s at a porosity of ~6.6%, the velocity variation can be classified into three groups based on γ parameter as well. The samples in these three groups have the similar water saturation, which are lower than 50% (Figure 4.8). With the similar porosity and fluid content, the other possible factors causing compressional velocity variation might be the mineral composition, pore type and fracture. As observed from thin section analysis, it can be found that the major mineral composition of group 1, 2 and 3 in zone B are either dolomite or dolomitized limestone shown in Figure 4.10-a,b,c. However, a big difference between these groups is pore type. In group 2, the major pore type is interparticle between dolomite crystals with good sorting, which created with limestone being transformed into dolomite (Figure 4.10-b, c). In group 1, there are some dissolution pore spaces existing in the thin section besides interparticle pore space (Figure 4.10-a). The average diameter of these dissolution pore spaces is much bigger than that of the interparticle pore space that is visible in thin section. Capillary curve analysis also proves there are two major pore spaces existing in the group 1 of zone B.

From the column of pore diameter, it could be found there are two peaks of pore diameter, one is around 9.35 um and another is 0.034 um (Figure 4.10-d). Based on some studies, the large dissolution pore space, for example the round moldic or vuggy, tends to make the rock hard with high aspect ratio than that in micropore and consequently the wave moves faster than that in the rock lack of large dissolution pore space. The FMI data indicates that there are fractures developing in the group 3, which is the major reason causing the lowest velocity in zone B.

Relative homogenous pore type, mineral composition and fluid types explain a small velocity variation for the samples with high porosity. For points with porosity > 7% in ChangXing reservoir, velocity demonstrates very weak scattering at a given porosity. The thin section analysis shows that the major pore type is the interparticle (Figure 4.10-e, f). The major mineral composition is coarse dolomite with very good rhombic crystal shape and good sorting. Meanwhile, the water saturation of the samples with porosity >7% is <25%. However, an existence of two kinds of pore type mixture still could cause velocity scattering in high velocity range, even though this scattering is not so dramatic. For example, some samples with a porosity of ~12%, the velocity presents a considerable scattering, ~ 500m/s. This section analysis reveals that there are some big dissolution pore spaces existing in some samples, for example the sample of well 101-3-21 (Figure 4.10-d).

As a summary, it could be found that the pore types and mineral compositions variations and fracture are the major factors causing velocity-porosity complexity and this complexity could be characterized by γ parameter (Figure 4.11). For the zone with γ

parameter lower than 2.2, the major pore types are the mixture of two kinds of pore spaces, either a mixture of intercrystalline and interparticle or a mixture of interparticle and dissolution pore space, for example the moldic. The major mineral composition in this zone is dolomitized limestone or dolomite. For the sample with γ parameter between 2.2 and 6, its major pore types are either intercryslline or interparticle. For the sample with intercryslline pore type, it is developed in the low porosity zones in limestone. For sample with interparticle pore space, it is developed in the high porosity zones and its major mineral composition is dolomite and these interparticle pore spaces are created by the dolomitization. For the zones with γ parameter higher than 6, it is fracture zones which have been proven by thin section and FMI. Figure 4.11 is a classification of the pore types variation in velocity-porosity crossplot based on γ parameter.

DISCUSSION

In carbonate reservoir, permeability heterogeneity is much more intensive than that in clastic reservoir because of its complicated mineral composition, pore types and rock textures. How to characterize permeability heterogeneity is a big challenge for both geologist and geophysicist. The above studies show that frame flexibility factor (γ) is helpful to characterize carbonate reservoir pore type variation. Is that the γ parameter can be useful to delineate permeability heterogeneity?

Basically, porosity is the major factor that affects reservoir permeability in ChangXing gas reservoir, but the pore type variations are another important controlling factor at the similar porosity, especially in the zones with porosity lower than 5%.

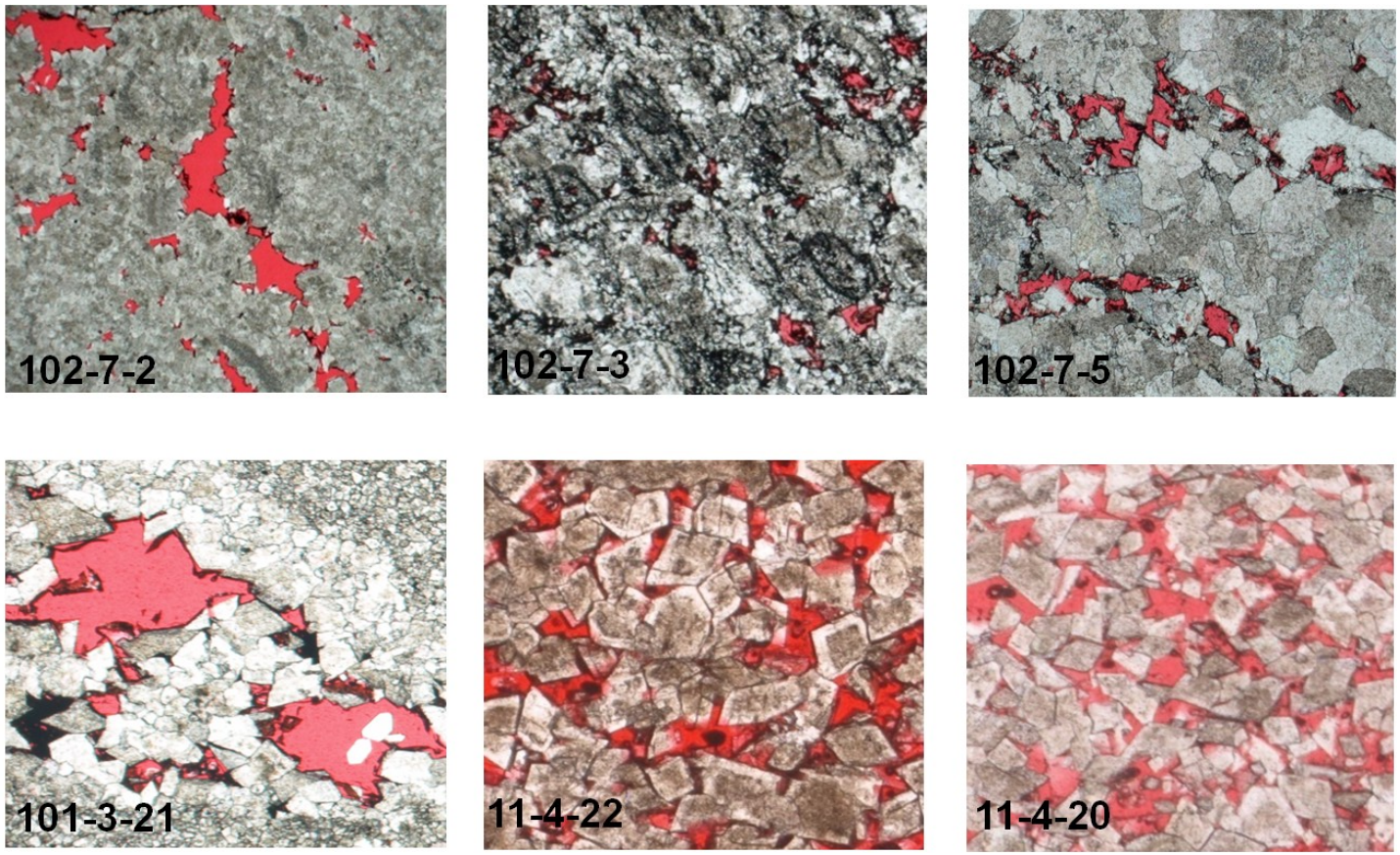

Figure 4.10 Thin Section Photos to Represent Mineral Composition, Pore Types and Diagenesis Events of Selected Samples, ChangXing Reservoir

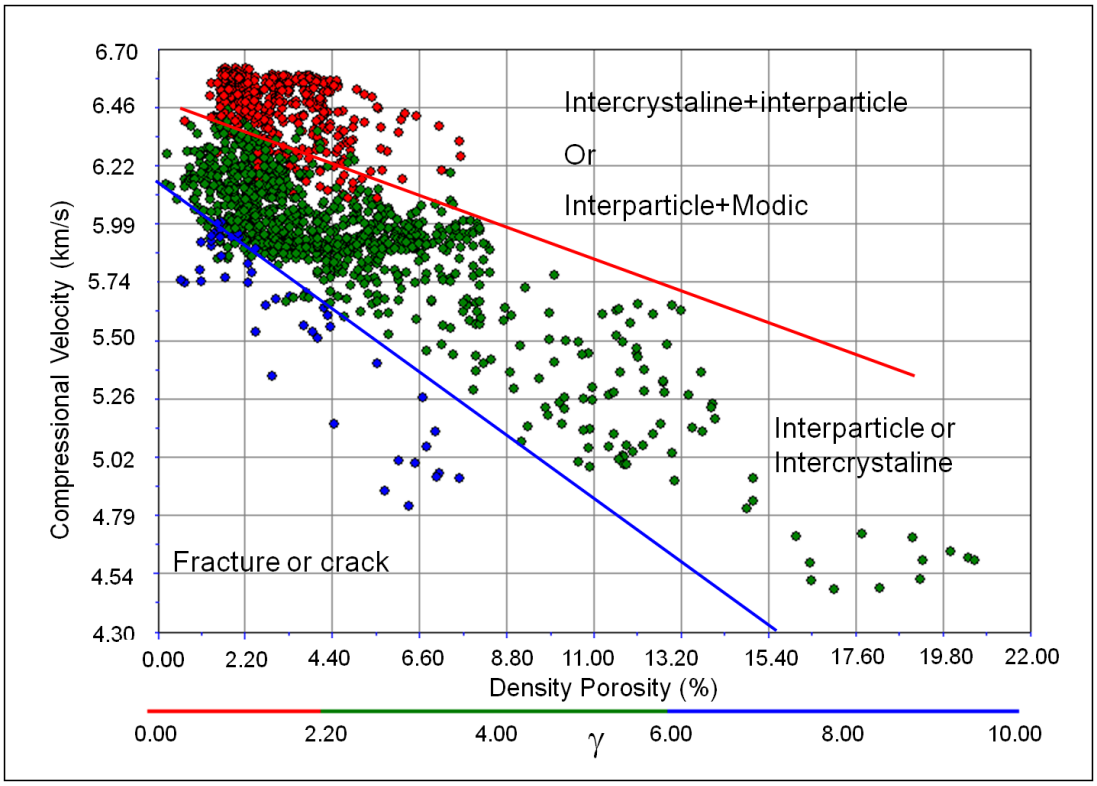

Figure 4.11 Density Porosity and Compressional Velocity with a Summary of Pore Types Indicated by γ

For example in zone A, group 1 and group 2 represent similar porosity around 2% (Figure 4.12-a,b), but the average permeability of group 1 is larger than that of group 2 by 2 orders, which are 0.12md and 0.0034md based on core samples lab measurement (Figure 4.12-d,e), respectively. Besides the mineral difference between these two groups, the major differences causing the permeability variations is the pore structure differences. For the sample in group 2, the major pore type is the intercrystalline invisible revealing by thin section analysis. Besides the invisible intercrystalline pore type in group 2

samples, some large interparticle or dissolution pore space developed by the dolomitization diagenesis. Based on the thin section imaging analysis, the peak pore diameter in group 2 is ~0.036um in group 2 samples, however, it could be high up to ~0.213 um in group 1 samples (Figure 4.13-a,b). The increasing pore throat in group definitely improve the reservoir permeability from lower than 0.001md to higher than 0.1md, which is higher enough for gas to flow in ChangXing gas reservoir.

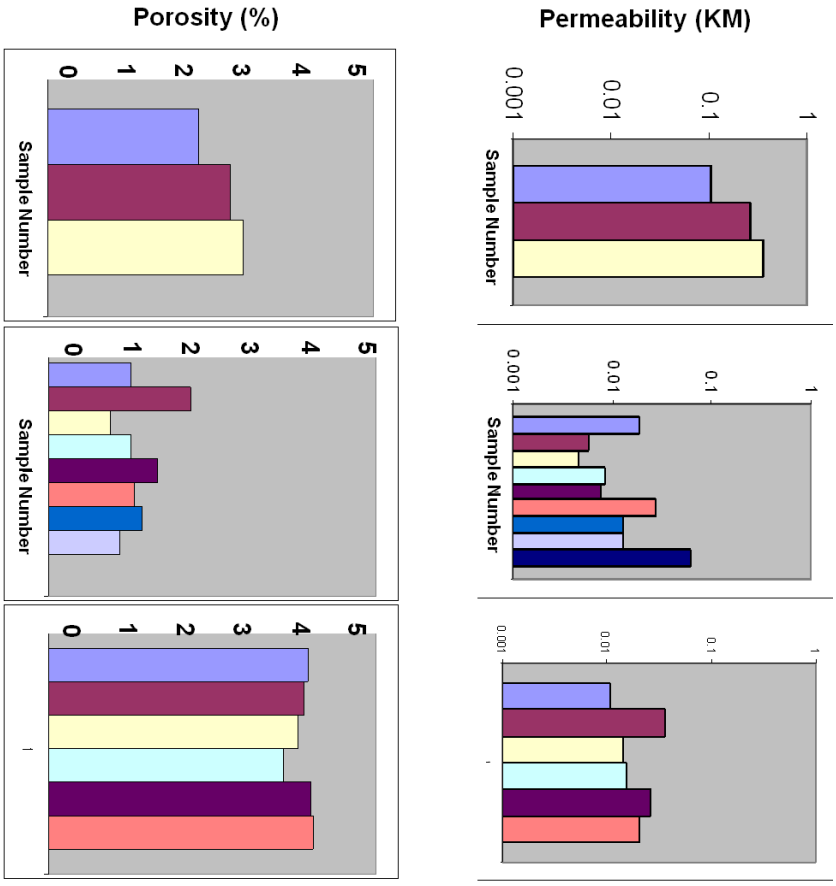

Figure 4.12 Porosity and Permeability Histogram of Core Measurement Samples

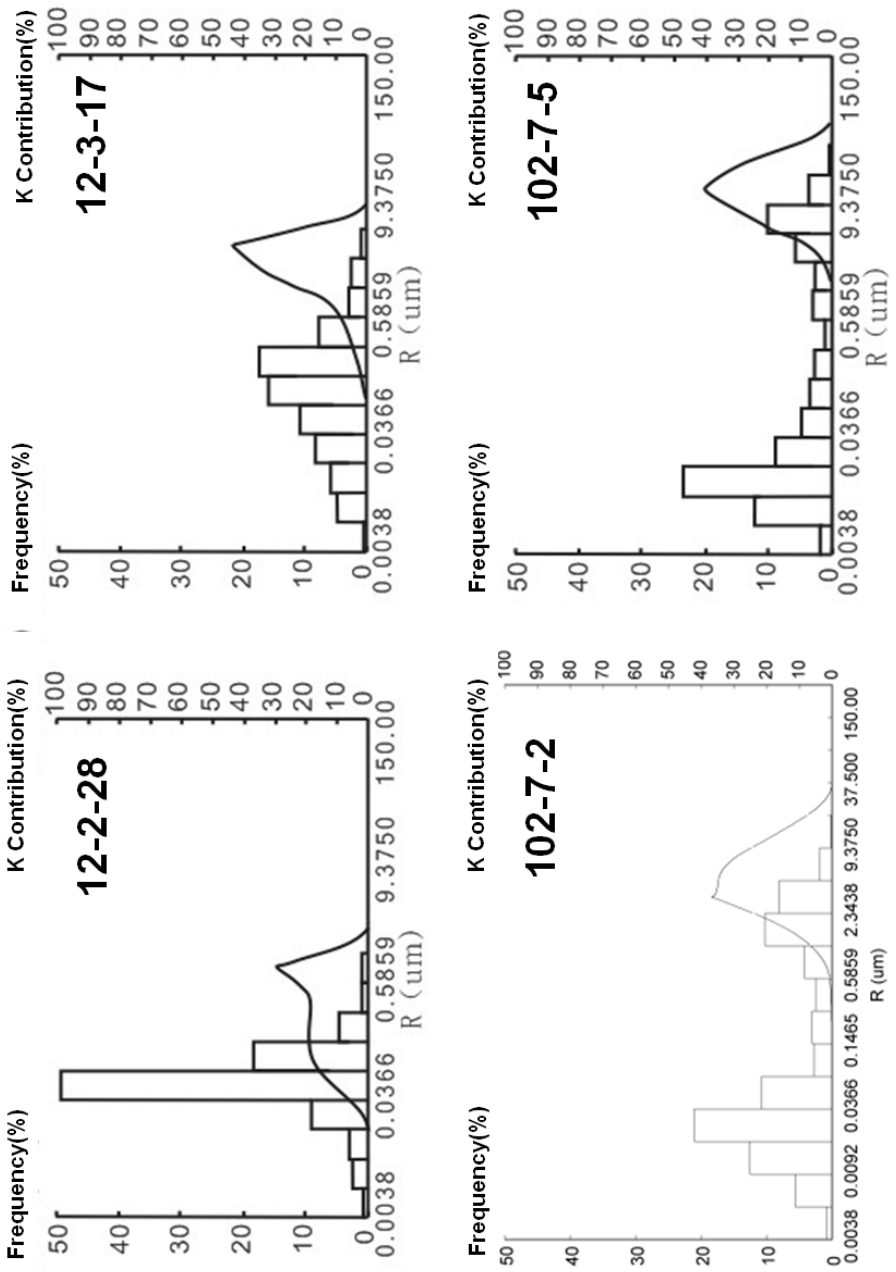

Figure 4.13 Histogram of Pore Throat Diameter from Core Sample Imaging Analysis

Compared to porosity, pore structure variation exhibits much stronger influences on permeability. As we discussed above, the samples in group 1 is a mixture of interparticle and intercryslline with an average porosity and permeability ~2% and ~0.12md learned from core measurements. The core samples in group 4 represent higher porosity than that in group 1, which is ~ 4%, however, lower permeability than that in group 1, which is around 0.032md (Figure 4.12-c,f). Thin sections analysis from these two groups reveals that there are lithological and pore types differences between these two groups. The major pore type of the samples in group 4 is micro-intercrystalline developed in clastic-carbonate deposition (Figure4.9-e,f). So, the above analysis proves that pore structure and pore types variation is another major factor affecting permeability in carbonate reservoir which can't neglected for reservoir evaluation.

For samples in zone B, pore type variation shows certain influences on permeability heterogeneity as well. For example, two samples from group 1 (well102-7-2) and group 2 (well102-7-5) in zone B which represent a permeability of 1.785md and 0.564md, respectively. Thin section analysis shows the pore type differences based on above study. For sample of well101-7-2, it demonstrates a mixture of interparticle and moldic pore spaces, however, it is dominated by interparticle in sample of ya102-7-5. Capillary curve and pore diameter analysis also prove the affecting of pore structure differences on permeability variations. For sample of well102-7-2, it second peak of high diameter is ~9.3μm, however, it is 2.34 μm in sample of well102-7-5, respectively (Figure 4.13-c, d).

For the samples with a porosity> 10%, the porosity is the major factor controlling permeability in ChangXing super-deep carbonate reservoir. The reason is that the main pore types for the samples in this porosity domain is interparticle, which means there is no large pore type or pore structure variation, and porosity is the main controlling factors to permeability heterogeneity. And 80% of with a porosity >10%, represent high permeability >1md.

For this low-grade reservoir with an average porosity lower than 5%, fracture is another important contribution to improve reservoir permeability. For example the sample well102-B6_11, its permeability is higher up to 26.56 md, however, with very low porosity ~ 2%. Thin section analysis reveals the fracture existing in this sample which improves reservoir permeability greatly. Based on the petrophysical analysis, the thickness of fracture zone is very thin, ~2-4 meters. So, it is a huge challenge to characterize fracture using conventional seismic data.

Another more important issue in reservoir description is the prediction of fluid types. Figure 4.8 is the density porosity- compressional velocity crossplot and the color bar is water saturation for ChangXing gas reservoir. From this Figure, it could be found the zones with a porosity > ~ 5%, it represents a very lower water saturation and consequently higher gas saturation, which could be classified as pure gas zones. Zones with a porosity varying from to 5% to 3.5%, the water saturation is demonstrate a big changes, however, 95% samples are less than 50%, which could be considered as a transition zone from gas to water. For the zone with porosity lower than 3.5%, it shows a huge water saturation variation from 0% to 100%. Further study reveals that pure water

zones with 100% water saturation is gathered in group 2 in zone A, however, group 1 and group 3 in zone A represent a low water saturation, <50%, which could be consider as a either gas zone or water-gas transition zones. Why these three groups with similar porosity represent a big water saturation differences? Based on the above analysis, the permeability in these three groups shows a big difference, the group 2 with lowest permeability ~0.001-0.01md, group 1 is much higher, >0.1md. The major geological factors affecting permeability is the pore type differences. For the samples in group 2, the major pore type is the micropore of intercryslline, however, it is a mixture of intercrystalline and interparticle for the samples in group 1. Group 3 is a fracture zone learning from thin section and FMI data. So, these pore type differences cause the permeability difference and consequently cause fluid type differences among these three groups. Higher permeability consequently benefits the hydrocarbonate accumulation.

Based on above analysis, the influence of pore type variation is very important in reservoir permeability and fluid evaluation. As a summary for ChangXing gas reservoir, the porosity is a major factor controlling permeability for the zones with porosity higher than 5%. For the zones with porosity lower than 5%, pore type variation affects the permeability more than the porosity does. Similar as permeability, pore types variation in low porosity zones is a key controlling factor for fluid differences as well. Figure 4.14 is crossplot of bulk module against γ parameter, and color indicator is water saturation. Combining these two parameters, gas zone, gas-water transition zone and water zones could be separated successfully. The points above pink curve are water zones and the

points below yellow curve are pure gas zone and it is gas-water transition between these two curves.

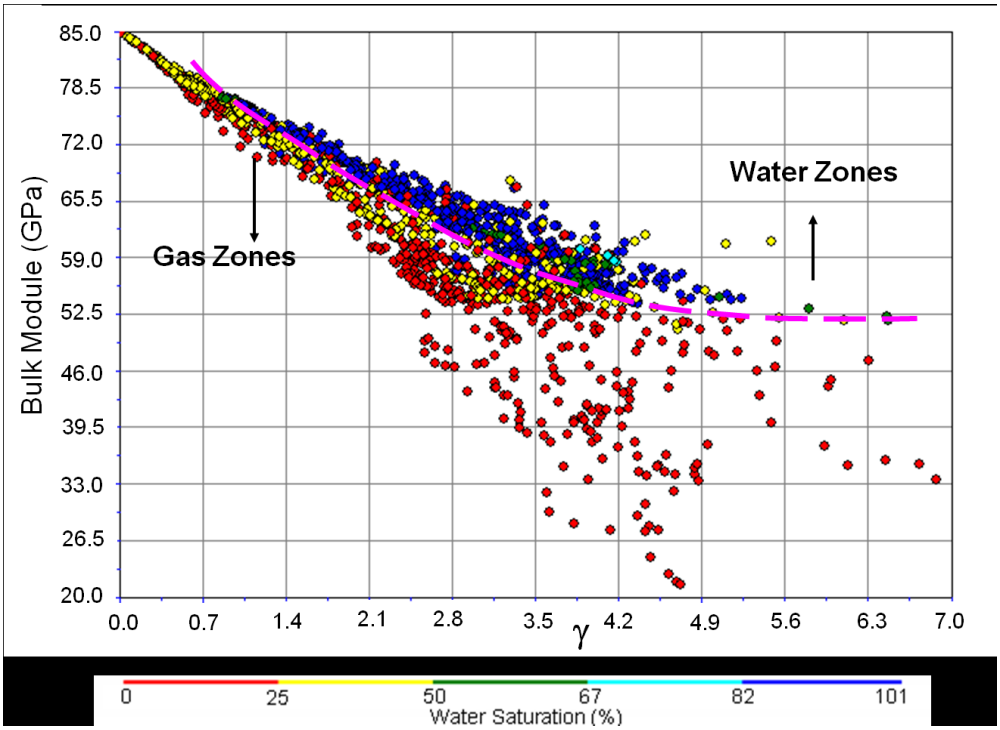

Figure 4.14 Crossplot of γ to Bulk Module for Fluid Type Identification with Water Saturation Color Bar

CONCLUSIONS

Field study from ChangXing low-porosity carbonate reservoirs proved that rock-physics based pore type evaluation approach is helpful for characterizing the influences of pore types variation permeability heterogeneity and improving fluid feature evaluation. The knowledge gained in this study is being used in seismic inversion of porosity and permeability under investigation.

CHAPTER V

POROSITY AND FRAME FLEXIBILITY FACTOR (γ) SEISMIC INVERSION AND RESERVOIR PERMEABILITY HETEROGENEITY EVALUATION

OVERVIEW

Petrophysical study demonstrates that in ultra-deep carbonate gas reservoirs with porosity < 5%, pore type variations and dolomitization could control permeability-porosity relationship and the spatial distribution of gas-bearing zones. A frame flexibility factor (γ) defined using a rock physics model is found to be able to classify different pore types and quantify their effects on acoustic wave velocity and permeability heterogeneity in low-porosity carbonate reservoir rocks. After calibration with core and log measurements, this parameter could be potentially estimated from seismic data. Nevertheless, how to use 3D seismic data to characterize pore types and further predict permeability heterogeneity in ultra-deep low-porosity carbonate reservoirs is a new challenge for reservoir geologists and geophysicists. For the first time, we report an integrated approach by combing angle-stack seismic inversion with the rock physics model to evaluate 3D variations of reservoir porosity, pore types and permeability heterogeneity for an ultra-deep carbonate gas reservoir, Sichuan basin, China.

Two-step seismic inversions are used to calculate reservoir porosity and frame flexibility factor (γ). In the first-step inversion, acoustic impedance, elastic impedance and shear impedance are obtained using model-based inversion method from angle-stack seismic data, which are functions of compressional velocity, shear velocity, density and

incident angle. Classified by elastic impedance, acoustic impedance and shear impedance are further used to derive density, compressional and shear velocity. In the second-step inversion, the rock physics model is used to calculate reservoir porosity and frame flexibility factor (γ). Porosity and frame flexibility factor (γ) are then combined to estimate reservoir permeability heterogeneity.

Compared to conventional methods of permeability calculation by which a best-fit function between porosity and permeability is usually used, our integrated approach results in a better permeability heterogeneity estimation which correlates quite well with the known high-permeability gas-bearing zones in the studied reservoir. This integrated approach could be useful for building accurate reservoir 3D model for similar deep low-porosity carbonate reservoirs worldwide.

INTRODUCTION

Based on the studies in Chapter III and IV, we understand that pore type variation is a major affecting factor on sonic velocity-porosity relationship and permeability heterogeneity in a carbonate reservoir. Using petrophysical data calibrated by core measurement and analysis, the influence of pore type changes on sonic velocity and permeability heterogeneity can be evaluated and characterized by a rock-physics-model based approach.

However, how to apply 3-D seismic data to evaluate porosity and pore structure variation and further to estimate permeability heterogeneity in carbonate reservoir is a huge challenge to geophysicist and geologist and there are few documents reported

about this study. A traditional method to derive porosity from seismic data is to transform seismic acoustic impedance data cube into porosity in terms of the best-fit function between acoustic impedance and porosity. This approach might be applicable for clastic reservoir with simple pore structure. The diversity of pore types in carbonate reservoir causes a complex relationship between acoustic impedance and porosity as well, just like that existing between the compressional velocity and porosity.

Gartner et al., in 2006 proposed an approach by using 3D seismic data to evaluate carbonate reservoir pore structure variations and then relate a pore geometry factor to matrix-dominant permeability at a given porosity for a single mineralogy and great volume of thickness Middle East carbonate reservoir. Based on their study, the pore geometry factor could describe 3D pore structure and connectivity and therefore be related to permeability, which could be extracted from post-stack data. This is the first time to estimate carbonate reservoir pore structure variations and is a major step forward to evaluate average interval matrix permeability from 3D seismic data as well.

One limitation for post-stack seismic data is that velocity information that could be extracted is just compressional velocity, however, without shear velocity. Based on the study in Chapter IV, the frame flexibility factor (γ), which is effective in pore type variations delineation for carbonate reservoirs, is a function of bulk density, compressional and shear velocity. In order to get compressional and shear velocity and bulk density, pre-stack seismic data is useful and necessary. In this chapter, a approach about porosity and frame flexibility factor (γ) inversion and further permeability

heterogeneity evaluation would be tested by using post-stack and angle-stack seismic data from a ChangXing gas reservoir, Sichuan Basin, Central China.

METHODS

Two-step inversion would be used to estimate porosity and frame flexibility factor (γ) from post-stack and angle-stack seismic data. The first step is to conduct conventional seismic inversion so as to get acoustic impedance, elastic impedance and elastic shear impedance, which are the function of bulk density, compressional velocity, shear velocity and incident angle. The second step is to derive porosity and frame flexibility factor (γ) from above impedance data cubes by integrating rock physics model.

In order to ensure the well-to-well accuracy, consistence and comparison, multi-well normalization is necessary, especially for compressional and shear velocity and bulk density curves. For the model-based inversion, a very important part during this procedure is to build an initial model from well log by interpolation and extropolation between wells and outside of wells. However, a reality is that well log collection would cover a very long time as well as may be collected by different tools for an old field with a long production history. So, this collection time and tools differences would cause inconsistencies for a multi-well log analysis, which would transport a well log tool's error into subsurface reservoir geological interpretation from well log. Large practical experiences prove that there are >50% of wells requiring some normalization for superior accuracy in reservoir characterization.

Seismic inversion has been widely used in reservoir geophysical characterization since the 1970s, which could transform seismic reflection data into a quantitative reservoir rock and fluid property parameters, such as porosity, clay content and water saturation and so on. Because seismic inversion could be referred as a form of deconvolution in theory, it could create a higher resolution display by removing wavelet from seismic data.

Basically, there are three kinds of seismic inversion methods including band-limited or Recursive Inversion (Lindseth, 1978), Sparse-Spike and Model Based (Hampson and Russell, 1991) based on inversion algorithms differences.

For the first two inversions methods, all the problems in the seismic data itself could be as part of the final inversion result, for example, noise, poor amplitude recovery as well as the frequency band-limited nature of seismic data.

In order to weaken the influences from the above problems in seismic inversion, model-based inversion is proposed by Hampson and Ressell in 1991. In this approach, a geological model will be built first and then compare this model to real seismic data. The comparison between real data and model is used to iteratively update initial model as to better match the seismic data. Mathematically, the above method could be written as,

$$F(M) = F(M_0) + \frac{\partial F(M_0)}{\partial M}\Delta M \quad \text{.....5.1}$$

where M_0 is initial geological model, M is true earth model, $F(M_0)$ is calculated values from initial model; $F(M)$ is observation; ΔM is change in model parameters, and

$\frac{\partial\ '(M_0)}{\partial\ 1}$ is change in calculated values. The error between the observation and computed values could be written into a matrix equation:

$$\Delta F = A\ \Delta M \quad \text{.....5.2}$$

where A is a matrix of derivatives with n rows and k columns.

Using lease square method, ΔM could be solved and is written as:

$$\Delta M = (A^T A)^{-1} A^T \Delta F \quad \text{.....5.3}$$

Basically, the initial model is built from the well log and horizon interpretation from seismic data. So, the final inversion results not only tie to all the wells and also honor all the seismic data, which could be considered as a combinations of well logs and seismic data. In this study, model-based seismic inversion would be used to conduct impedance inversion.

In terms of seismic data type, seismic inversions consist of post-stack, pres-stack and angle-stack inversion. In post-stack seismic inversion, acoustic impedance section or data volume could be generated, which is related to reservoir lithology and fluid features. One limitation in post-stack inversion is that only compressional velocity can be derived from seismic data. For the carbonate reservoirs with complex pore structure, a combination of shear velocity with compressional velocity is much helpful for fluid discrimination and permeability heterogeneity evaluation. So, pre-stack seismic inversion was used widely when post-stack inversion failed in some cases sometimes. Not only acoustic impedance but also shear impedance and density as well could be derived from pre-stack seismic inversion. Consequently, V_p/V_s ratio or Possion ratio

could be calculated from shear and acoustic impedances to improve fluid and lithology identification. However, one limitation in pre-stack inversion is the huge calculation, which limits its application widely.

A more robust and simple approach is to use post-stack seismic inversion method on angle-stack seismic data so that not only avoid the huge calculation in pre-stack inversion but also shear velocity could be extracted from angle-stack data. This angle-stack inversion mainly includes the elastic impedance inversion proposed by Connolly in 1999 and elastic shear impedance inversion introduced by Duffaut et al., in 2000.

By approximating the linearization of the Zoeppritz equation for P-wave reflectivity in a low incident angle range, elastic impedance (EI) is expressed as,

$$EI = \gamma_p^{(1=\tan^{2\theta})} V_S^{(-K\sin^2\theta)} \rho^{(1-K\sin^2\theta} \quad \text{.....5.4}$$

where: V_p, V_s and ρ are P-wave, S-wave and density, respectively. θ is incident angle and K is average ratio of P-wave to S-wave in study interval, which could be obtained from well log analysis.

In terms of the above formula, *EI* is a generation of acoustic impedance at variable incident angle, which could be applied to calibrate and invert nonzero-offset seismic data in the way as the *AI* does at zero-offset data.

Similar to *EI*, shear wave elastic impedance could be used to link P-S wave reflection to wells using a linearization of the Zoeppritz equation and it is written into,

$$SEI(\theta = \gamma_s^{m(K,\theta} \rho^{n(K,\theta} \quad \text{.....5.5}$$

where

$$m(K,\theta = 4K\sin(\theta [1-\frac{1}{2}(1+ 2K)\sin^2(\theta] \text{.....5.6}$$

$$n(K,\theta = 1+ 2K)\sin(\theta [1-\frac{K(1+ .5K)}{1+ 2K}\sin^2(\theta \text{.....5.7}$$

where K is V_p/V_s ratio and θ is incident angle. When V_s/V_p is 0.5 and incident angle close to critical angle, *SEI* approximately equals to shear impedance (*SI*).

In order to conduct angle-stack inversion to get *EI* and *EI* using the approach as AI inversion does, angle-stack processing is necessary. Now, it is a common technique to do partial offset data volume processing from 3-D seismic sets to obtain AVO information and the most common offset consists of near, middle and far offset which are lower than critical incident angle.

How to relate the above three impedances to porosity and flame flexibility factor (γ) is a key part for second step inversion. Two approaches would be used to derive porosity and flame flexibility factor (γ) from the above three impedances.

Basically, all of the three above inversed impedance either from post-stack or angle-stack is the function of compressional velocity, shear velocity, density and incident angle. Based on the two fundamental compressional and shear velocity formula below, the impedance and some related AVO parameters could be expressed into bulk and shear module:

$$V_p = \sqrt{\frac{K+\frac{4}{3}\mu}{\rho}} \text{.....5.8}$$

$$V_s = \sqrt{\frac{\mu}{\rho}} \text{..... 5.9}$$

where V_p and V_s are compressional and shear velocity, K, μ and ρ are the bulk module and shear module and bulk density.

The first method tested in this study is to calculate K, μ from the above three impedances and then derive porosity and γ from K and μ. By combining these three kinds of impedance, bulk density could be removed from bulk and shear module calculation as followings:

$$\frac{EI}{AI^{(2c-\quad)}} = K + \frac{4}{3}\mu^{(a+\ .5b-\ )}\mu^{\ .5b} \qquad \text{.....5.10}$$

$$\frac{Lambda}{AI^2} = \frac{3K - 4\mu}{3K + \ \iota} \qquad \text{.....5.11}$$

where K and μ are written as the following by using rock physics model introduced by SUN, respectively,

$$K = \frac{K_s[(1-\ \text{Þ})^{\gamma}(\Phi K_f - \ \text{Þ}K_s + K_f) - K_f]}{K_f(1-\phi^{\ \gamma} - K_f + (K_f - K_s)\Phi} \qquad \text{.....5.12}$$

$$\mu = \iota_s(1-\ \text{Þ}^{\ \gamma} \qquad \text{.....5.13}$$

where EI is elastic impedance; AI is acoustic impedance; Lambda is lame's constant which is a function of acoustic impedance and shear impedance; K and μ are bulk and shear module; a, b, c are constant coefficient in elastic impedance calculation (Connolly, 1999); $\varnothing$ and γ are porosity and frame flexibility factor respectively; K_s, K_f, and μ_s are frame and fluid bulk modulus, matrix shear modulus, respectively, d is gamma ratio (Sun, 2004).

The above four equations reveal a non-linear relations between impedance data volumes and frame flexibility factor (γ) as well as the porosity. By solving the above equations, the porosity and γ can be determined from *EI, AI* and *Lambda*. One assumption in applying the above method to calculate porosity and γ is that the knowledge of K_s, K_f, and μ_s are required.

The second approach applied in this study is to derive bulk density, compressional velocity and shear velocity first from acoustic impedance, shear impedance and elastic impedance and then calculate porosity and γ using introduced rock-physics model. The formula to calculate bulk density derived from the above three impedances is written as,

$$Den = \left(\frac{EI}{AI^{a} SI^{b}}\right)^{\frac{1}{c-1-}} \quad \text{.....5.14}$$

where *Den* is bulk density, *EI, AI and SI* are elastic impedance, acoustic impedance and shear impedance, respectively; a, b, c are constant in *EI* formula, which is related to incident angle and ratio of shear velocity to compressional velocity. After bulk density calculation, acoustic impedance and shear impedance are used to derive compressional and shear velocity.

Finally, we also would compare the permeability calculated by the above proposed approach to which from conventional method of best-fit function between permeability and porosity.

RESULTS

Multi-well normalization is conducted to get an accurate and consistent well log data for building forward model before seismic inversion. In multi-well normalization, a key step is to select a standard depositional layer. Two key criteria for standard depositional layer: an enough extending area as well as similar depositional features. Enough extending space could ensure that standard layer is correlated in most wells of studied reservoir (~90% wells) at a similar depth range. Similar geological feature is to ensure that the well log differences in standard layer from each well are mainly caused by tool calibration differences but not subsurface reservoir geological variations. Based on the above two major criteria, the standard layer used in multi-well normalization generally is a marine shale, low porosity carbonate or evaporate deposition layer. A marine shale deposition in the upper Feixianguan formation is selected as standard depositional layer with an average thickness of ~30 meters for ChangXing gas reservoir, Sichuan Basin, Central China. This layer is easily correlated in each well over the entire fields with a very high GR and Low resistivity values comparing to nearby layers, see Figure 5.1.

Totally, there are three kinds of methods to conduct multi-well normalization, including histograms, crossplots and depth-based logs. Histogram normalization is widely used to correct errors caused by tool calibration, which is a plot of frequency of data vs data values, referred as a distribution by statistics. Basically, the mean, mode and standard deviation and number of samples are documented. Histogram normalization method is used to finish multi-well normalization.

Four wells in this field will be normalized for density, compressional and shear velocity. During this procedure, the histogram of Well 12 was used as standard histogram. The other four wells were normalized by comparing individual histogram with standard histogram for each well log curve. Figures 5.2, 5.3, 5.4 are the histogram of bulk density, compressional and shear velocity of each well.

Production data is used to test multi-well normalization result. Figures 5.5 and 5.6 are the AI forward model across Well 101 before and after multi-well normalization. After normalization, a reservoir layer in ChangXing formation with low AI is easily identified in AI section, meanwhile its AI differences from Well 12 well is decreased apparently. The difference after well log normalization agrees with production data much well between these two wells, which are ~300,000 m^3 and ~ 400,000 m^3, respectively. So, the multi-well normalization in this field ensures the accuracy and consistency of each curve from these 4 wells by removing the relative errors from tool calibration of each well.

Acoustic impedance, elastic impedance and shear elastic impedance inversion from near-off set and far-off set angle-gather seismic data are conducted after multi-well normalization. Figure 5.7 is a wavelet extracted from seismic data around Well 12, Well 11, Well 101 and Well 102 by statistic method. In the time domain, wavelet represents a near zero-angle phase with a strong peak at zero-angle and symmetric as well as weak side reflection. This zero-angle phase wavelet extracted from seismic data is an almost ideal wavelet for seismic inversion and deconvolution processing.

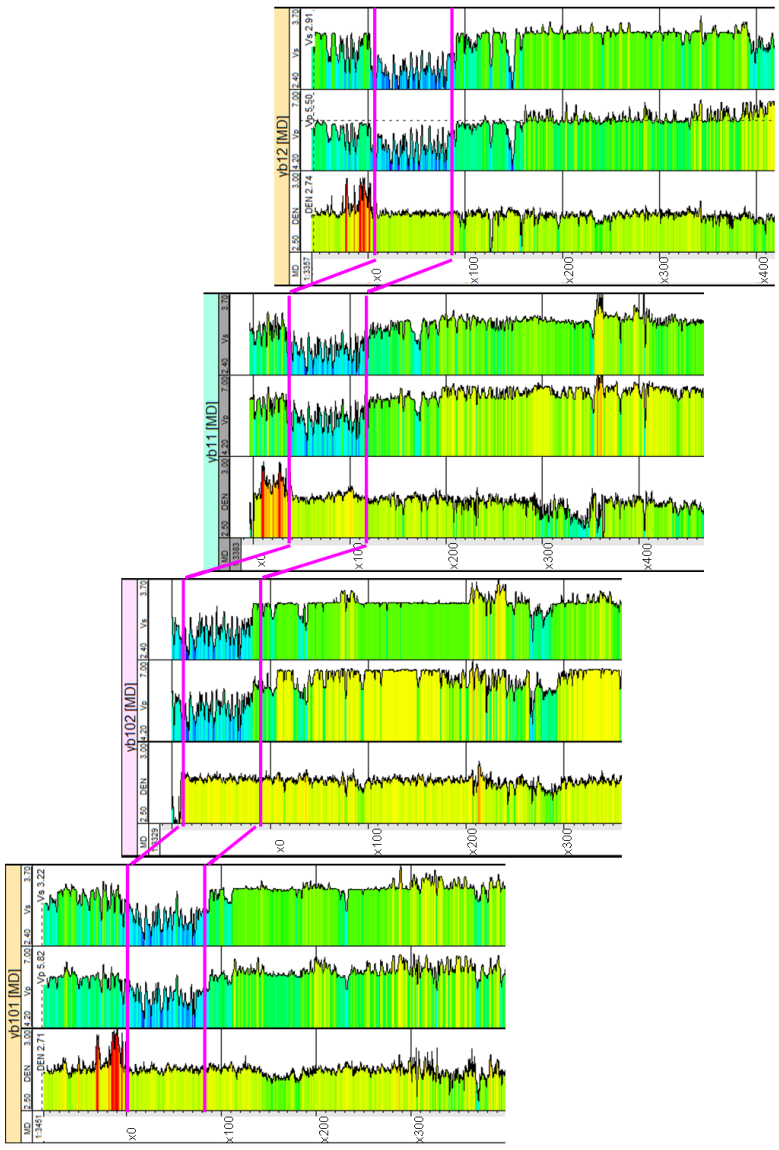

Figure 5.1 Cross-section from Well 101 to Well 102, which Shows the Depth Interval of Standard Layer within the Pink Box

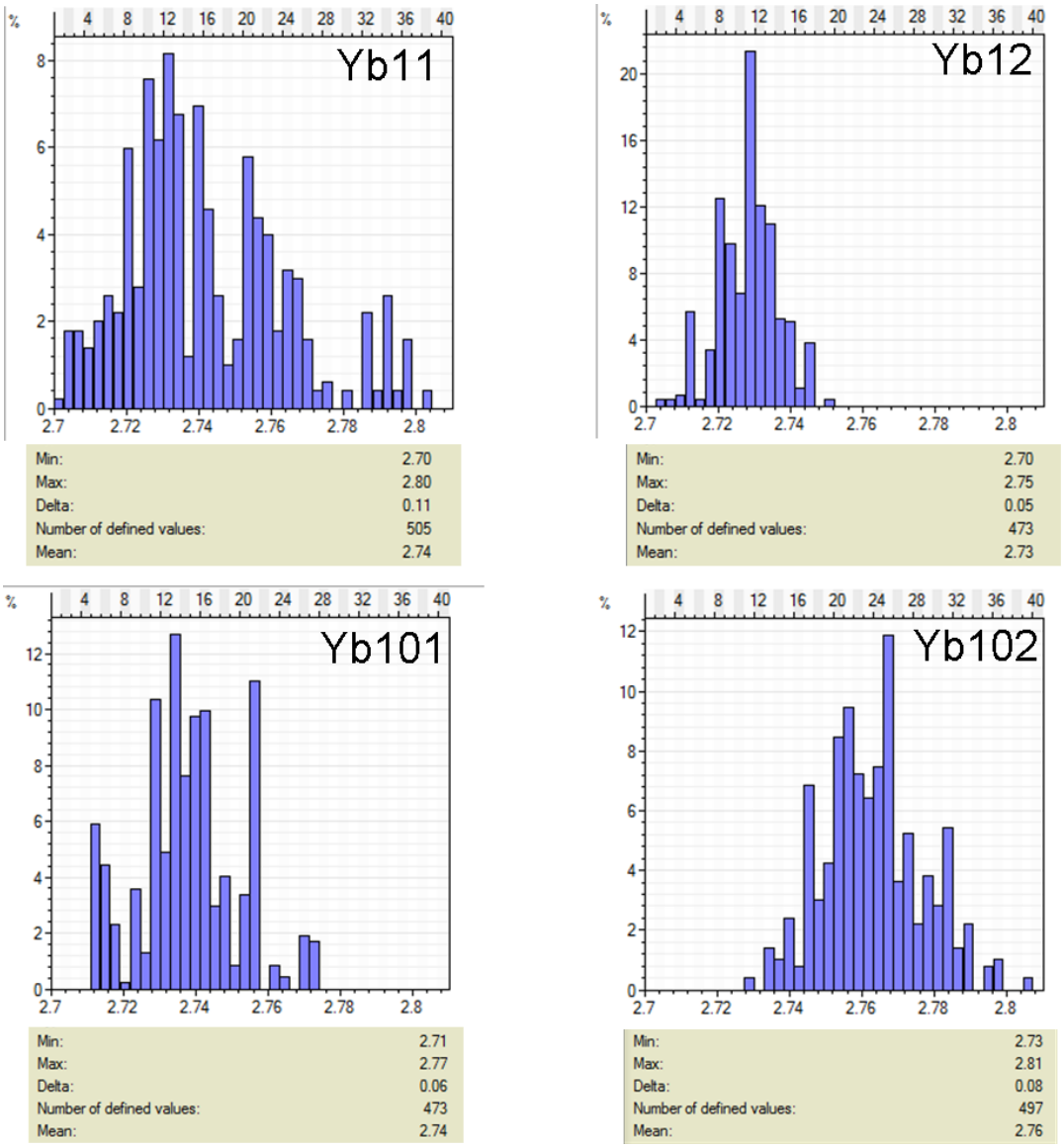

Figure 5.2 Density Histogram of Standard Layer for Well 11, Well 12, Well 101 and Well 102

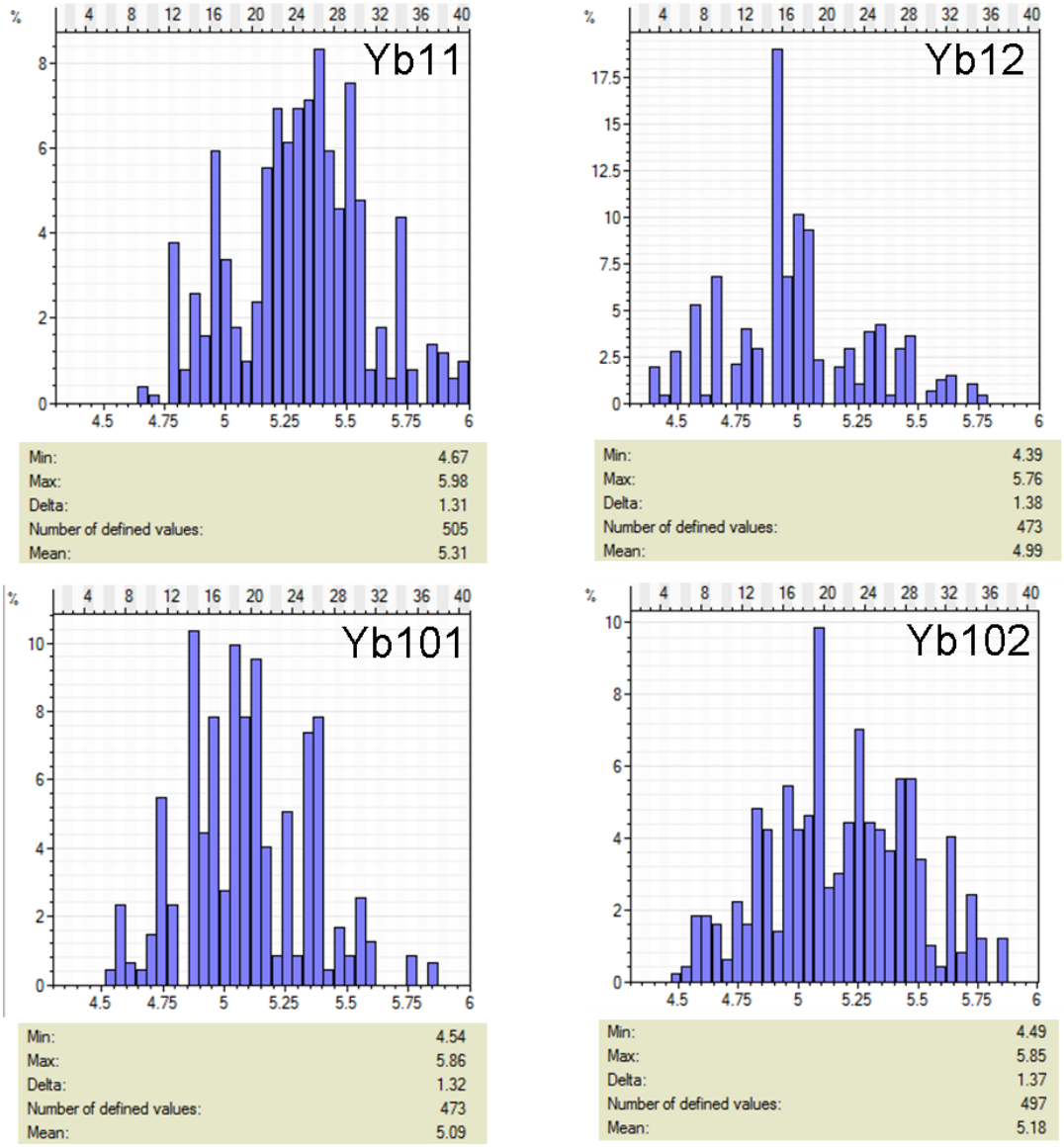

Figure 5.3 P-wave Histogram of Standard Layer for Well 11, Well 12, Well 101 and Well 102

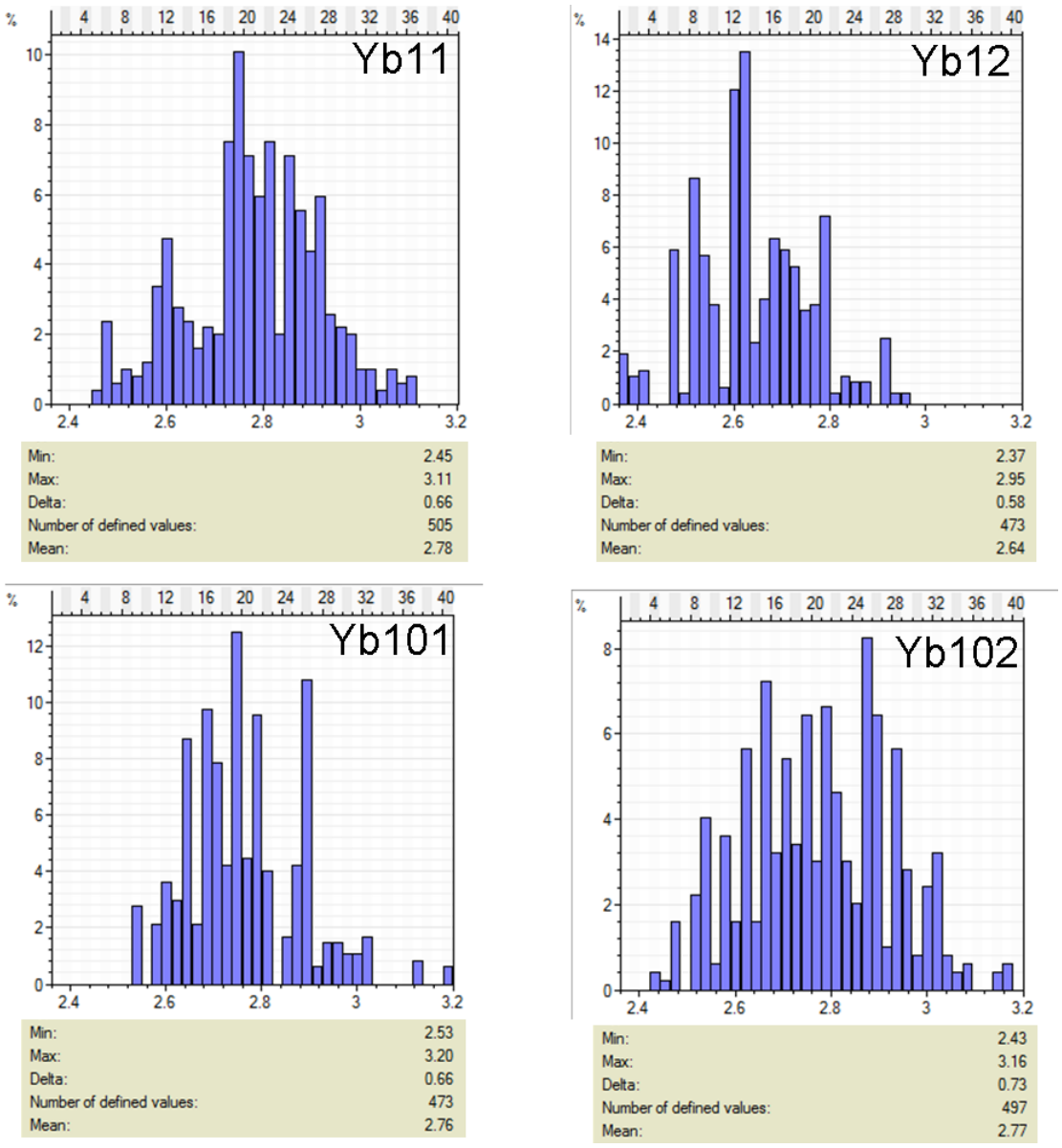

Figure 5.4 S-wave Histogram of Standard Layer for Well 11, Well 12, Well 101 and Well 102

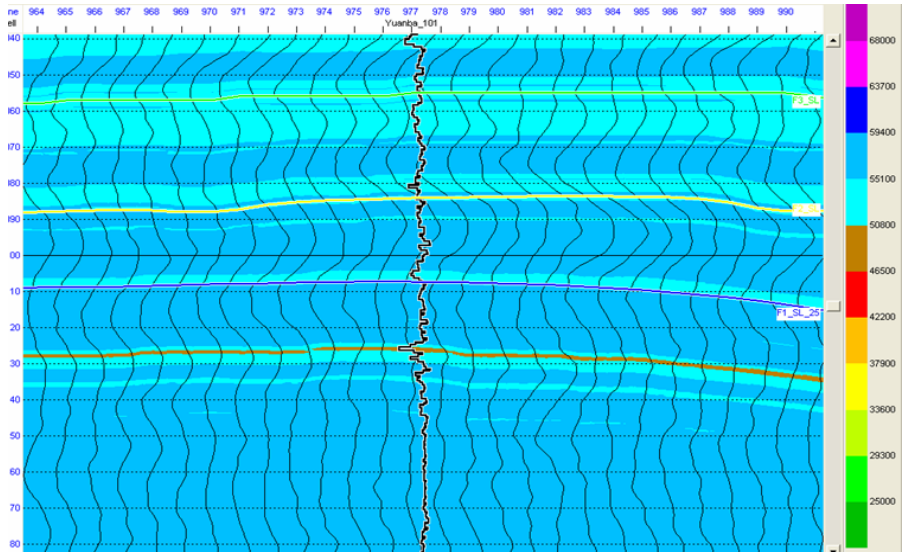

Figure 5.5 Acoustic Impedance Forward Model Section across Well 101 before Multi-well Normalization

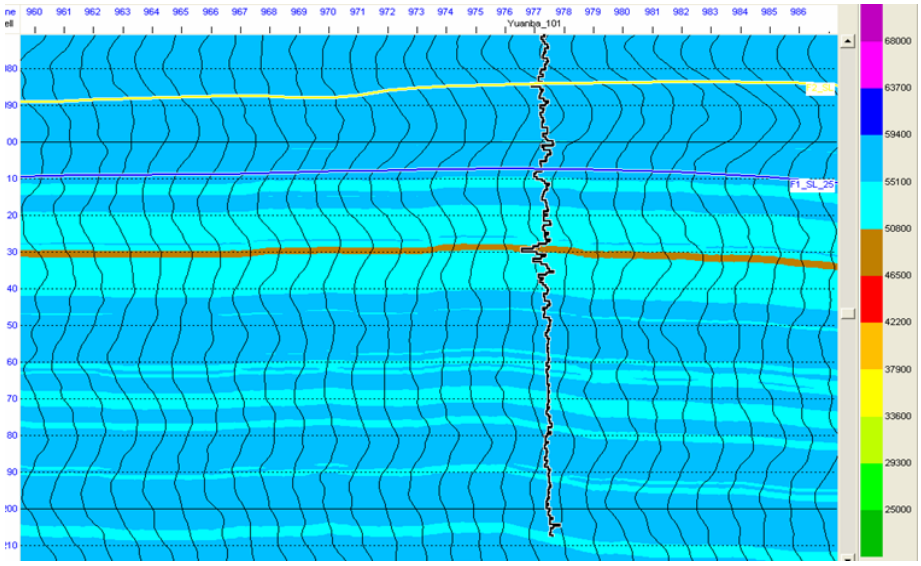

Figure 5.6 Acoustic Impedance Forward Model Section across Well 101 after Multi-well Normalization

Figure 5.8 is a synthetics for Well 12 which represents a very good match between real seismic trace and synthetics. Three major reflection interface featured by strong peak reflection, which is around the top of T2L, bottom of T2L and between T1f3 and T1f4 can be traced clearly in not only synthetics trance but also three angle-stack seismic data volume of 0-8°, 8-16° and 16-24°. The gas zone in ChangXing reservoir is within a trough (see the box zone in Figure 5.9) with a lower compressional and shear velocity, lower density and lower resistivity compared to the surrounding layers and apparent separation between deep-resistivity and shallow-resistivity curves, a typical feature of gas saturated layer.

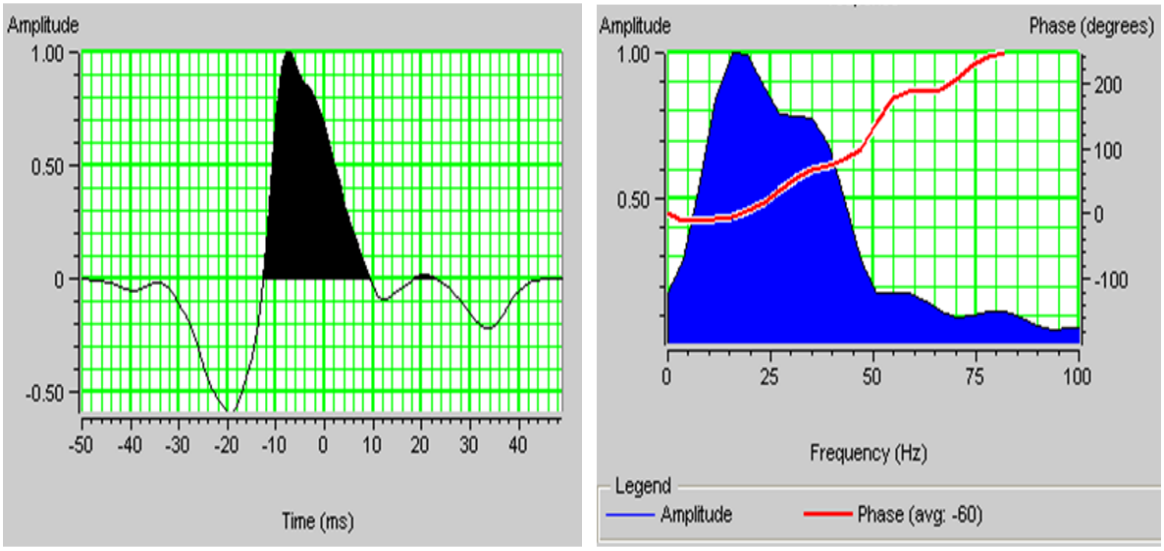

Figure 5.7 Wavelet Extracted from Seismic Data around Wells by Statistic Method. The Right: Wavelet in Time Domain; The Left: Wavelet in Frequency Domain

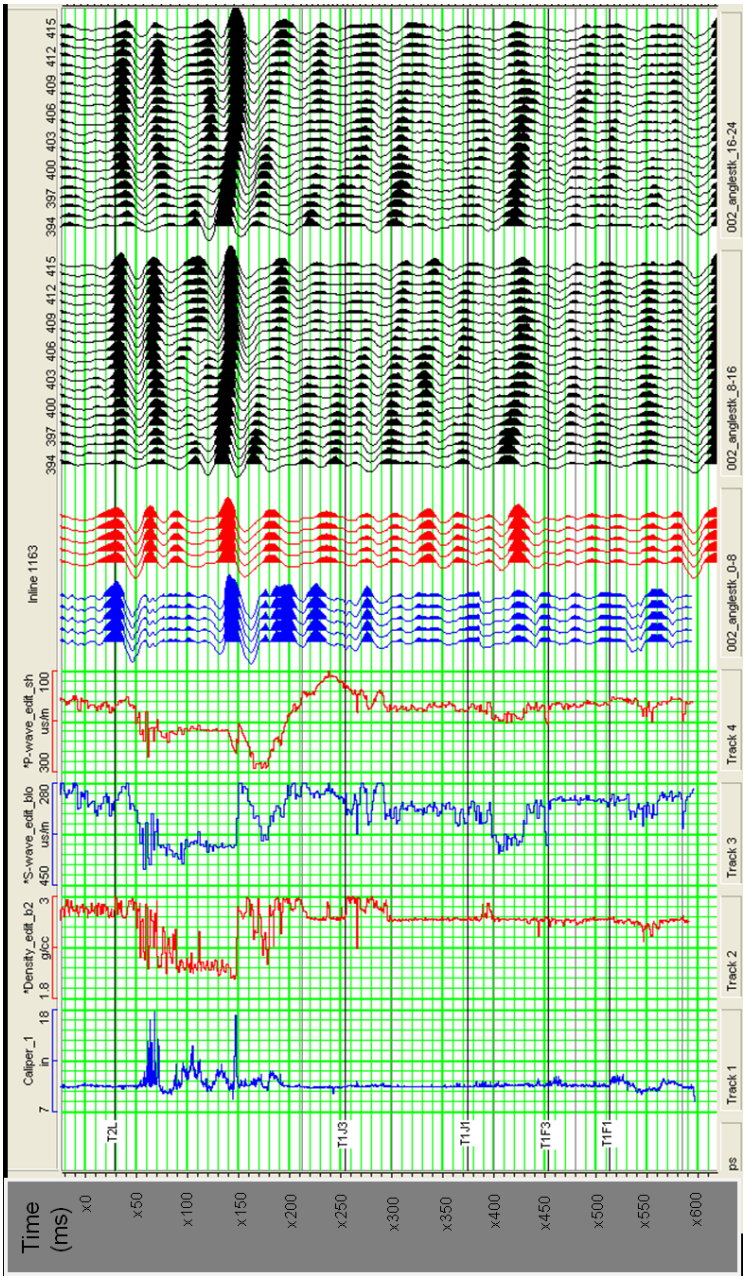

Figure 5.8 Synthetics of Well 12, which Matches with the Real Seismic Data Very Well

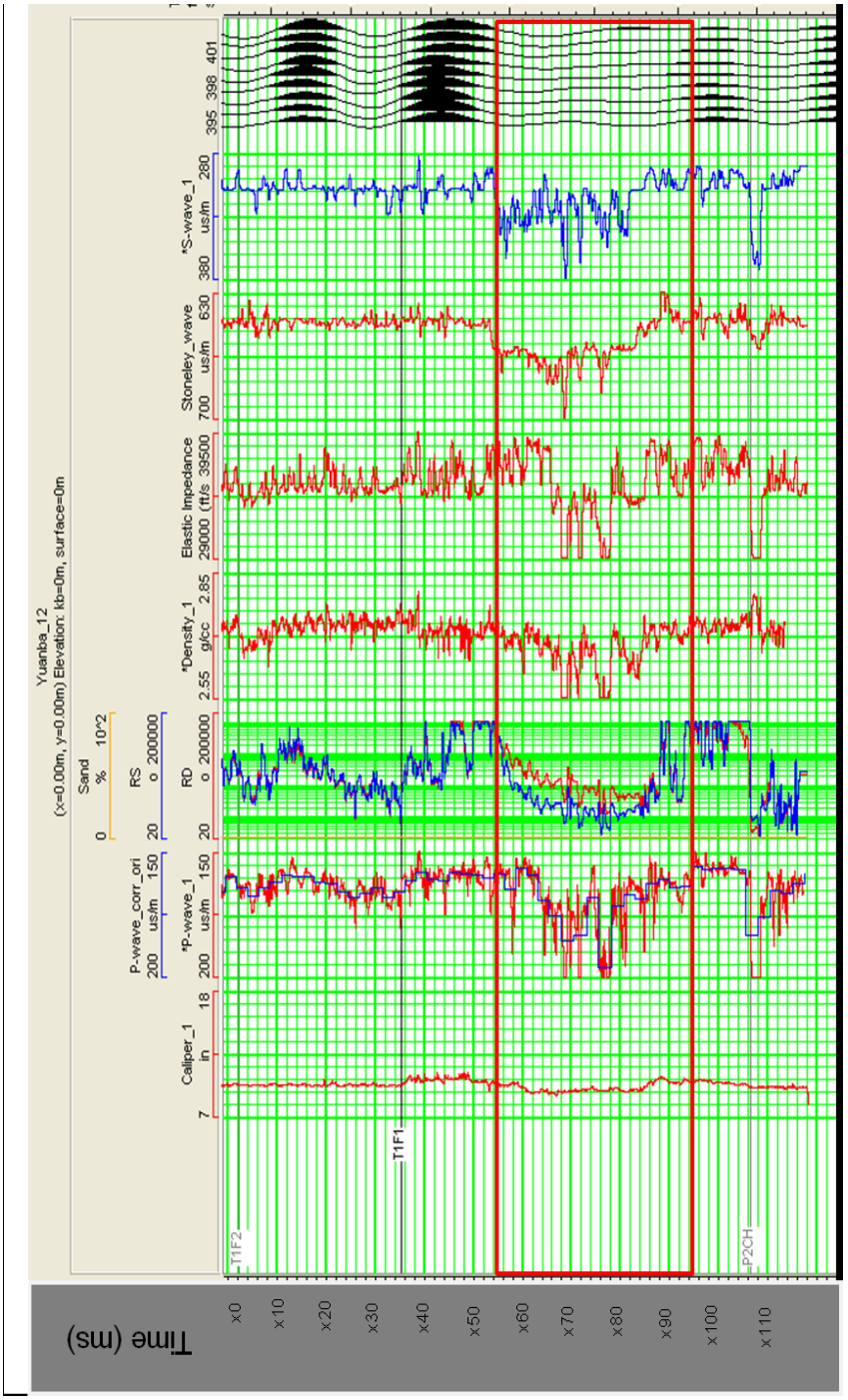

Figure 5.9 Petrophysical Feature of Reservoir Zone in Well 12

Figure 5.10 is an arbitrary seismic line from 0-8 angle-stack seismic data volume and it is across Well 12, Well 11, Well 101 and Well 102. The synthetics of each well are overlapped on this arbitrary section, which demonstrate a good match between synthetics and real seismic traces around each well. This arbitrary seismic line is used to test the proposed approach for porosity and frame flexibility factor (γ) inversion from seismic data.

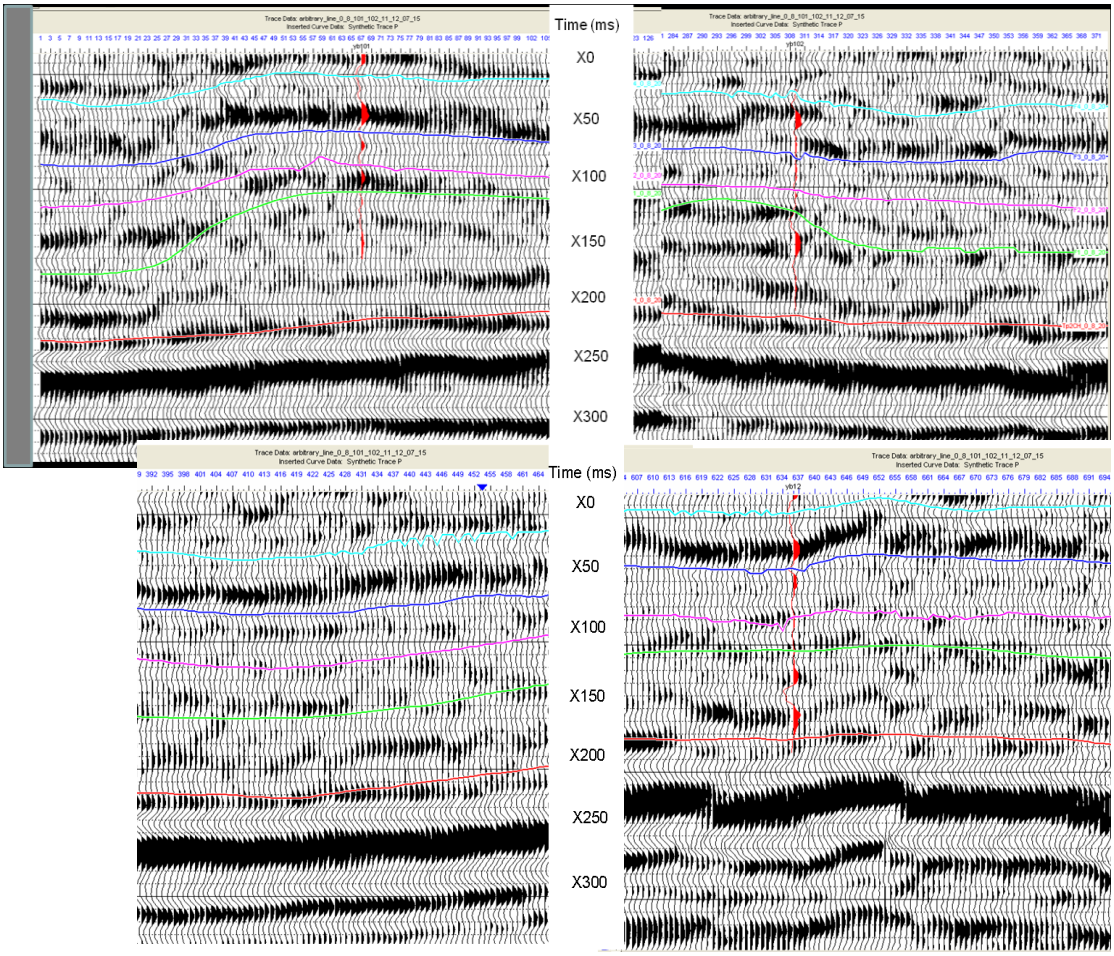

Figure 5.10 Arbitrary Seismic Section across Well 101, Well 102, Well 11 and Well 12 Posted with Synthetics of Each Well

Using model-based seismic inversion method, acoustic impedance is inversed from 0-8 ° angle-stack seismic data volume and elastic impedance and shear impedance are inversed from 8-16 ° angle-stack seismic data volume. Figures 5.11, 5.12, 5.13 are acoustic impedance, elastic impedance and shear impedance, respectively across Well 12 and Well 11. Calibrated by log curves, gas zones in these two sections are featured by low acoustic impedance, low elastic impedance and shear impedance. The sea-level variations cause sequence and depositional facies changes representing in three impedance section. On the platform crest around Well 12, shoal dolomitized oolite is developed with low impedance features.Far away from platform-margin to either basin or inner ramp, fine-size limestone or bio-limestone is developed featured by high impedance.

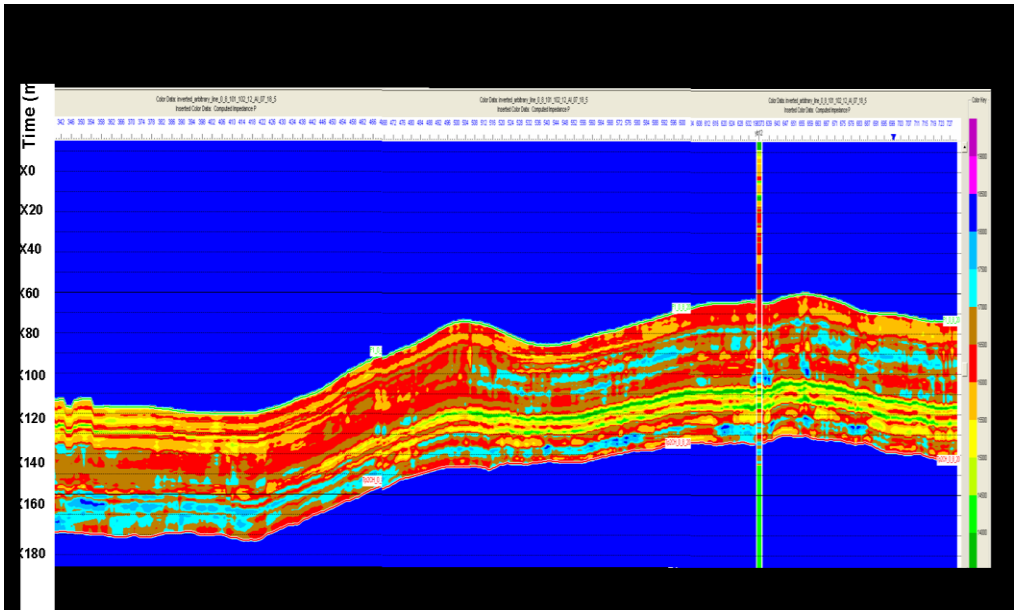

Figure 5.11 Acoustic Impedance Inversion Section across

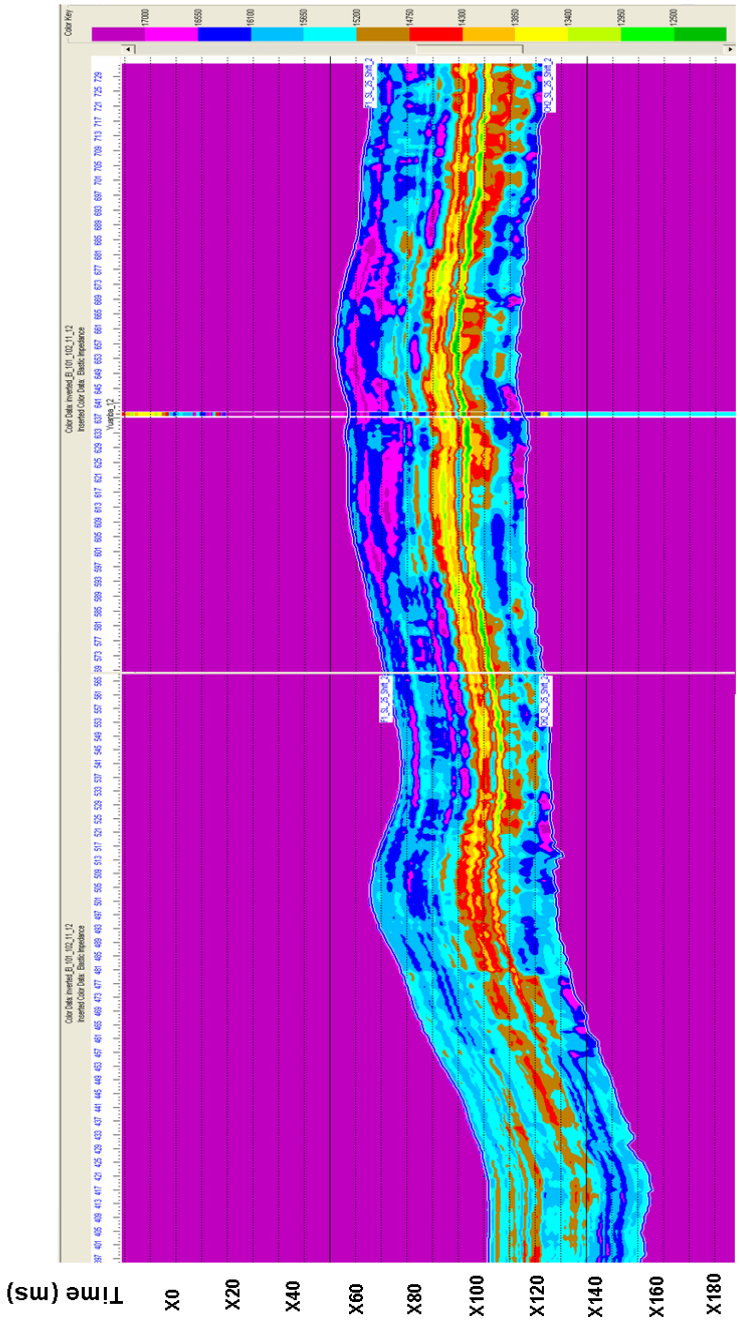

Figure 5.12 Elastic impedance inversion Section across Well 12

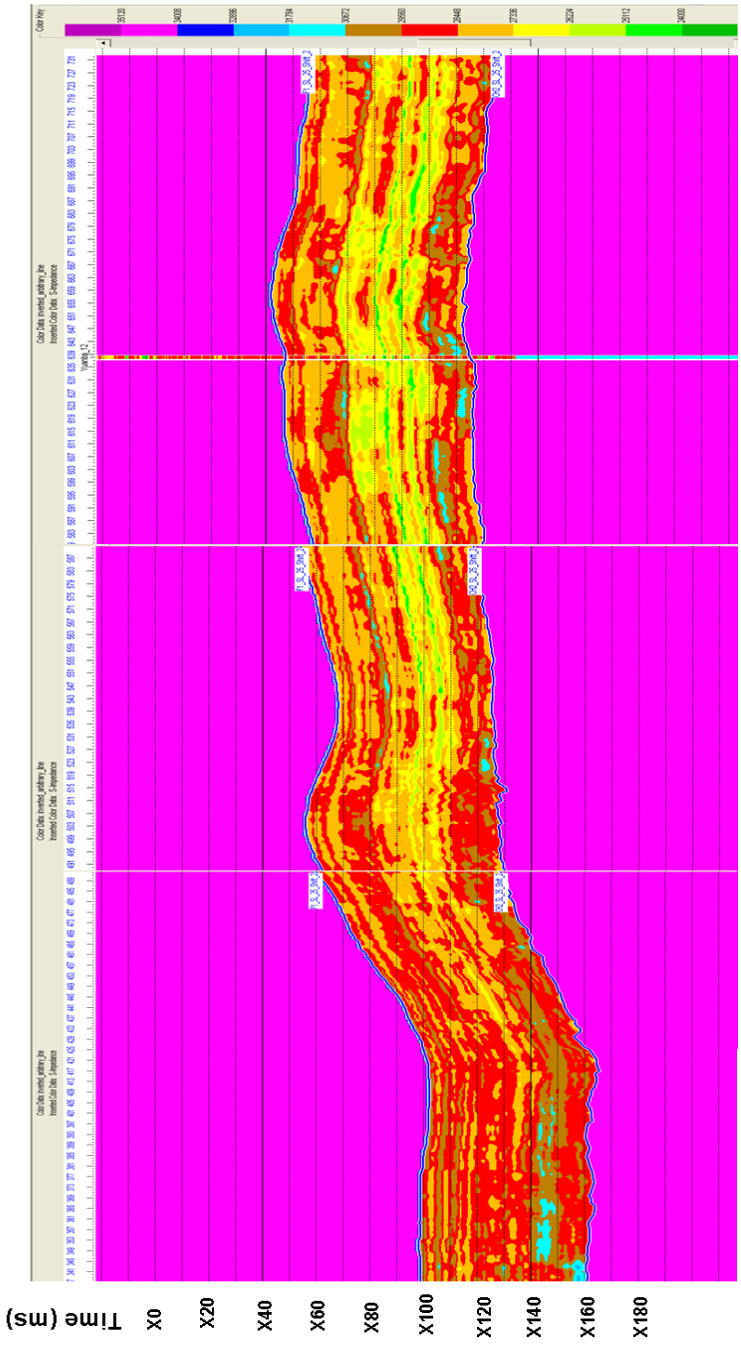

Figure 5.13 Shear Impedance Inversion Section across well 12

Figures 5.14, 5.15, 5.16 are acoustic impedance, elastic impedance and shear impedance, respectively across Well 101 and Well 102. Different from southern part around Well 12, the eastern part around Well 101 and Well 102 is dominated by carbonated reef depositional environment. For the zones around reef crest, it is featured by low impedance representing high-grade reservoir in ChangXing formation.

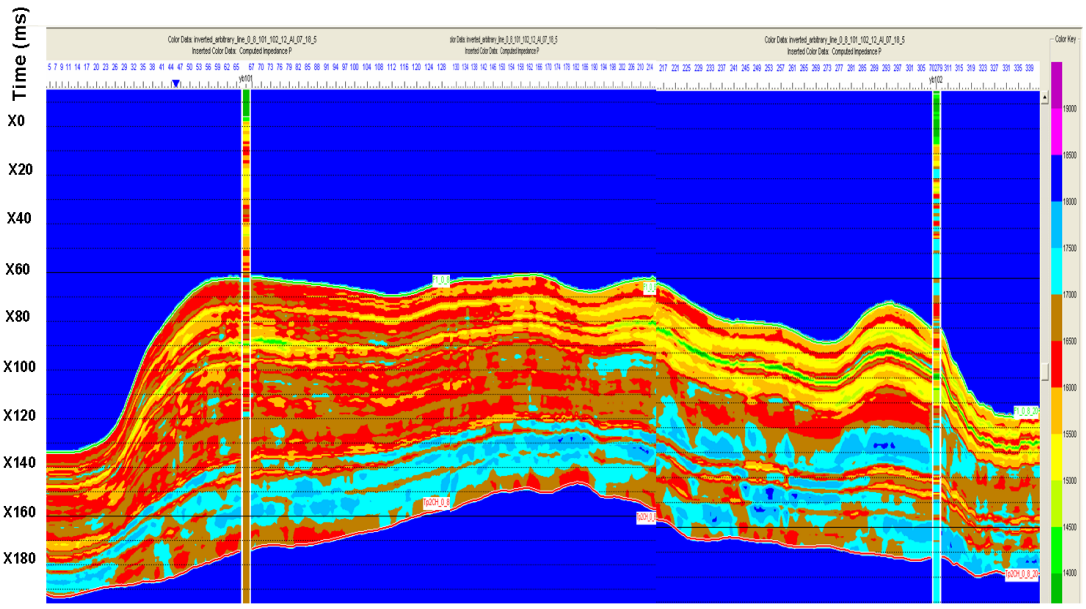

Figure 5.14 Acoustic Impedance Inversion Section across Well 101 and Well 102

With depositional facies varying into back-reef and basin, fine-size limestone deposition is featured by high-impedance. Compared reef crest to reef core, another interesting discovery is that reef core demonstrates much higher impedance than that in

reef crest which means the reservoir quality in reef crest is much better than that in reef core. This reservoir quality differences between these two zones mainly caused by diagenesis process variation. There is more opportunity for reef crest to expose to the surface and consequently experience more dissolution caused by fresh water. This dissolution process in reef crest results into much more secondary-dissolution pore space than that in reef core, which consequently lead low impedance response in seismic inversion.

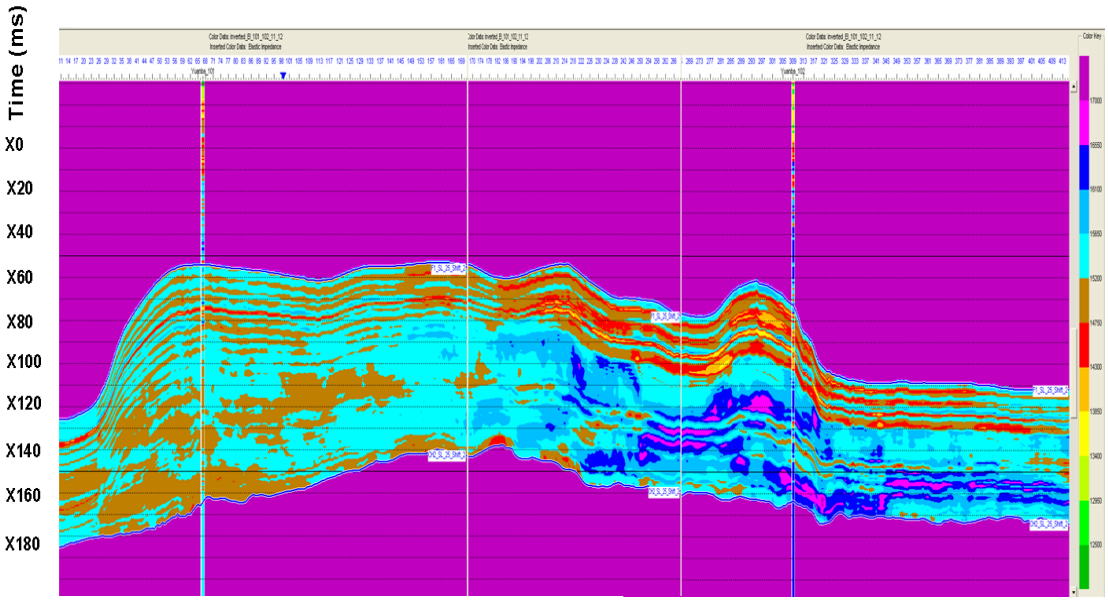

Figure 5.15 Elastic Impedance Inversion Section across Well 101 and Well 102

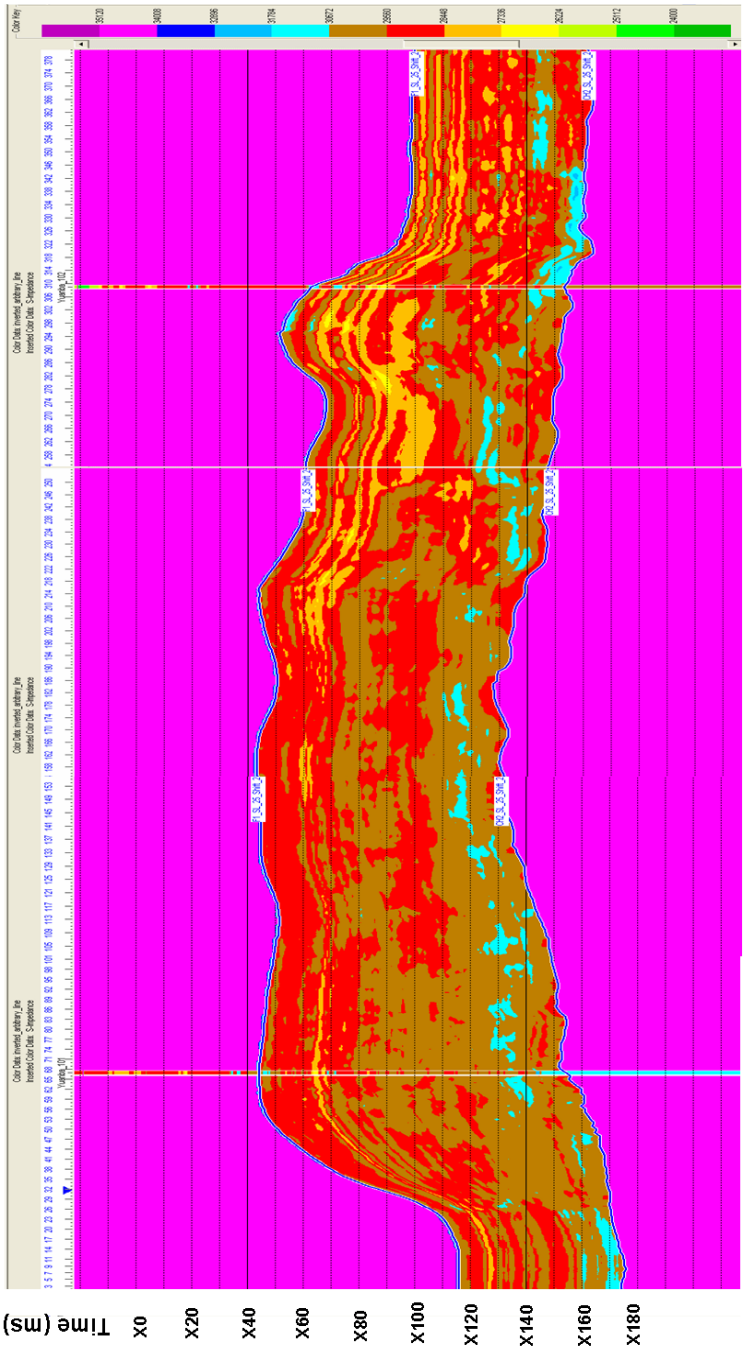

Figure 5.16 Shear Impedance Inversion Section across Well 101 and Well 102

Figures 5.17, 5.18, 5.19 and 5.20 are time structure and the acoustic impedance, elastic impedance and shear impedance slice extracted along horizon one which is 25 ms below the top of ChangXing reservoir. Figure 5.17 shows that it dips into north from carbonate platform to the basin. Compared Figures 5.18 and 5.19 with Figure 5.20, shear elastic impedance represents large differences from acoustic and elastic impedance. The later part would explain the reason causing the impedance differences among the three figures.

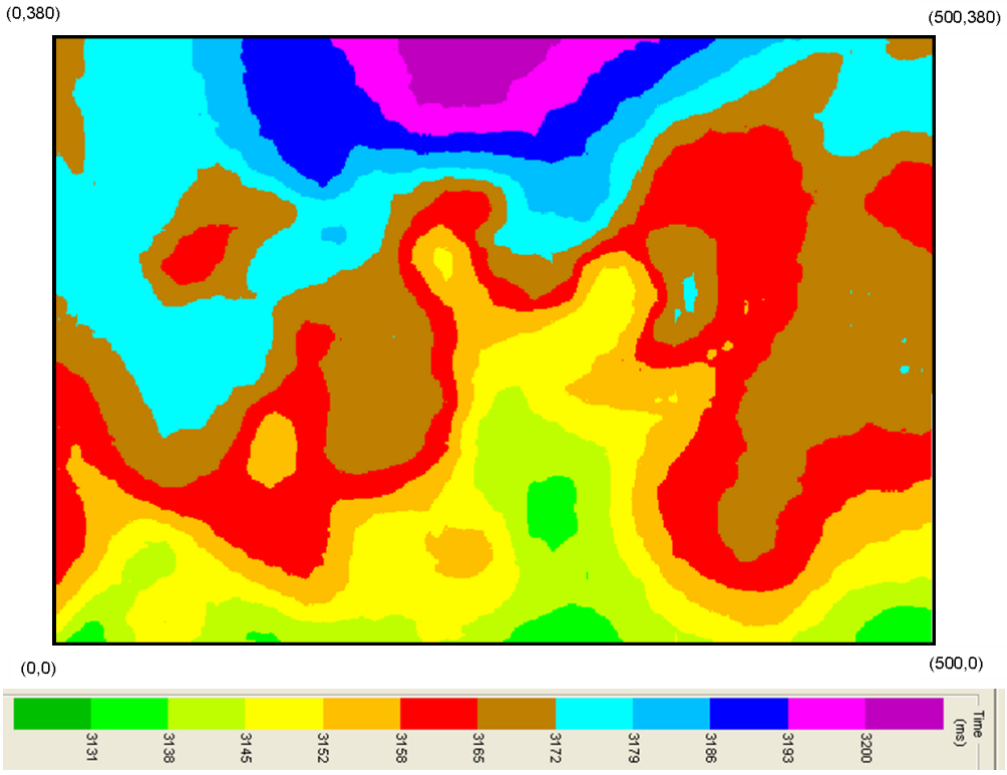

Figure 5.17 Time Structure of Horizon One

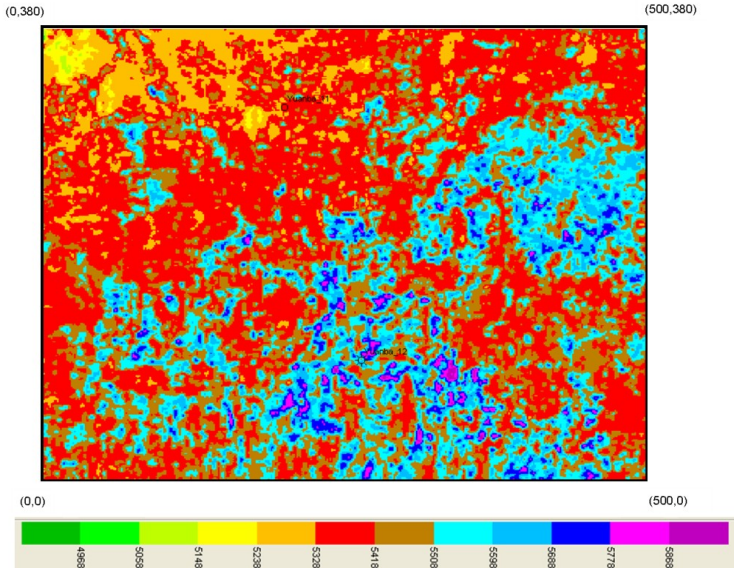

Figure 5.18 Acoustic Impedance Slice of Horizon One

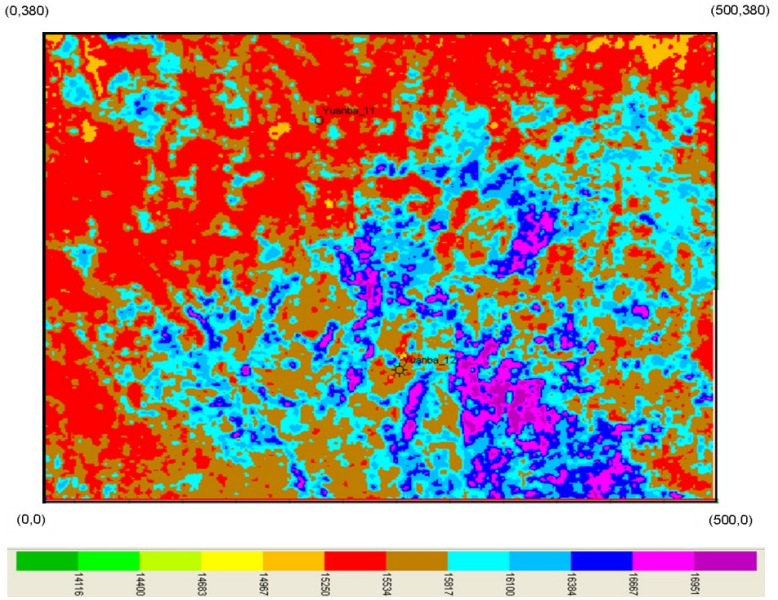

Figure 5.19 Elastic Impedance Slice of Horizon One

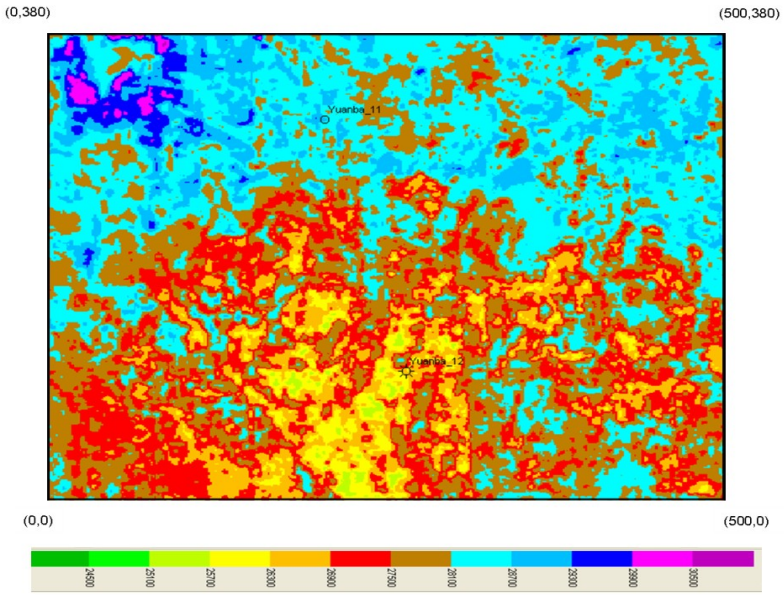

Figure 5.20 Shear Impedance Slice of Horizon One

Figures 5.21, 5.22, 5.23 and 5.24 are time structure and the acoustic impedance, elastic impedance and shear impedance slice extracted along horizon two which is 35 ms below the top of ChangXing reservoir. From platform to the basin, three kinds of impedance vary from low impedance at the platform into the high impedance in the basin, which is caused by the depositional environments variations. On the carbonate platform, dolomite depositions with high porosity developed and consequently with low impedance seismic response. Moving into the basin, tight limestone deposited with low porosity and consequently results in high velocity, high density and high impedance seismic response.

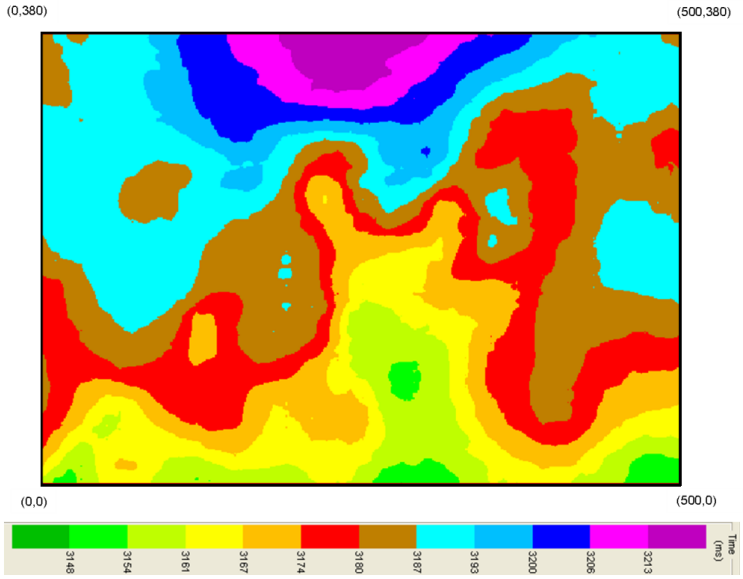

Figure 5.21 Time Structure of Horizon Two

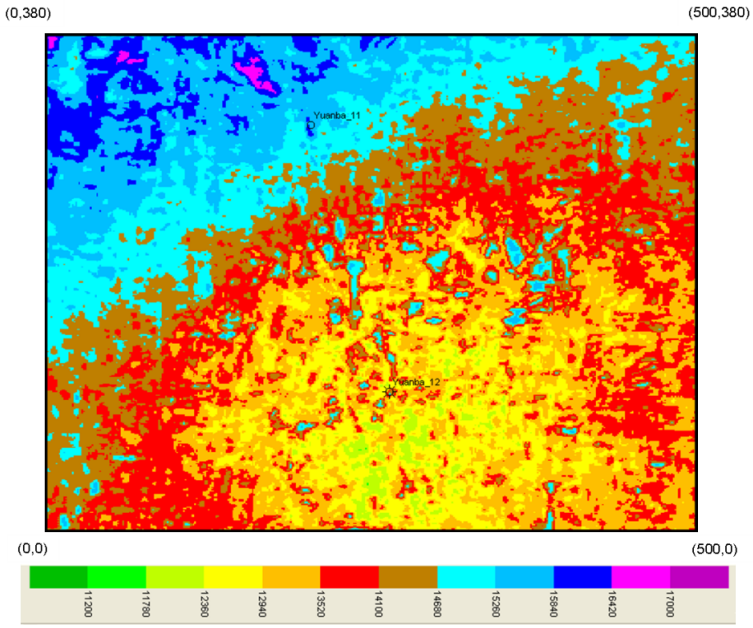

Figure 5.22 Acoustic Impedance of Horizon Two

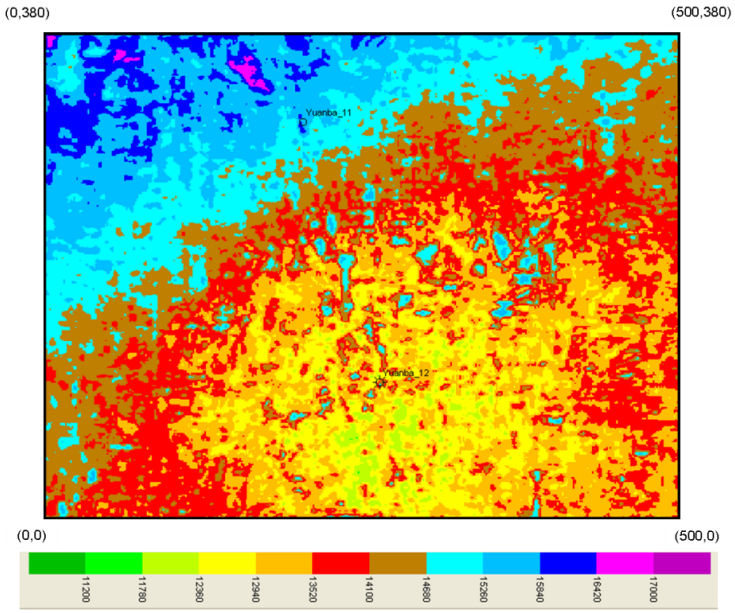

Figure 5.23 Elastic Impedance of Horizon Two

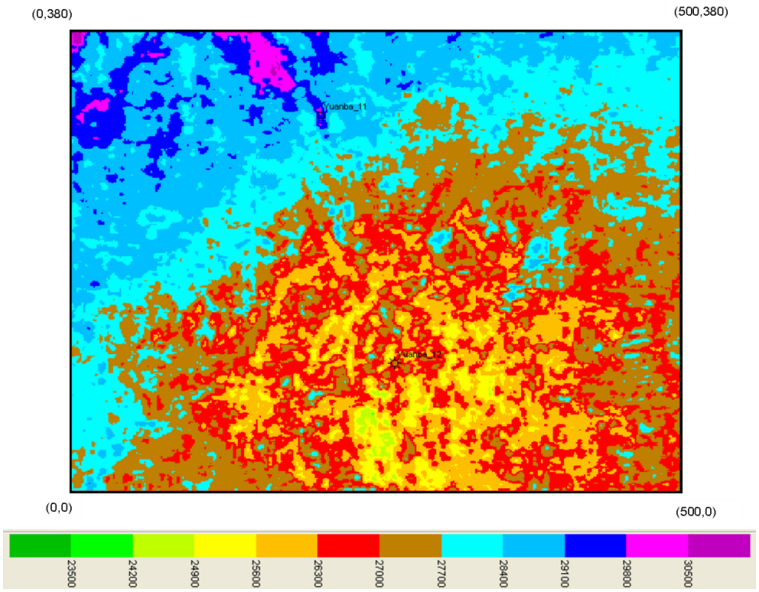

Figure 5.24 Shear Impedance of Horizon Two

Comparing inverted EI, AI and SI from seismic data extracted around Well 12 with that calculated from petrophysical data, the relative error of inverted EI, AI and SI are lower than 5%, respectively, see Figure 5.25, which means that the inversion accuracy is high enough for porosity and frame flexibility factor (γ) calculation.

After AI, EI and SI seismic inversion, porosity and frame flexibility factor (γ) calculated were conducted using two approaches introduced in the method section. In the first approach, Parameter "d" is the ratio of γ to γ_μ, which is a constant based on Sun studies for the Middle East reservoir with high porosity, ~0.8-0.6. Parameter "d" is calculated using Well 12 well in studies reservoir and Figure 5.26 is the crossplot of

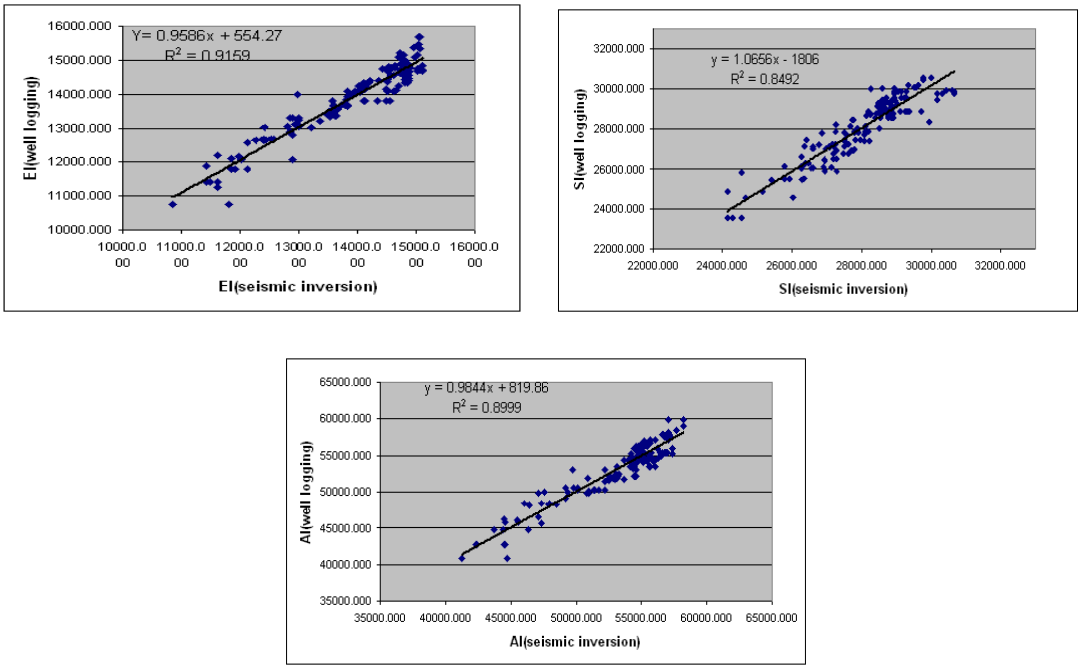

Figure 5.25 Crossplot of Inversed Impedance to Calculated Impedance from Log Curves

porosity and "d", and the color indicator is the acoustic impedance. From this figure, it could be found that "d' represents a very small variation for the zones with porosity h> 5-6%, which is around 0.6. However, it demonstrates a dramatic variation for the zones with a porosity < 5%, from 0.3 to 4. In terms of the color indicator of acoustic impedance, the above approach could be used to evaluate porosity and γ parameter for the zones with a porosity > 5%. However, for other zones with acoustic impedance higher than 15.6 (km/s) (g/cc), it isn't applicable because of huge variation of Parameter "d". More than 50% zones in ChangXing formation is featured by low porosity < 5%.

Using petrophysical data of the same well as that in method one, approach two was tested as well. Using formula 5.19, density was calculated from the above impedances data volume extracted around Well 12, Figure 5.27 is the crossplot of calculated density to bulk density curve. The crossplot shows a very poor correlation between calculated density and density log curve, which means a very poor calculating accuracy of density from above impedance volume. A case with incident angle of 20° and Vs/Vp of 0.523 is used to explain the huge calculation error of bulk density. Learned from formula 5.19, the constant exponent in density calculating formula is ~90. So, a very low impedance inversion error could generate dramatic density calculation error caused by the very big exponent constant. The big density prediction error consequently would cause huge shear and compressional velocity prediction from shear and compressional impedance. So, the second approach isn't applicable to porosity and γ calculation using the above three impedances.

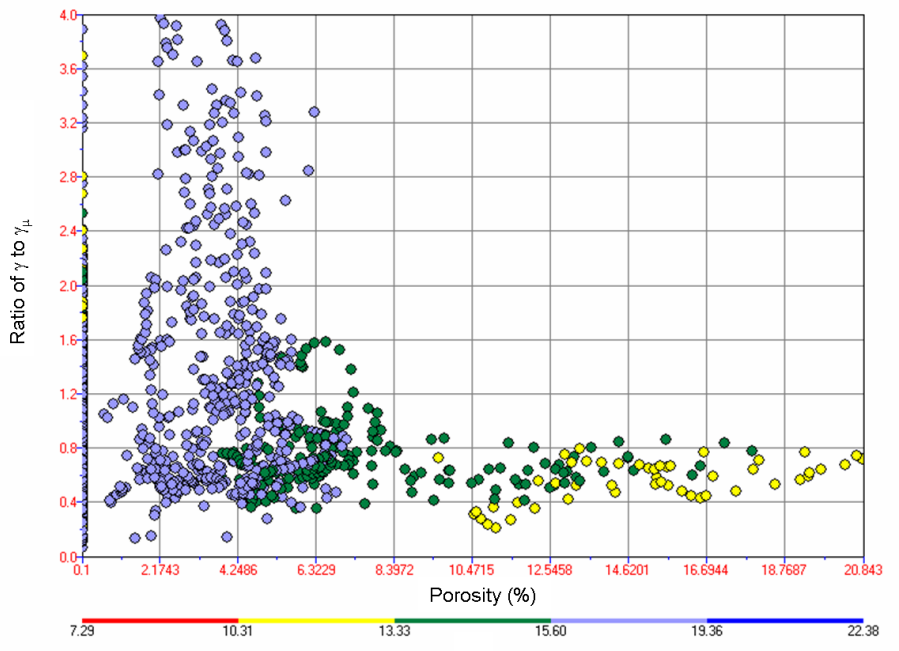

Figure 5.26 Crossplot of Porosity to γ to γ_μ Ratio with a Color Indicator of Acoustic Impedance

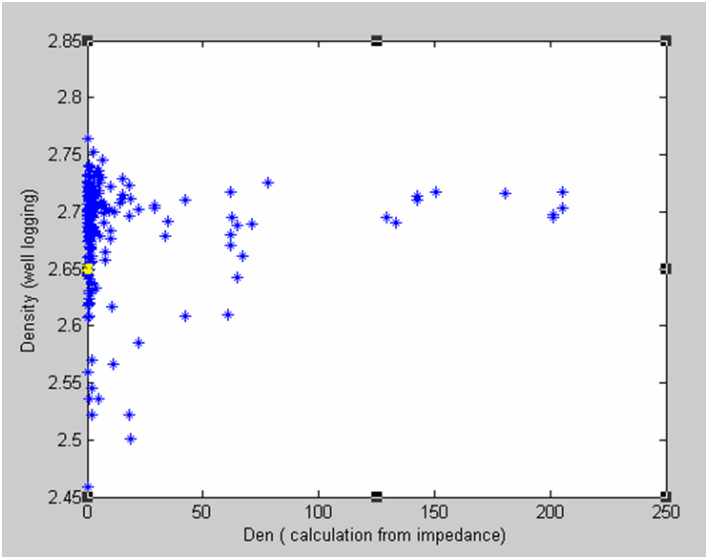

Figure 5.27 Crossplot of Inversed Density to Bulk Density

In order to decrease the error progradation from impedance inversion to density, Vp and Vs, a linear transform from acoustic impedance to density was used instead of the above non-linear formula. Figure 5.28 is the crossplot of bulk density against acoustic impedance in reservoir interval, ChangXing formation. In this figure, it could be found that acoustic impedance shows a considerable variation at bulk density, especially at a bulk density > 2.6 g/cc. Because the AI is the combination of bulk density and compressional velocity, the variation of AI at a give density might be caused by velocity variation. Learned from color bar of SI/AI, it could be found that this variation of density at a given AI could be characterized approximately.

In terms of Vs/Vp ratio, the bulk density and acoustic impedance could be divided into three trends and formula for each trend is:

For Vs/Vp < 0.52,

Den=0.08485* AI + 1.375.....5.15

For 0.52 < =Vs/Vp < 0.56

Den=0.07302* AI + 1.516.....5.16

For 0.56 <= Vs/Vp

Den=0.06356* AI + 1.717.....5.17

Where Den, AI and Vs/Vp, SI are bulk density, acoustic impedance and ratio of shear velocity to compressional velocity, shear impedance, respectively.

Using the indication of P-wave to S-wave ratio, bulk density can be transformed from the above transform accurately. After density calculation, the P-wave and S-wave can be derived from acoustic impedance and shear impedance.

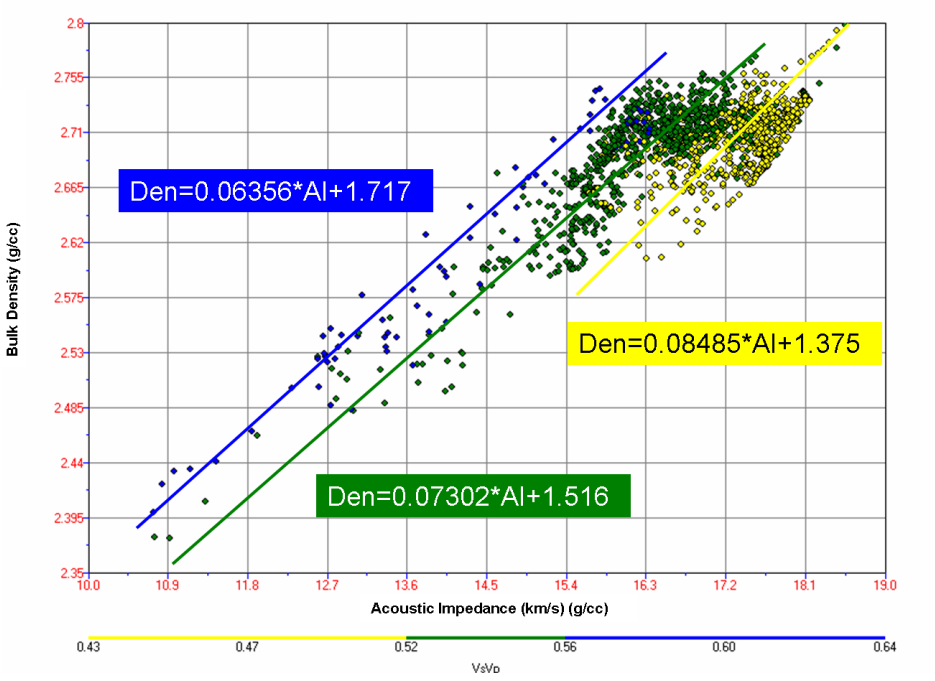

Figure 5.28 Crossplot of Acoustic Impedance to Bulk Density with a Color Indicator of P-wave to S-wave Ratio

Based on an assumption that the fluid types and mineral composition are constant as water and dolomite, porosity and frame flexibility factor (γ) are calculated using the above inversed density, compressional velocity and shear velocity from seismic data around well locations. Figures 5.29, 5.30, 5.31 and 5.32 are inversed porosity and frame flexibility factor (γ) across Well 12, respectively from AI, EI and SI using approach III overlapped by P-wave and S-wave velocity. From Figure 5.29, we could see a very thick interval with porosity > 5%, which is 35 ~ 40 m and other zones are with low porosity < 5%. Basically, this high porosity zone corresponds to dolomitized oolite shoal platform deposition and low porosity represents outer platform and inner platform. Compared Figure 5.30 with Figure 5.29, this high porosity zones demonstrate higher $\gamma > 4$, however,

the low porosity zones show a large γ variation from 0 to 5. Based on studies in Chapter IV, this large γ variation in low porosity zones is caused by complexity of pore structure and mineral composition. For the zones with porosity <5% and γ <2.5, it represents a mixture pore types of interparticle and intercrystalline with dolomitized limestone. For the zones with porosity <5% and 2.5<γ <5, it is featured by microporosity in the bio-limestone dominant depositional environments. Pore structure and mineral composition differences consequently result in permeability variations between these two zones. The zones with porosity <5% and γ <2.5 represent 2-3 orders higher permeability than that in the zones with porosity <5% and 2.5<γ <5. For the zones with porosity >5%, it represents a dominant interparticle pore type and dolomite mineral composition as well as demonstrates higher permeability than that in low porosity zones.

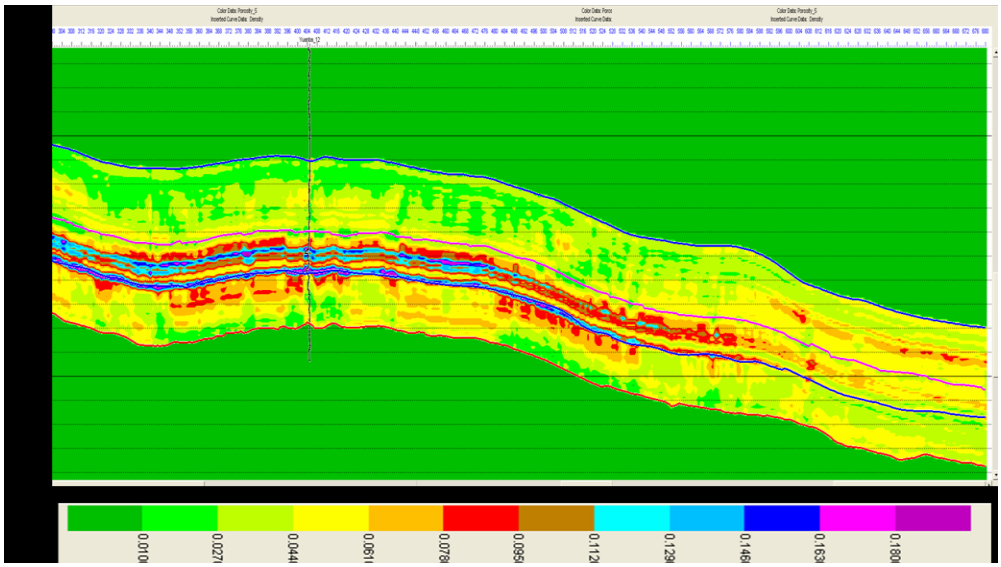

Figure 5.29 Porosity Inversion Section (inline) across Well 12

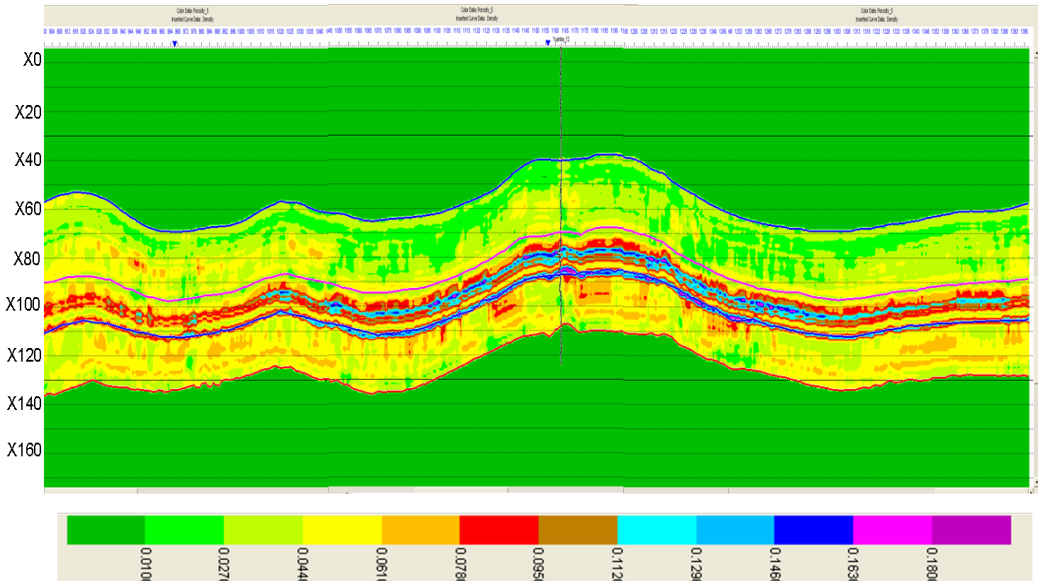

Figure 5.30 Porosity Inversion Section (crossline) across Well 12

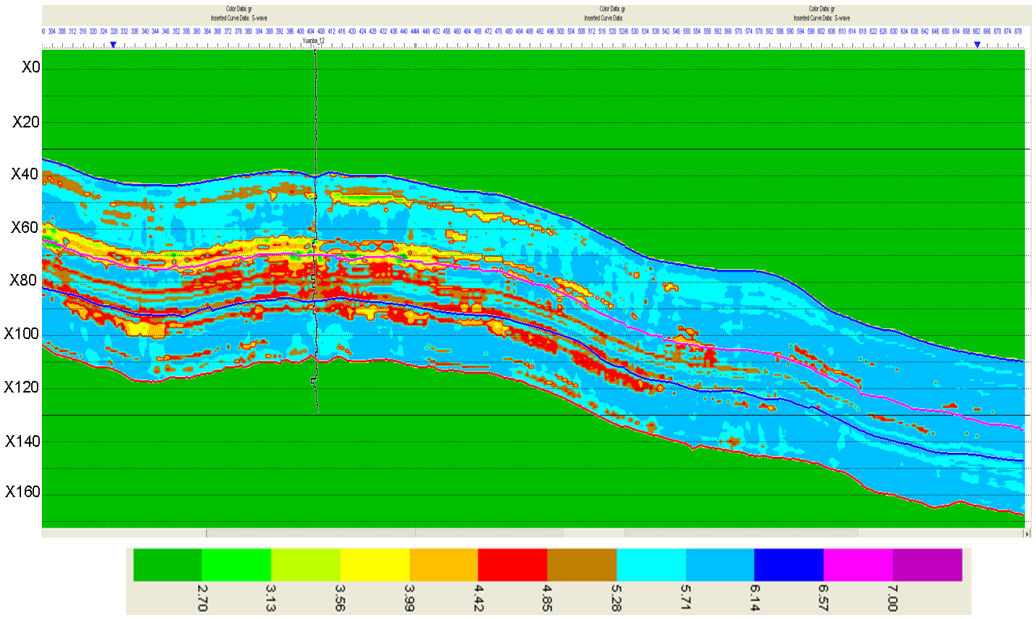

Figure 5.31 γ Parameter Inversion Section (inline) across Well 12

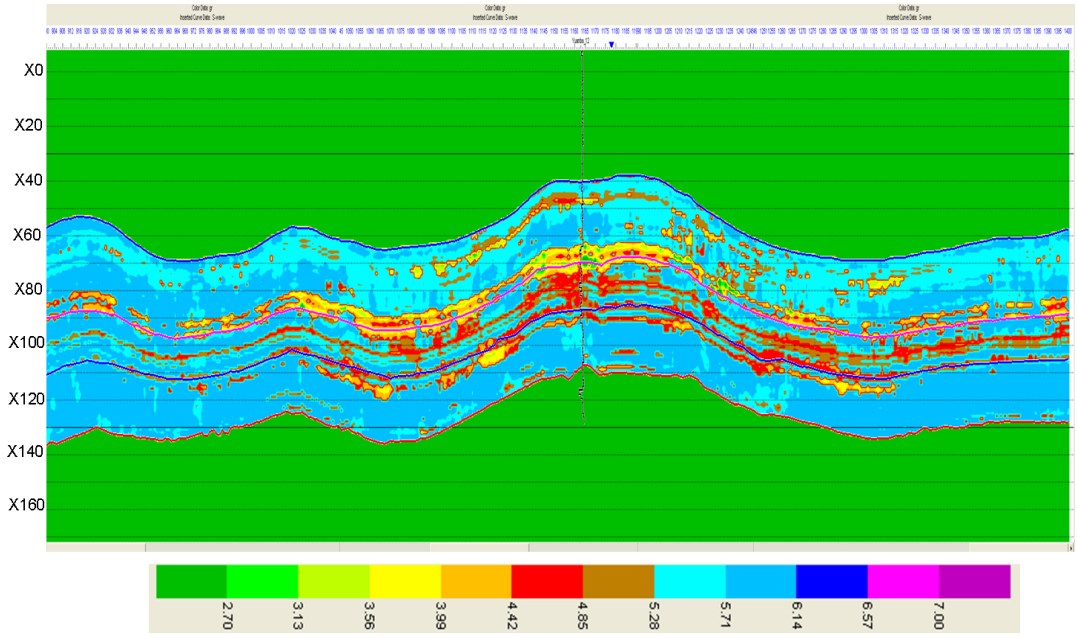

Figure 5.32 γ Parameter Inversion Section (crossline) across Well 12

Figures 5.33 and 5.34, and Figures 5.35 and 5.36 are porosity and γ parameter slice for horizon one and horizon two, respectively. Figure 5.33, a porosity slice extracted along the horizon, represents low average porosity < 5% except small area in the northeast part. With sea level decreasing, accommodation space moved to the basin and consequently para-sequence moved to basin too. The progradation of para-sequence produced reservoir moving into the low part of platform, which produces relatively higher porosity zone > 5% in the northeast area. Figure 5.34 is the γ parameter slice of horizon one. The area on the platform is featured by low γ value <3.5, however, it is increasing down dip into the basin. Learned from Figure 5.35, porosity varies from > 15% on the platform to <5% in the outer platform, which is controlled by depositional

facies and mineral composition variation. On the platform margin, the dominant mineral composition is dolomitized limestone with enlarged interparticle and dissolution pore space compared to the tight limestone deposited in the basin with microporosity, for example, intercrystalline. The γ parameter is featured by high value >3.5, except for a small area in the circle. This γ parameter can represent pore types, mineral composition and depositional environment variation, and consequently can be used to characterize the permeability changes at a given porosity.

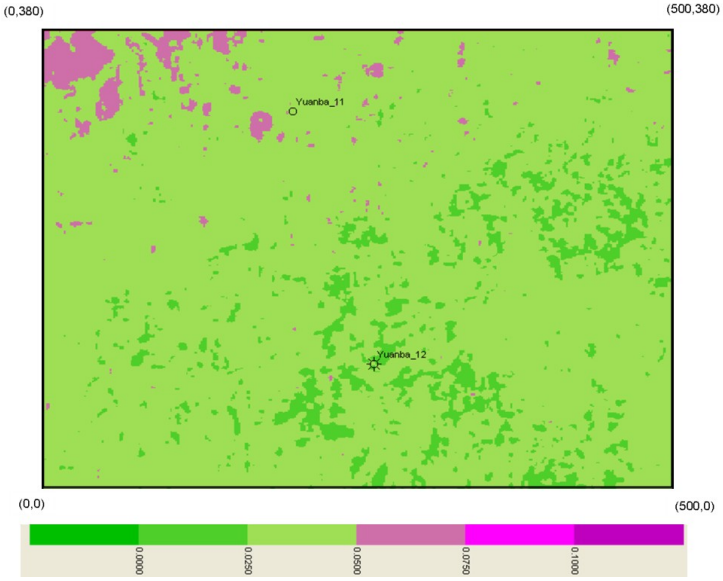

Figure 5.33 Porosity Slice of Horizon One

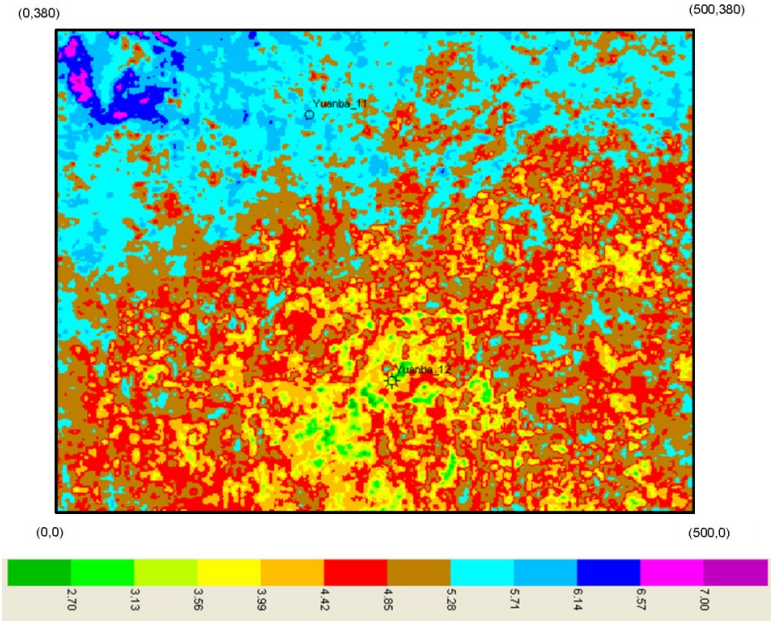

Figure 5.34 γ Parameter Slice of Horizon One

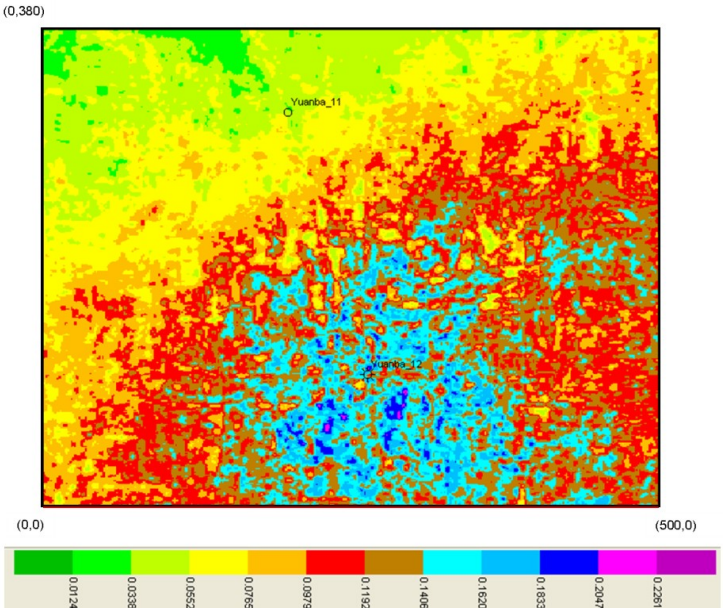

Figure 5.35 Porosity Slice of Horizon Two

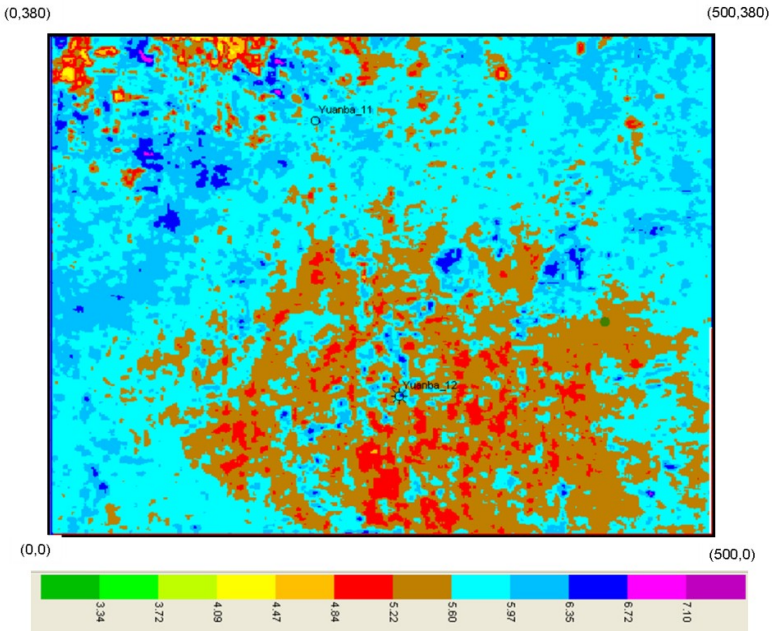

Figure 5.36 γ Parameter Slice of Horizon Two

DISCUSSION

The traditional method to evaluate reservoir permeability is to transfer porosity into permeability using best-fit function between them. For some clastic reservoir with simple pore structure, this approach could characterize permeability heterogeneity because that porosity is the major controlling factor on permeability variation. But, this approach can't succeed in its application in carbonate reservoir with complex pore structure variation which has more influences on permeability heterogeneity than porosity does. For our studied reservoir, ChangXing reservoir, it represents diversity of pore types composed of micropore, interparticle pore space, dissolution (moldic) pore space and fracture as what we discussed above, and this pore structure variations cause intensive permeability heterogeneity. In the following part, permeability heterogeneity

evaluation using traditional method would be compared to that using rock-model based approach.

Core measurement samples were used to build porosity-permeability transform formula using traditional method and rock-physics model based approach. By γ parameter, core porosity and core permeability is classified into two regression trends compared that without γ parameter indicator, see Figure 5.37 and Figure 5.38. These regression formulas were used to calculate permeability from porosity respectively.

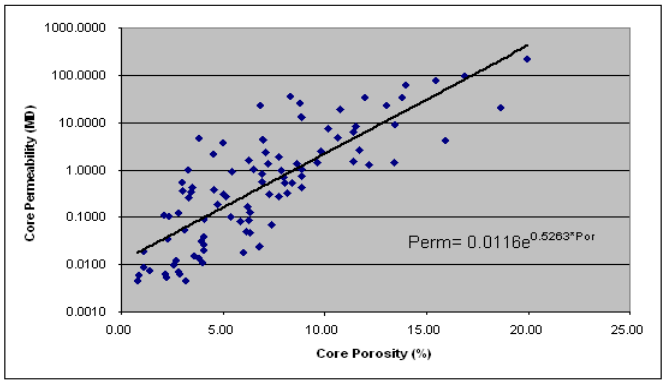

Figure 5.37 Crossplot of Core Porosity to Core Permeability

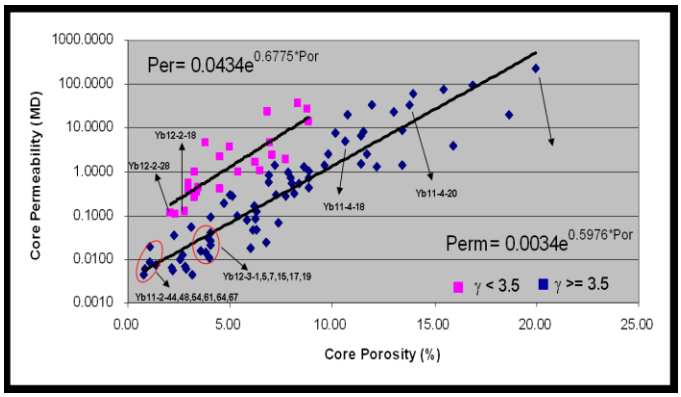

Figure 5.38 Crossplot of Core Porosity to Core Permeability with Color Indicator of γ

Figures 5.39 and 5.40 is the inversed permeability slice of horizon one using two methods, one is porosity-permeability best-fit function method and another one is rock-physics based method. Learned from Figure 5.39, most areas in this slice presents low permeability <0.001 MD except some areas in the northeast part that agrees with its porosity variation trend. In Figure 5.40, some discontinuously and relatively high permeability areas, 0.01-0.1 MD, are present on the platform, which are calculated from porosity with indication of γ parameter. Production data from Well 12 proved that the relatively high permeability areas are gas production areas. Core measurement in Well 12 also proves that permeability calculation using the γ parameter is more accurate than that calculated by using traditional method, just like what is shown in Figure 5.45. Petrophysical data from Well 12 also prove that these relatively high permeability zones are gas zones with low water saturation (< 50%).

Figure 5.41 and Figure 5.42 are inversed permeability slice of horizon one using two methods, one is porosity-permeability best-fit function method and another one is rock-physics based method, respectively. Except for the small area within the circle, the permeability in the whole area in these two figures is similar. The major reason is that the γ parameter in this slice is >3.5 in 95% areas, which indicates a relatively homogeneous pore type and porosity is the major controlling factor for permeability heterogeneity.

The comparison result between these two approaches prove that rock-physics model based method is more powerful than the best-fit function method in production

zones identification and permeability heterogeneity characterization in low porosity reservoir.

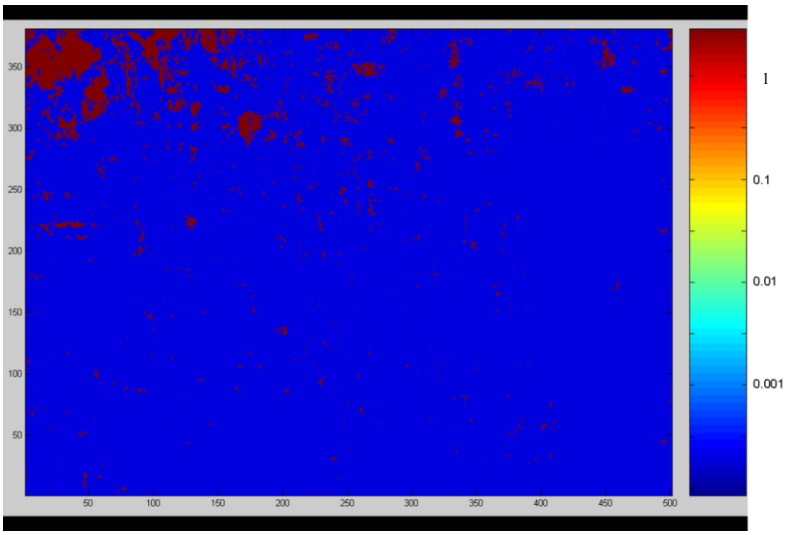

Figure 5.39 Permeability Inversion Slice of Horizon One by Using Traditional Method

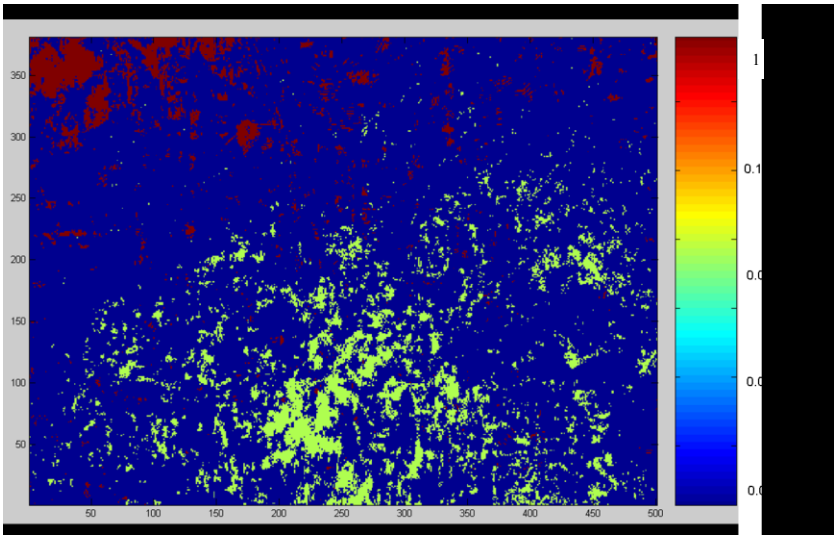

Figure 5.40 Permeability Inversion Slice of Horizon One by Using γ Parameter Indication

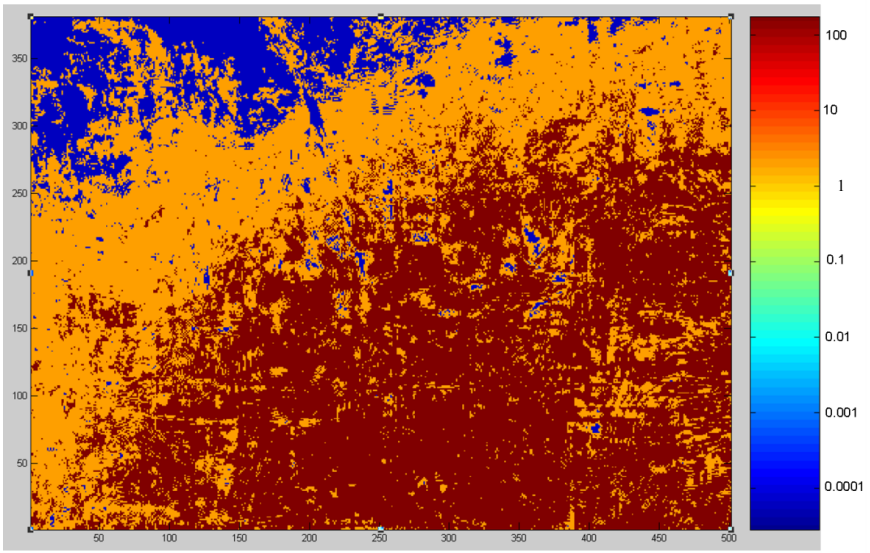

Figure 5.41 Permeability Inversion Slice of Horizon Two by Using Traditional Method

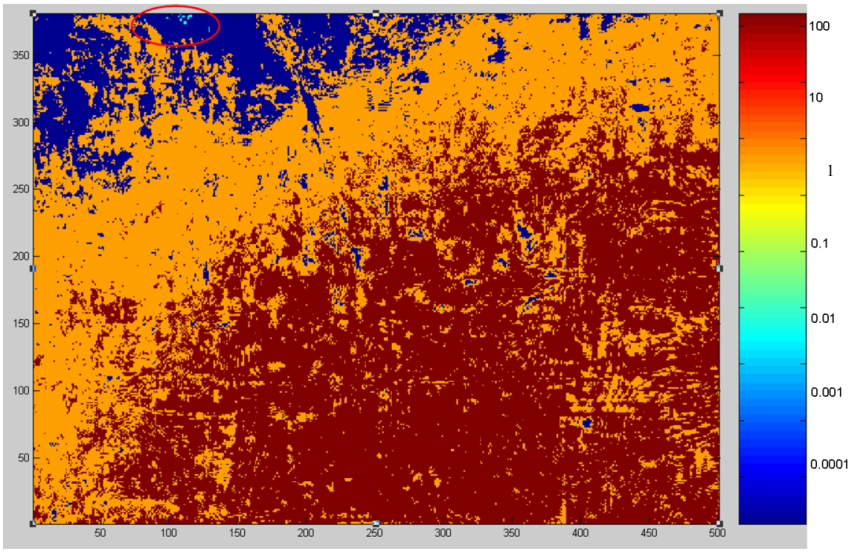

Figure 5.42 Permeability Inversion Slice of Horizon Two by Using γ Parameter Indication

CONCLUSIONS

The study in this chapter proves that the approach by combining seismic data and rock physics model is effective for characterizing carbonate reservoir permeability heterogeneity caused by not only porosity but also pore structure variations. Learned from this study, frame flexibility factor (γ) is helpful to characterize reservoir pore type variation and further predict gas-bearing layers in low porosity zone, which would be missed from porosity inversion interpretation only. In the first step inversion, multiwell normalization is the key part to remove tools calibration error to get consistent and accurate well log information for the forward model building. Classified by Vs/Vp ratio, acoustic impedance can be transformed into density and further to calculate compressional and shear velocity from both acoustic and shear impedance. Two challenges still existing in this study are as follows: reservoir mineral composition and fluid types are the required porosity and frame flexibility factor (γ) inversion from seismic data and the further research is necessary to solve this problem. Meanwhile, time-shift of the same reflection event in different angle-stack seismic data, which is caused by the velocity lateral heterogeneity during migration in the time domain is another one for applying the above approach.

CHAPTER VI

SUMMARY AND CONCLUSIONS

The 3-D distribution of the collapsed paleokarst system in Upper San Andres reservoir was delineated by detail seismic characterization by integrating core, well log and rock physics data. Tight, fine-scale collapsed paleokarst system was discovered in the area of high volume production with higher acoustic impedance compared to reservoir zones, which exhibited low and uniform porosity development. The model-based seismic inversion method is thus a useful tool to characterize the vertical and lateral extent of this paleokarst system. For large-scale collapsed paleokarst systems along the transition from platform into basin, seismic geometric attribute analysis is a good tool to map its 3D spatial distribution. The development of the paleokarst complex system detected in the San Andres Formation was explained by a proposed carbonate platform hydrological model. Two other collapsed paleokarst system were predicted in the structurally high area of the lower San Andres Formation, G3 and G4 HFS. Production data proved the influence of tight paleokarst system on reservoir compartmentalization.

Study from two carbonate reservoirs with different reservoir quality demonstrates that the frame flexibility factor (γ) is helpful for characterizing the diversity of pore types and improving permeability prediction accuracy in carbonate reservoirs.

It is found in ChangXing gas reservoir that samples with frame flexibility factor (γ) <2.2 represent a mixing pore type of intercrystalline and interparticle in low porosity range $< 5\%$, or a mixture of interparticle and dissolution pore space as porosity is $> 5\%$.

Samples with frame flexibility factor (γ) between 2.2 and 6 show either intercraystalline pore space in low porosity range <5% or dominant inerparticle pore space in relative high porosity range >5%. Fractures can be determined by a feature of high frame flexibility factor (γ) > 6.

Similar as the ChangXing gas reservoir, frame flexibility factor (γ) is applicable for pore type complexity characterization too for an Upper San Andres reservoir. Different from ChangXing gas reservoir, the dramatic velocity scattering happens at a high porosity range >~7% in Upper San Andres reservoir, however, it does in a low porosity range <~7% in ChangXing gas reservoir. In this case, samples with frame flexibility factor (γ) <3.85 is featured by either visible moldic pore space in or dolopackstone or intercrystalline pore space in dolowackstone. On the other hand, samples with frame flexibility factor (γ) >3.85 demonstrate either dominant interparticle pore space in dolopackstone or microcrack pore space in dolowackstone or dolomudstone.

Frame flexibility factor (γ) is not only helpful to delineate pore type diversity, but also characterize permeability heterogeneity. In the ChangXing gas reservoir with an average depth of ~7000 meters, porosity is a major controlling factor to reservoir permeability for samples with relatively high porosity >~6-7%, which have a relative homogeneous mineral composition and pore structure. However, for sample in a low porosity range <5%, it presents a much big mineral composition and pore type variation. In this case, frame flexibility factor (γ) is an indicator to differentiate relative high permeability zones (>~0.1md) from nonreservoir zones (average permeability <

~0.001md) for the samples in a low porosity range <5%. Meanwhile, high frame flexibility factor (γ) value is an indicator of fracture zones with dramatic high permeability, >~10md. In terms of frame flexibility factor (γ), different porosity-permeability trends were generated in Upper San Andres reservoir for samples with a porosity >6%. These two different trends include clear geologic interpretation such as pore type and rock texture variations, and consequently improve permeability prediction accuracy compared to a traditional method.

Fluid types variation in ChangXing gas reservoir were demonstrated by combining bulk module and frame flexibility factor (γ) which considers the influences from not only porosity but also pore type variations, which shows a much improvement for fluid identification than that learn from conventional porosity-acoustic impedance crossplot.

The results from ChangXing gas reservoir studies proved that two-step seismic inversion is successful in calculating reservoir porosity and frame flexibility factor (γ). In the first step inversion, acoustic impedance, elastic impedance and shear impedance were generated using model-based inversion method from angle-stack seismic data. Classified by Vs/Vp ratio, acoustic impedance and shear impedance were applied to calculate density, compressional and shear velocity. In the second step inversion, rock physics model was applied to derive reservoir porosity and frame flexibility factor (γ). By combining porosity and frame flexibility factor (γ), permeability heterogeneity was evaluated further. Compared to the conventional permeability calculation method by best-fit function between porosity and permeability, additional relative high permeability

gas zones were easily interpreted using the above integrated permeability characterization method and it also improved permeability prediction accuracy.

More efforts and work are necessary for the following two challenges in the future: the first one is the assumption that reservoir mineral composition and fluid types are constant for porosity and frame flexibility factor (γ) inversion from seismic data, which doesn't exist in most carbonate reservoirs. Time-shift of the same reflection events in different angle-stack seismic data, which is caused by the velocity lateral heterogeneity during migration in time domain, is another one for applying the above approach.

REFERENCES

Adams, D.C., Keller, G.R.,1996. Precambrian basement geology of the Permian Basin region of the west Texas and eastern New Mexico: A geophysical perspective. American Association of Petroleum Geologists Bulletin 80, 410-431.

Anselmetti, F.S., Eberli, G.P., 1993. Controls on sonic velocity in carbonates. Pure and Applied Geophysics 141, 287-293.

Anselmetti, F.S., Eberli, G.P., 1999. The velocity-deviation log: A tool to predict pore type and permeability trends in carbonate drill holes from sonic and porosity or density logs. American Association of Petroleum Geologists Bulletin 83, 450–466.

Berger, Z., Davies, G., 1995. The development of linear hydrothermal dolomite reservoir facies along wrench or slip fault systems in the western Canadian Sedimentary Basin. Canadian Society of Petroleum Geologists Reservoir 26, 34-38.

Bracco Gartner, G.L., Wagner, P.D., Baechle, G.T., Sun, Y.F., Weger, R., Eberli, G.P., Asyee, W., Hillgartner, H., Van der Kolk, K., Leguijt, J., Nasser, M.R., Massaferro, J., 2005. Obtaining permeability from seismic data: a new breakthrough in carbonate reservoir modeling. Proceeding of the International Petroleum Technology Conference, p.10577.

Brite, A., Johnson, D.L., Nurmi, R.D., 1985. Effect of Spherical Pores on Sonic and Resistivity Measurements. 26th Annual Logging Symposium, Society of Professional Well Log Analysts, 10-20.

Buenafama, P., Gibson R.L., 2004. Case history: Acoustic impedance inversion of the Lower Permian carbonate buildups in Permian Basin, Texas. Society of Exploration Geophysicists Extended Abstract 23, 529-533.

Burlington/Schlumber IPM, 2003. Core Description Report, #1261 well W.N. Waddell Field in Crane County, Texas, 1-20.

Castagan, J.P., Batzle, M.L., Eastwood, R.L., 1985. Relationship between compressional-wave and shear-wave velocities in clastic silicate rocks. Geophysics 50, 571-581.

Chopra, S., Marfurt, K.J., 2008. Emerging and future trends in seismic attributes. The Leading Edge 27 (3), 298-319.

Connolly, P., 1999. Elastic impedance. The Leading Edge 18(4), 438-452.

Craig D.H., 1988. Caves and other features of Permian karst in San Andres dolomite, Yetes field reservoir, west Texas. In N.P. James and P.W. Choquette, eds., Paleokarst, New York, Springer-Verlag, 342-363.

Dembicki, E.A., 1996. Recognition and delineation of paleokarst zones by the use of wireline logs in the bitumen-saturated Upper Devonian Grosmont Formation of northeastern Alberta Canada. American Association of Petroleum Geologists Bulletin 80 (5), 695-712.

Dou, Q.F., Sun, Y.F., Sullivan, C., 2009. Seismic detection of paleokarst system and its influence on carbonate reservoir compartmentalization. Society of Exploration Geophysicists Expanded Abstract, 1731-1736.

Eberli, G., Massaferro, J. L., Weger, R., Sun, Y. F., Bächle G., Bracco G., 2006. Permeability from seismic in carbonate reservoirs, Part I: Dream or reality? American Association of Petroleum Geologists Bulletin, 90, 120-123.

French, V.L., 2000. Reservoir characterization and geostatistical modeling of the West Jordan unit, San Andres Formation, Central Basin Platform, Rector and Crane counties, west Texas. PhD dissertation, University of Oklahoma, Norman, OK,1-80.

French, V.L., Kerans, C., 2004. Accommodation-controlled system-tract-specific faces partitioning and resulting geometric development of reservoir grainstone ramp-crest shoal bodies. American Association of Petroleum Geologists Memoir 80, 171-190.

Gardner, M.H., Sonnenfeld, MD, 1996. Recognition criteria for establishing a high-resolution sequence stratigraphic framework for high net-to-gross slope sandstones, Permian Brushy Canyon Formation, Texas. American Association of Petroleum Geologists Abstract 15, 50.

Geertsma, J., 1961. Velocity-log Interpretation: The effect of rock bulk compressibility. Society of Petroleum Engineers 1, 235-248.

Han, D.H., 1986. Effects of porosity and clay content on acoustic properties of sandstone and unconsolidated sediments. Ph.D.dissertation, Stanford University. Stanford, CA, 1-90.

Hayes, P.T., 1964. Geology of the Guadalupe Mountain, New Mexico, U.S. Geological Survey Professional Paper, 446-480.

Hardage, B. A., Carr, D. L., Lancaster, D. E., Simmons, J. L., Hamilton, D. S., Elphick, R. Y., Oliver, K. L., Johns, R. A., 1998. 3-D seismic evidence of effects of carbonate karst collapse on overlying clastic stratigraphy and reservoir compartmentalization. Geophysics 61 (5), 1336-1448.

Hills, J.M., 1984. Sedimentation, tectonism, and hydrocarbon generation in Delaware Basin, west Texas and southeastern New Mexico. American Association of Petroleum Geologists Bulletin 68, 250-267.

Hills, J.M., 1970. Late Paleozoic structural directions in southern Permian basin, west Texas and southern New Mexico. American Association of Petroleum Geologists Bulletin 54, 1809-1827.

Hills, J.M., 1972. Late Paleozoic sedimentation in west Texas Permian Basin. American Association of Petroleum Geologists Bulletin 56, 2303-2322.

Keller, G.R., Hill, J.M., Djeddi, R., 1980. A regional geological and geophysical study of the Delaware Basin, New Mexico and west Texas. New Mexico Geological Society, 31st Field Conference Guidebook, 105-111.

Kerans, C., 1988. Karst-controlled reservoir heterogeneity in Ellenburger group carbonate of west Texas. American Association of Petroleum Geologists Bulletin 72 (10), 1160-1183.

Kerans, C., Fitchen, W.M., 1995. Sequence hierarchy and facies architecture of a carbonate-ramp system: San Andres Formation of Algerita Escarpment and western Guadalupe Mountains, west Texas and New Mexico. University of Texas at Austin, Bureau of Economic Geology Report of Investigation 235, 86-100.

Kerans, C., Lucia, F.J, Senger, R.K., 1994. Integrated characterization of carbonate ramp reservoir using San Andres Formation outcrop analogies. American Association of Petroleum Geologists Bulletin 78 (2), 181-216.

Kittridge, M.G., Laker, L.W., Lucia, F.J., 1990. Outcrop/subsurface comparisons of heterogeneity in the San Andres Formation. Society of Petroleum Engineering Formation Evaluation 5, 233-240.

Lindseth, R.O.,1978, Synthetic sonic logs: A process for stratigraphic interpretation. Geophysics 44, 3-26.

Lorenz, J.C., Sterling, L., Schecher, D.S., Whigham, C.L., Jensen, J.L., 2002. Natural fractures in the Spraberry Formation, Midland Basin, Texas: The effects of mechanical stratigraphy on fracture variability and reservoir behavior. American Association of Petroleum Geologists Bulletin 86 (3), 505-524.

Lucia, F. J., 1983. Petrophysical parameters estimated from visual descriptions of carbonate rocks: A field classification of carbonate pore space. Journal of Petroleum Technology 35, 629–637.

Lucia, F.J., 1995. Lower Paleozoic cavern development, collapse, and dolomitization, Franklin Mountain, El Paso, Texas. American Association of Petroleum Geologists Memoir 63, 279-300.

Loucks, R.G., 1999. Paleocave carbonate reservoirs: Origin, burial-depth modification, spatial complexity and reservoir implications. American Association of Petroleum Geologists Bulletin 83 (11), 1795-1834.

Loucks, R.G, Mescher, P., 2001. Paleocave facies classification and associated pore types. American Association of Petroleum Geologists SW Section Annual Convention, p.18-30.

Lyndon A.Y., Jim S.S., Amy S.R., Andy G., Imelda G.J., 2006. Three-dimensional characterization of a heterogeneous carbonate reservoir Lower Cretaceous, Abu Dhabi. American Association of Petroleum Geologists Memoir 74, 172-205.

Ma, Y.S., Guo, X.S., Guo, T.L., Huang, R., Cai, X.Y., Li, G.X., 2006. The Puguang gas field: new giant discovery in the mature Sichuan Basin, southwest, China. American Association of Petroleum Geologists Bulletin 90 (5), 627-643.

Meese, A.D., Walther, H.C., 1967. An investigation of sonic velocities in vugular carbonates. 8th Annual Logging Symposium, Society of Professional well Log Analysts, paper P, p.4-30.

Murphy, W. F., 1984, Acoustic measures of partial gas saturation in tight sandstones. Journal of Geophysics Research 89, 11549-l1559.

Murphy, W. F., 1985, Sonic and ultrasonic velocities: Theory versus experiment. Geophysics Research Letter 12, 85-88.

Mylroie, J.E., Carew, J.L., 1995. Karst development on carbonate islands. American Association of Petroleum Geologists Memoir 63, 55-76.

Nissen, S.E., Sullivan, E.C., Givens, N.B., 2005. Improving geological and engineering models of mid-continent fracture and karst-modified reservoir using 3-d seismic attributes. DOE Semiannual Scientific/Technical Report, 23-24.

Nissen, S.E., Doveton, J.H., Watney, W.L., 2008. Petrophysical and geophysical characterization of karst in a Permian San Andres reservoir, Waddell field, west Texas. American Association of Petroleum Geologists Abstract, 90078.

Plummer, L.N., 1975. Mixing of sea water with calcium carbonate ground water. Geological Studies of America Memoir 142, 219-236.

Pranter, M., 1999. Use of a Petrophysical-based reservoir zonation and multicomponent seismic attributes for improved geological modeling, Vacuum field, New Mexico. Ph.D. dissertation, Colorado School of Mines, Golden, CO, 15-50.

Robert G.K., Xu, S.Y., 2002. An approximation for Xu-White velocity model. Geophysics 65 (5), 1406-1414.

Russell, B., Hampson, D., 1991, Comparison of poststack inversion method. Society of Exploration Geophysicists Expanded Abstracts 61, 876-878.

Saleh, A. A., Castagna, J.P., 2004. Revisiting the Wyllie time average equation in the case of near-spherical pores. Geophysics 69, 45-55.

Saller, A., Ball, B., Robertson, S., McPherson, B., Wene, C., Nims, R., Gogas, J., 2001. Reservoir characterization of Devonian cherts and their control on oil recovery: Dollarhide field, West Texas. American Association of Petroleum Geologists Bulletin 85 (10), 35-50.

Schlumberger, Inc., 1974. Log interpretation applications. Schlumberger Educational Service, 1-23.

Scotellaro C., Vanorio, T., Mavko, G., 2007. The effect of mineral composition and pressure on carbonate rocks. Society of Exploration Geophysicists Expanded abstract, p.1684.

Smart, P.L., Whitaker, F.F., 1993. Controls on the distribution and extent of porosity development in paleokarst terrains. AAPG program of Hedberg Conference on the Unconformities and Porosity development in Carbonate Strata: Recognition, Controls and Predictive Strategies, p.69.

Sullivan, E.C., Marfurt, K.J., Lacazette, A., Ammerman, M., 2006. Application of new seismic attributes to collapse chimneys in Fort Worth Basin. Geophysics 71(4), B111-B119.

Sun, Y.F., 2000. Core-log-seismic integration in hemipelagic marine sediments on the eastern flank of the Juan De Fuca Ridge. Ocean Drilling Program Scientific Results 168, 21-35.

Sun, Y.F., 2004. Effects of pore structure on elastic wave propagation in rocks, AVO modeling. Journal of Geophysics and Engineering 1, 268-276.

Sun, Y.F., 2007. Upscaling of a proxy parameters for pores structure in sedimentary rocks. Society of Exploration Geophysicists Expanded Abstract, 1649-1654.

Sun, Y.F., Goldberg, D., 1997a. Effects of aspect ratio changes on wave velocities in fractured rocks. Society of Exploration Geophysicists Expanded Abstract 67, 925-928.

Sun, Y.F., Goldberg, D., 1997b. Estimation of aspect ratio changes with pressure from seismic velocities, in: Lovell, M.A., Harvey, P.K., (eds.), Developments in Petrophysics. Geological Societ Special Publication, 122, 131-139.

Sun, Y. F., Berteussen, K., Vega, S., Eberli, G. P. , Baechle, G. T. , Weger, R. J., Massaferro, J. L., Bracco Gartner, G. L., Wagner, P. D. 2006. Effects of pore structure on 4D seismic signals in carbonate reservoirs. Society of Exploration Geophysicists Expanded Abstracts, 3260–3264.

Tosoya, C., Nur, A., 1982. Effects of diagenesis and clays on compressional velocities in rocks. Geophysics Research Letter 9, 5-8.

Weger, R.J., Eberli, G.P., Baechle, G.T., Massaferro J.L, Sun, Y.F., 2009. Quantification of pore structure and its effect on sonic velocity and permeability in carbonates, American Association of Petroleum Geologists Bulletin 93(10), 1297-1317

Xu, S.Y., Payne, M.A., 2009. Modeling elastic properties in carbonate rocks. The Leading Edge 28, 66-74.

Xu, S.Y., Chen, G., Zhu, Y., Payne, M.A., Deffenbaugh, M., Song, L., Dunsmuir, J., 2007. Carbonate rock physics: Analytical models and validations using computational approaches and log/lad measurement. International Petroleum Technology Conference, December 2007, Dubai, United Arab Emirates, 11308-MS.

Xu, W.L., Wrolstard, K., Kramer, D., Dooley, P., Dominque, K., Vo, D.T., 2006. Brazos A-105 D_sand reservoir modeling by integration of seismic elastic inversion results with geostatistical techniques. American Association of Petroleum Geologists Computer Application in Geology 5, 269-278.

Yang, K.M., Dorobek, S.L.,1995. The Permian Basin of west Texas and New Mexico: tectonic history of a ‘composite' foreland basin and its effect on stratigraphic development. Society for Sedimentary Geology Special Publication 52, 149–174.

Zeng, H.L., Kerans, C., Lucia, J.F., 2006. 3-D seismic detection of collapsed paleocave system in the clear Fork/Glorieta Platform, Hobbs field, New Mexico. Society of Exploration Geophysicists Extended Abstract, 1023-1026.

VITA

Name: Qifeng Dou

Mailing Address: Shell Exploration and Production Company, USA
200 N. Dairy Ashford Rd.
Houston, TX 77079

Email Address: bjdouqf@yahoo.com.cn

Education:

B.S.	(1995)	China University of Petroleum (East China)
M.S.	(1998)	China University of Petroleum (Beijing)
Ph.D.	(2011)	Texas A&M University (College Station)

Experience:

06/1998-07/2005	Assistant Professor at China University of Petroleum (Beijing)
08/2005-08/2006	Research Assistant at University of Houston
05/2007-08/2007	Assistant Geophysicist at Application Geophysical Group, Total E&P Company, USA
05/2008-08/2008	Assistant Geophysicist at Unconventional Reservoir Group, EOG Resource Company, USA
05/2009-08/2009	Assistant Geophysicist at Quantitative Interpretation Group, Geophysics Division, URC, ExxonMobil